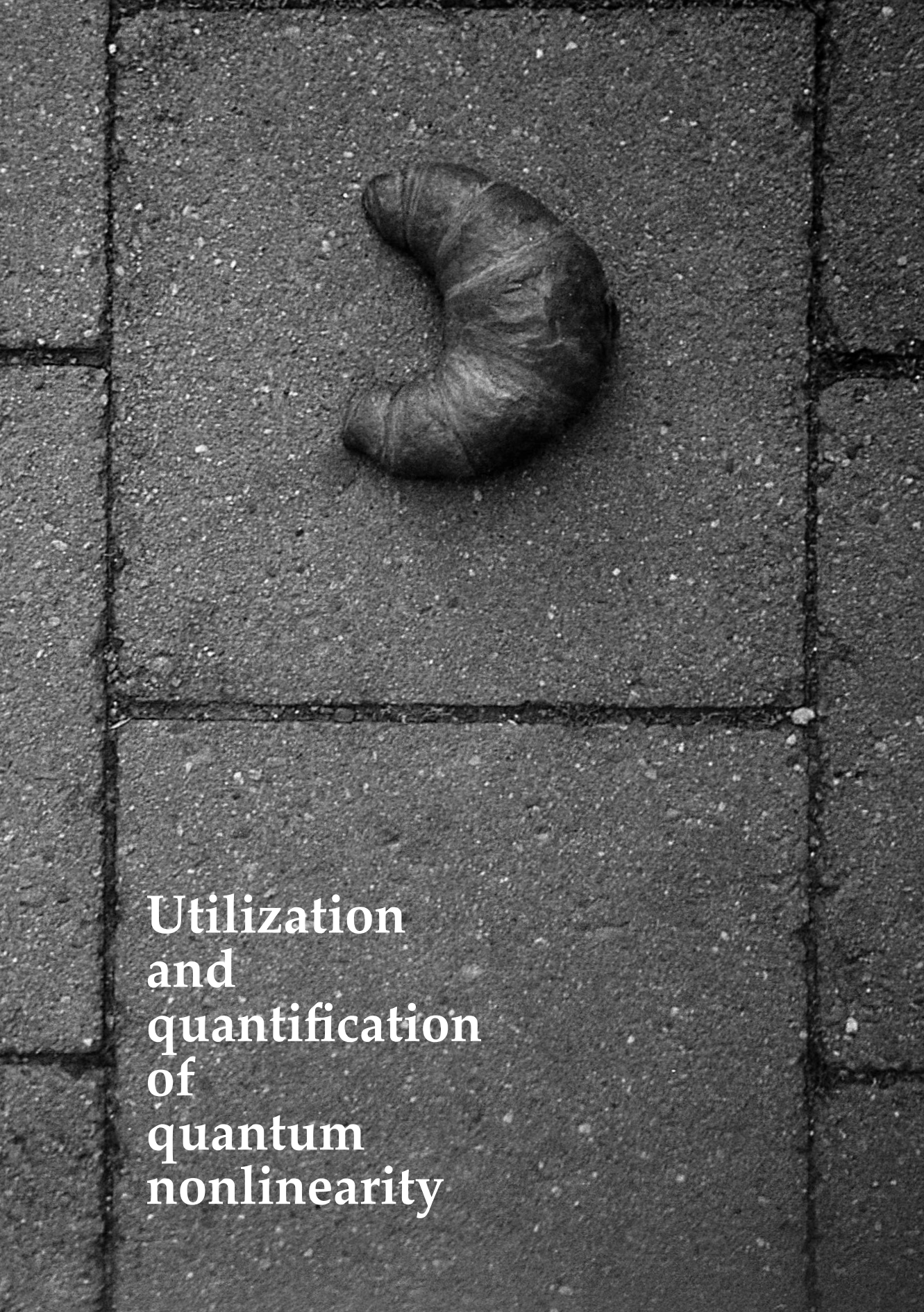

Utilization and quantification of quantum nonlinearity

Utilization and quantification of quantum nonlinearity

a Ph.D. thesis by **Šimon Bräuer**

Faculty
of Science

Palacký University
Olomouc

Department of Optics

2024

Annotation in English

The thesis focuses on two key directions, namely, the use of nonlinearities in quantum thermodynamics and, subsequently, the generation of nonlinear states and their quantification. The thermodynamic part describes the realization of a nonlinear interferometer as the smallest possible quantum heat machine, where the nonlinear process is an integral part of the scheme. With four input modes, it is possible to concentrate energy in one preselected mode at the output of the scheme. The second segment focuses on the realization and quantification of nonlinearly squeezed states — cubic and quartic, where it is a deterministic process with the use of a non-linear operation (Kerr operations). The follow-up is the generalization of the nonlinear squeezing parameter so that it can be used for the classification of different types of states in different systems.

KEYWORDS: quantum optics, quantum thermodynamics, Kerr nonlinearity, nonlinear squeezing

TITLE: Utilization and quantification of quantum nonlinearity

AUTHOR: Šimon Bräuer
ADVISOR: Tomáš Opatrný
CO-ADVISOR: Petr Marek

STUDY PROGRAM: Optics and optoelectronics

STUDY FORM: Full-time
YEAR: 2024
PAGES: 105

DEPARTMENT OF OPTICS
FACULTY OF SCIENCE
PALACKÝ UNIVERSITY OLOMOUC

Anotace v češtině

Práce se zaměřuje na dva klavní směry a to využití nelinearit v kvantové termodynamice a následně na generaci nelineárních stavů a jejich kvantifikaci. V termodynamická část popisuje realizace nelineárního interferometru jako nejmenšího možného kvantového tepelného stroje, kdy nelinární proces je nedílnou součástí schématu. Při vstupních čtyřech módech je možné na výstupu schématu koncentrovat energii do jednoho předvybraného módu. Druhý segment se zaměřuje na realizaci a kvantifikaci nelineárně stlačených stavů — kubicky a kvarticky, kdy se jedná o deterministický proces právě s využitím nelineární operace (Kerrovské operace). Na to navazuje zobecnění parametru nelineárního stlačení tak, aby bylo možné ho využít pro klasifikaci různých typů stavů v různých systémech.

KLÍČOVÁ SLOVA: kvantová optika, kvantová termodynamika, Kerrova nelinearita, nelineární stlačení

NÁZEV: Využití a kvantifikace kvantové nelinearity

AUTOR: Šimon Bräuer
ŠKOLITEL: Tomáš Opatrný
KONZULTANT: Petr Marek

STUDIJNÍ PROGRAM: Optika a optoelektronika

VE FORMĚ: Prezenční
ROK: 2024
STRANY: 105

KATEDRA OPTIKY
PŘÍRODOVĚDECKÁ FAKULTA
UNIVERZITA PALACKÉHO V OLOMOUCI

Acknowledgments

I want to thank my supervisor, Tomáš Opatrný, for guiding the direction of my PhD studies. My co-supervisor, Petr Marek, also participated in the formation process during the studies. I am grateful to both of them for their time, advice, and, most of all, their patience with me.

I would like to thank my colleagues from the Department of Optics in Olomouc, specifically Jaromír Mika, Vojtěch Kala, Jan Provazník, Martin Bielak, and Michal Matulík for the scientific discussions. Also, to my colleagues, for the support during the Ph.D. studies, and for providing a cup of good tea to Radim Hošák, Michal Neset, Jiří Fadrný, Nikola Horová, Olga Leskovjanová, Glib Mazin and Vojtěch Švarc. I must not forget to thank the administrative workers, thanks to whom it was possible to survive the bureaucracy, namely Lenka Jarnotová, Petra Cabišová, Ilona Kašpírová, Elena Kučerová and Mrs. Věra.

Many thanks to Klaus Mølmer for the opportunity to be part of his scientific group in Aarhus and Copenhagen. Also, I thank Mads Lund and Fan Young for taking me in and helping me through the problematic beginnings of a new scientific field (for me). And to Mads, for the fact that it was not purely a matter of scientific cooperation but also of establishing a friendship.

My biggest thanks go to my wife and family for supporting me throughout my studies, surrounding me with love, and enabling me to reach my goal.

Declaration

This thesis is the author's original work. It is based on scientific works that were published in collaboration with other authors and co-authors. A statement of the work done on the articles by the authors and co-authors is attached on the following pages. The co-authors are credited in References. Any other sources are cited there as well.

Date:

Šimon Bräuer

Co-author statement

I hereby declare that I am aware that the work in the paper/manuscript entitled:

> *Generation of quantum states with nonlinear squeezing by Kerr nonlinearity*

of which I am a co-author, will form part of the PhD dissertation by PhD student:

> *Šimon Bräuer*

The PhD student made a major contribution to the research and in the writing phase. I agree to use the materials published in the article for this dissertation.

Date: _____

Petr Marek

Co-author statement

I hereby declare that I am aware that the work in the paper/manuscript entitled:

Nonlinear coherent heat machines

of which I am a co-author, will form part of the PhD dissertation by PhD student:

Šimon Bräuer

The PhD student made a significant contribution to the research and writing phase. I agree to use the materials published in the article for this dissertation.

Date: _____

Tomáš Opatrný

Table of contents

List of Figures

Chapter I

Introduction

Quantum information is an interdisciplinary field with the goal of utilizing the quantum properties of various physical systems in order to drive new applications. The most promising areas of development are quantum communication [1–4], expanding the tools of secure communication towards real-life applications, quantum metrology [5–7], practically enhancing the most powerful measurement tools of the modern times, and quantum computation [8–10], already achieving results that would require unacceptably long time on classical computers. Quantum information is not tied to any particular physical system. It aims at devising universal protocols, which then can be adapted by any capable platform. The protocols can be divided into two broad categories. The

first relies on discrete quantum systems represented by a specific number of two-level qubits. The second one considers continuous systems described by infinite-dimensional Hilbert spaces. These can be modes of optical [11–13] or microwave fields [14, 15], or vibrational modes of mechanical oscillators [16]. Alternatively, they can also be the systems of such a large number of qubits that their collective behavior is essentially continuous, such as in the case of the collections of magnetic spins [17, 18].

For universal processing of continuous-variable (CV) systems, one needs the ability to implement an arbitrary quantum operation [19]. This can be achieved by having access to the class of the Gaussian operations that linearly transform the quadrature operators of the system [12], together with at least a single non-Gaussian operation [19, 20]. The non-Gaussian nature can be imparted by suitable projective measurements [21, 22], but scalable applications ultimately demand a deterministic implementation.

For these reasons, this work focuses on both the use of nonlinearities to generate non-Gaussian states and the evaluation of relevant parameters of these states. During the experimental realization of the states, it is crucial to assess the quality of the state we have created and determine whether it meets the expected properties, such as a given level of squeezing, non-Gaussianity, and other characteristics. In this dissertation, we focus on the use of Kerr nonlinearity for the generation of nonlinearly squeezed states [23] (Chapter V); we also focus on the evaluation of relevant parameters of these states. We study both harmonic oscillators and other systems (Chapter VI).

Since classical information processing is a physical process [24], the computational and thermodynamic processes are closely linked [25]. A typical example is the resetting of a register in a computer, which, in thermodynamic terms, corresponds to cooling. If we move from classical information theory to quantum information theory, quantum information theory still intersects with quantum thermodynamics [26] in understanding the costs of information processing, storage, and communication [27, 28]. Insights from quantum thermodynamics can be helpful for the design of more efficient quantum algorithms [28] and error correction schemes [29, 30], ultimately enhancing the performance of quantum computers [29, 31]. Quantum thermodynamics paves the way for the development of quantum heat engines and refrigerators. These engines could potentially surpass the efficiency limits imposed by classical thermodynamics, leading to more efficient energy conversion and utilization technologies, leading to more efficient manipulation of quantum information. In this work, we deal with the realization of a heat engine designed as a nonlinear interferometer. Its most significant feature is that it uses the smallest possible heat reservoirs composed

of only 4 working modes.

An integral part of the dissertation thesis is a theoretical basis for easier access to the work carried out during the doctoral studies. Therefore, in the chapter II, we describe the system of collective spins: linear operation, possible description of states, and basic spin states. We will also focus on more complex operations that can be used to generate squeezed states. The chapter concludes with a presentation of the Holstein-Primakoff transformation - an approximation of a system of collective spins by phase space.

In chapter III, we deal with the basic description of the linear harmonic oscillator (LHO), the definition of quadrature operators, and their properties. We continue with possible descriptions of LHO states and quasi-probability distributions. We finish with the definition of LHO states and their division according to the property of the quasi-probability distribution of these states.

In chapter IV, we mainly focus on the use of Kerr nonlinearity to generate a non-Gaussian state for realizing a heat engine with the smallest possible number of modes. Without using a nonlinear phenomenon, it would not be possible to realize such a machine. In this project, we use Kerr nonlinearities to generate non-Gaussian states, allowing us to concentrate energy into one of the four modes in such a way that the energy of this state exceeds the energy of each of the individual input states. Additionally, the photon statistics of this state change from a Bose-Einstein distribution to a distribution that approaches Poisson distribution.

In chapter V, we focus on connecting the use of nonlinearity for generating nonlinearly squeezed non-Gaussian states with the use of Kerr nonlinearity, specifically cubically squeezed and quartically squeezed states. In this context, the quantification of the states themselves is also necessary. We introduce a squeezing parameter with which we quantify the resulting states.

In chapter VI, we expand the squeezing parameter used in chapter V so that it can also be applied to systems other than the linear harmonic oscillator. An example of this is cubic squeezing in systems of collective spins.

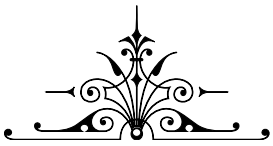

Chapter II

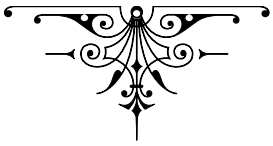

Theoretical basis of Collective spins

In this chapter, we describe the formalism of collective spin systems. We will define them as sums of individual spins or two n-boson modes. We will focus on operations that can be implemented in current experiments and divide them into classes according to the power of the Hamiltonian. We will do the same with quantum states, divide them into classes, and present the operations by which these states can be achieved. A necessary part of this chapter for a better understanding will be the visualization and description of states through quasi-probability distributions.

II.1 Definition

Spin is a quantum property of elementary particles, which has no equivalent in classical physics. It is the internal angular momentum of a particle independent of its orbital motion. This would describe a single particle with spin $\frac{1}{2}$ (using $\hbar = 1$) by angular momentum operator

$$\hat{S} = \frac{1}{2}\hat{\sigma}, \tag{II.1}$$

where $\hat{\sigma}$ is Pauli spin operator composed of $\hat{\sigma}_x, \hat{\sigma}_y$ and $\hat{\sigma}_z$ Pauli matrices

$$\hat{\sigma}_x = |0\rangle\langle 1| + |1\rangle\langle 0|, \tag{II.2}$$
$$\hat{\sigma}_y = -i\left(|0\rangle\langle 1| - |1\rangle\langle 0|\right), \tag{II.3}$$
$$\hat{\sigma}_z = |0\rangle\langle 0| - |1\rangle\langle 1|, \tag{II.4}$$

where

$$|0\rangle = \begin{pmatrix}1\\0\end{pmatrix}, |1\rangle = \begin{pmatrix}0\\1\end{pmatrix}. \tag{II.5}$$

Pauli operators satisfy commutation relations

$$[\hat{\sigma}_k, \hat{\sigma}_l] = 2i\epsilon_{klm}\hat{\sigma}_m, \tag{II.6}$$

where the ϵ_{klm} is the Levi-Civita symbol($k, l, m \in \{x, y, z\}$), also known as a permutation symbol

$$\epsilon_{klm} = 1 \text{ if } (k, l, m) \text{ is even permutation }, \tag{II.7}$$
$$\epsilon_{klm} = -1 \text{ if } (k, l, m) \text{ is odd permutation }, \tag{II.8}$$
$$\epsilon_{klm} = 0 \text{ if any two indices are equal.} \tag{II.9}$$

II.1.1 Operators $\hat{J}_x, \hat{J}_y, \hat{J}_z$

We can describe total collective spin by a collective spin operator for systems composed of more such particles. It is possible to define the collective spin operator in two different ways.

The first of them is to consider that this operator is formed as a sum of spin operators of N individual particles

$$\hat{J}_k = \frac{1}{2}\sum_{n=1}^{N}\hat{\sigma}_k^{(n)}, \tag{II.10}$$

for $k = x, y, z$. The dimension of N spins is 2^N; however, if only symmetrical states are involved, the dimension is reduced to $N + 1$.

For this purpose, we can use Swinger's representation [32] equivalent to two bosonic modes with annihilation operators $\hat{a}_{1,2}$ and creation operators $\hat{a}^\dagger_{1,2}$. These operators satisfy the bosonic commutation rules

$$\left[\hat{a}_k, \hat{a}^\dagger_l\right] = \delta_{kl}. \tag{II.11}$$

The collective spin operators have the form

$$\hat{J}_x = \frac{1}{2}\left(\hat{a}^\dagger_1\hat{a}_2 + \hat{a}_1\hat{a}^\dagger_2\right), \tag{II.12}$$

$$\hat{J}_y = \frac{1}{2i}\left(\hat{a}^\dagger_1\hat{a}_2 - \hat{a}_1\hat{a}^\dagger_2\right), \tag{II.13}$$

$$\hat{J}_z = \frac{1}{2}\left(\hat{a}^\dagger_1\hat{a}_1 - \hat{a}^\dagger_2\hat{a}_2\right), \tag{II.14}$$

and satisfy commutation relations

$$\left[\hat{J}_k, \hat{J}_l\right] = i\epsilon_{klm}\hat{J}_m, \tag{II.15}$$

in the same manner as the operators defined in (II.10). The total number of particles corresponds to

$$\hat{N} = \hat{a}^\dagger_1\hat{a}_1 + \hat{a}^\dagger_2\hat{a}_2. \tag{II.16}$$

The square of the total angular momentum operator

$$\hat{J}^2 = \hat{J}^2_x + \hat{J}^2_y + \hat{J}^2_z, \tag{II.17}$$

can be expressed as

$$\hat{J}^2 = \frac{\hat{N}}{2}\left(\frac{\hat{N}}{2} + 1\right). \tag{II.18}$$

That means that the system of N spins $\frac{1}{2}$ can be described as one system with the total angular momentum $\hat{J}$, where $\hat{N}$ and $\hat{J}$ are connected by (II.18).

It is also useful to define the so-called ladder operators $\hat{J}_+$ and $\hat{J}_-$

$$\begin{aligned} \hat{J}_+ &= \hat{J}_x + i\hat{J}_y, \\ \hat{J}_- &= \hat{J}_x - i\hat{J}_y. \end{aligned} \tag{II.19}$$

They satisfy the commutation relations

$$\left[\hat{J}_+, \hat{J}_-\right] = 2\hat{J}_z, \tag{II.20}$$

$$\left[\hat{J}_z, \hat{J}_\pm\right] = \pm\hat{J}_\pm. \tag{II.21}$$

II.1.2 Dicke states

The states that are the eigenstates of the operator $\hat{J}_z$ and $\hat{J}^2$, are called the Dicke states $|J, M\rangle$ and they are defined by

$$\hat{J}^2 |J, M\rangle = J(J+1) |J, M\rangle , \tag{II.22}$$

$$\hat{J}_z |J, M\rangle = M |J, M\rangle , \tag{II.23}$$

where $J = \frac{N}{2}$, $M = -J, -J+1, \cdots, J-1, J$ and N is the total number of atoms. These states have a precise number of particles in the two modes and a completely undefined phase. The lowest state that can be reached, the ground state $|J, -J\rangle$ of Hamiltonian $\hat{H} = \hat{J}_z$ (sometimes called the vacuum state), can be used to construct higher Dicke states as

$$\begin{aligned}
\hat{J}_+ |J, -J\rangle &= \sqrt{2J} |J, -J+1\rangle , \\
\hat{J}_+ |J, -J+1\rangle &= \sqrt{2(2J-1)} |J, -J+2\rangle , \\
&\vdots \\
\hat{J}_+ |J, M-1\rangle &= \sqrt{(J+M)(J-M+1)} |J, M\rangle .
\end{aligned}$$

Any Dicke state can be expressed in terms of the ground state as

$$|J, M\rangle = \frac{1}{(J+M)!} \sqrt{\binom{2J}{J+M}} \hat{J}_+^{M+J} |J, -J\rangle . \tag{II.24}$$

The extreme states $|J, \pm J\rangle$ satisfy

$$\hat{J}_- |J, -J\rangle = 0, \tag{II.25}$$

$$\hat{J}_+ |J, J\rangle = 0. \tag{II.26}$$

On the opposite side, we also have the highest possible excited state $|J, J\rangle$, satisfying

$$\hat{J}_+ |J, J\rangle = 0. \tag{II.27}$$

II.2 Basic operations

One of the most basic operations in the collective spin system is the rotation operation. By the unitary operation of rotation, it is possible to create a coherent spin state from the vacuum state, and therefore we will describe the operation of rotation in the definition of the coherent spin state.

II.2.1 Coherent spin state

A coherent spin state pointing in direction $\mathbf{n}$ [33–35] can be defined as the ground state of the Hamiltonian $\hat{H} = \mathbf{n}\cdot\hat{\mathbf{J}}$, where $\mathbf{n}$ is rotation axis and $\hat{\mathbf{J}} = \left(\hat{J}_x, \hat{J}_y, \hat{J}_z\right)$. So, we demonstrate an example of rotation, first, we rotate along J_z

$$\hat{J}_z = \hat{J}_z, \tag{II.28}$$

$$\hat{J}_n = \hat{J}_x \sin\phi - \hat{J}_y \cos\phi, \tag{II.29}$$

$$\hat{J}_k = \hat{J}_x \cos\phi + \hat{J}_y \sin\phi. \tag{II.30}$$

Now we have new axes J_z,J_n,J_k. If we perform a rotation along the J_n axis, then the rotation operator will have the form

$$\hat{R}^{(n)}(\theta,\phi) = \exp\left(-i\theta\hat{J}_n\right) \tag{II.31}$$

$$= \exp\left(-i\theta\left[\hat{J}_x\sin\phi - \hat{J}_y\cos\phi\right]\right), \tag{II.32}$$

$$= \exp\left(\alpha\hat{J}_x - i\alpha\hat{J}_y - \alpha^*\hat{J}_x - i\alpha^*\hat{J}_y\right), \tag{II.33}$$

$$= \exp\left(\alpha\hat{J}_+ - \alpha^*\hat{J}_-\right), \tag{II.34}$$

where $\alpha = \frac{\theta}{2}\exp(-i\phi)$. A spin coherent state with general rotation has the form

$$|\theta,\phi\rangle = \exp\left(\alpha\hat{J}_+ - \alpha^*\hat{J}_-\right)|J,-J\rangle\,. \tag{II.35}$$

Even though it is a rotated ground state, the coherent state is still an eigenstate of the total angular momentum operator, but no longer of the operator $\hat{J}_z$,

$$\hat{J}^2|\theta,\phi\rangle = J(J+1)|\theta,\phi\rangle\,. \tag{II.36}$$

It is also possible to write a coherent state in the basis of Dicke states. It is necessary to rewrite the rotation operator using the Baker-Hausdorf relation[36]

$$\hat{R}(\theta,\phi) = \exp\left(e^{-i\phi}\tan\left(\frac{\theta}{2}\right)\hat{J}_+\right)\exp\left(\ln\left(1+|e^{-i\phi}\tan\left(\frac{\theta}{2}\right)|^2\right)\hat{J}_z\right)\times$$
$$\times\exp\left(e^{+i\phi}\tan\left(\frac{\theta}{2}\right)\hat{J}_-\right). \tag{II.37}$$

For simplicity, we use the substitution $\tau = \exp(-i\phi)\tan\left(\frac{\theta}{2}\right)$. Then we express the coherent state as the rotated ground state

$$|\theta,\phi\rangle = \hat{R}(\theta,\phi)\,|J,-J\rangle\,, \tag{II.38}$$
$$= \frac{1}{(1+|\tau|^2)^J}\exp\left(\tau\hat{J}_+\right)|J,-J\rangle\,, \tag{II.39}$$
$$= \frac{1}{(1+|\tau|^2)^J}\sum_{M=-J}^{J}\frac{\tau^{M+J}}{(M+J)!}\hat{J}_+^{M+J}\,|J,-J\rangle\,, \tag{II.40}$$
$$= \frac{1}{(1+|\tau|^2)^J}\sum_{M=-J}^{J}\binom{2J}{J+M}^{\left(\frac{1}{2}\right)}\tau^{M+J}\,|J,M\rangle\,. \tag{II.41}$$

As is obvious, the only thing that the rotation operation causes is a change in the state's position on the Bloch sphere (more details in the section below), so it is a linear operation. The mean values in the individual operators $\hat{J}_k$ ($k \in \{x,y,z\}$) are in interval $-\frac{N}{2}$ to $\frac{N}{2}$.

II.3 Visualization

For the visualization of the states of collective spins, we are using the Bloch sphere. The Bloch sphere [37] (also known as Poincaré sphere in classical optics) is a geometrical representation of the state space of a two-level quantum system. The pure state of a two-level system can be described as a superposition of two ground states

$$|\psi\rangle = \alpha\,|0\rangle + \beta\,|1\rangle\,, \tag{II.42}$$

where $\alpha = \cos\left(\frac{\theta}{2}\right)$ and $\beta = e^{i\phi}\sin\left(\frac{\theta}{2}\right)$ and satisfy $|\alpha|^2 + |\beta|^2 = 1$. Angles θ and ϕ represent coordinates on the Bloch sphere, analogous to geographical latitude and longitude.

The position of a point on the sphere for spin is defined as the mean value of individual operators:

$$\langle \hat{\sigma}_x \rangle = r \sin(\theta) \cos(\psi), \tag{II.43}$$

$$\langle \hat{\sigma}_y \rangle = r \sin(\theta) \sin(\psi), \tag{II.44}$$

$$\langle \hat{\sigma}_z \rangle = r \cos(\theta), \tag{II.45}$$

where r is the sphere's radius.

This was for an one atom system; we will move to an N atom system where we will not represent a point on the Bloch sphere but a state in the form of a quasi-probability distribution (we will use the Q-function, but in some cases, it is also possible to use the Wigner function [38]).

Similarly, as in the previous case, the position of the center of mass of the state

$$\langle \hat{J}_x \rangle = r \sin(\theta) \cos(\psi), \tag{II.46}$$

$$\langle \hat{J}_y \rangle = r \sin(\theta) \sin(\psi), \tag{II.47}$$

$$\langle \hat{J}_z \rangle = r \cos(\theta), \tag{II.48}$$

where the radius of the Bloch sphere increases with the size of the system [39]

$$r = |\langle \hat{J} \rangle| = \sqrt{\frac{N}{2}\left(\frac{N}{2}+1\right)}. \tag{II.49}$$

Instead of describing quantum systems in terms of the states, we can also employ description using Husimi Q-function [40]. Q-function is a quasiprobability distribution that is defined by means of the coherent state

$$\mathcal{Q}(\theta,\phi) = \frac{1}{\pi} \mathrm{Tr}\left\{\hat{\rho}\,|\theta,\phi\rangle\,\langle\theta,\phi|\right\}, \tag{II.50}$$

$$= \frac{1}{\pi} \langle\theta,\phi|\,\hat{\rho}\,|\theta,\phi\rangle, \tag{II.51}$$

where $|\theta,\phi\rangle$ is the coherent spin state and $\hat{\rho} = |\Gamma\rangle\langle\Gamma|$ is the studied state. The value for specific angles θ and ψ corresponds to the overlap of the coherent spin state with the state under consideration.

II.4 Quadratic and higher-order operations

When defining a coherent spin state, we introduced a linear operation, rotation, that changes the mean values in the operators $\hat{J}_k$ ($k \in \{x,y,z\}$). Now we move

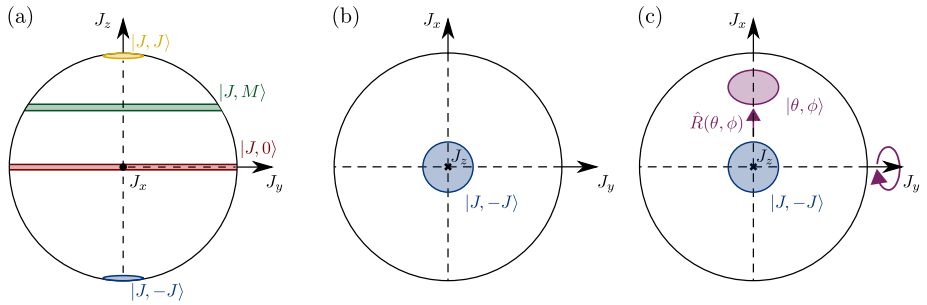

Figure II.1: Visualisation of the states on the Bloch sphere: (a) Dicke states on the Bloche sphere where blue $|J,-J\rangle$ is the ground state and yellow $|J,J\rangle$ is the highest excited state. (b) The ground state on the Bloch sphere with a view perpendicular to the J_z axis.(c) Generation of the coherent state $|\theta,\phi\rangle$ through the rotation of the ground state $|J,-J\rangle$.

to operations that not only rotate the states on the Bloch sphere but also deform and squeeze them in various ways.

II.4.1 Squeezing in collective spins

In defining squeezing in collective spins, it is suitable to rotate the coordinate system such that $\langle\hat{J}_k\rangle = \langle\hat{J}_l\rangle = 0, \langle\hat{J}_m\rangle \neq 0$.

Coherent states (ground states of $\hat{J}_m$) are states that minimize uncertainty relations

$$\mathrm{var}\left(\hat{J}_k\right)\mathrm{var}\left(\hat{J}_l\right) \geq \frac{1}{4}|\langle\hat{J}_m\rangle|^2, \tag{II.52}$$

where $\mathrm{var}\left(\hat{J}_k\right) = \langle\hat{J}_k^2\rangle - \langle\hat{J}_k\rangle^2$ (for $\langle\hat{J}_l\rangle = \langle\hat{J}_m\rangle = 0$). The uncertainty they acquire is $\frac{J}{2}$, equally distributed over any two orthogonal components normal to the (θ,ϕ) direction.

States with an uncertainty smaller than the coherent state (ground state) in just one of the two directions are called squeezed (in the case of a diagonal covariance matrix). For these cases, a squeezing parameter is also introduced,

$$\xi = \frac{\mathrm{var}(\hat{J}_k)}{\mathrm{var}_{|CSS\rangle}(\hat{J}_k)} \tag{II.53}$$

which is normalized precisely by the uncertainty of the coherent state. If $0 \leq \xi < 1$, we say that the state is squeezed in the variable $\hat{J}_k$.

II.4.2 Quadratic operations

We can generate squeezing through quadratic operations, and we have two basic types according to the number of axes along which we twist: *one-axis twisting* or *two-axis counter-twisting*.

- **One-axis twisting (OAT) operation**

  The lowest-order nonlinear interaction in collective spins is the one-axis twisting operation, defined by the unitary operator

  $$\hat{U}_{\mathrm{OAT}}(\chi t) = \exp\left(i\chi t \left(\frac{N}{2}\right)^{-\frac{2}{3}} \hat{J}_k^2\right), \tag{II.54}$$

  where χt is the effective coupling constant and $\left(\frac{N}{2}\right)^{-\frac{2}{3}}$ is the scaling parameter depending on the number of particles in the system. The Hamiltonian itself has the form

  $$\hat{H}_{\mathrm{OAT}}(\chi) = \chi \hat{J}_k^2. \tag{II.55}$$

  Let us demonstrate the dynamics for $k = z$ and for the coherent state in the x-axis:

  $$\left|\frac{\pi}{2}, 0\right\rangle = 2^{-J} \sum_{M=-J}^{J} \binom{2J}{J+M}^{\left(\frac{1}{2}\right)} |J, M\rangle\,. \tag{II.56}$$

  Now apply time-evolution operator (II.54) (for $k = z$), which results in

  $$|\chi t\rangle = 2^{-J} \sum_{M=-J}^{J} \binom{2J}{J+M}^{\left(\frac{1}{2}\right)} \exp(i\chi t M^2)\,|J, M\rangle\,. \tag{II.57}$$

  This interaction leads to rotation proportional to J_z, which twists the quantum fluctuations (state) as shown in FIG II.2 (b),(c). This type of operation is analogous to self-phase modulation in the photon system [41].

  The OAT operation can be used in preparing different states, for example, squeezed states used for the generation of cubic squeezing [42], i.e., the emulation of the $\hat{J}_z^3$ operation. Another application is, for example, the generation of cat states, when we get a superposition of Dicke states on the poles and interference fringes between the poles [43].

- **Two axis counter twisting (TACT) operation**

  OAT squeezing had a side effect in addition to squeezing - rotation of the state. This effect can be removed if the twisting is performed at the same time with right-hand helicity and left-hand helicity about two orthogonal axes in the plane normal to the mean-spin direction [39]. For example, the initial state is $|J,-J\rangle$, then twisting is about two orthogonal axes in the $\theta=\frac{\pi}{2},\phi=\frac{\pi}{4}$ and $\theta=\frac{\pi}{2},\phi=-\frac{\pi}{4}$ directions. Spin operators relevant to these directions are

$$\hat{J}_{\left(\frac{\pi}{2},\frac{\pi}{4}\right)}=\cos\left(\frac{\pi}{4}\right)\hat{J}_x+\sin\left(\frac{\pi}{4}\right)\hat{J}_y=\frac{1}{\sqrt{2}}\left(\hat{J}_x+\hat{J}_y\right), \tag{II.58}$$

$$\hat{J}_{\left(\frac{\pi}{2},-\frac{\pi}{4}\right)}=\cos\left(\frac{\pi}{4}\right)\hat{J}_x-\sin\left(\frac{\pi}{4}\right)\hat{J}_y=\frac{1}{\sqrt{2}}\left(\hat{J}_x-\hat{J}_y\right). \tag{II.59}$$

  Consequently, the form of the TACT Hamiltonian is

$$\hat{H}_{\mathrm{TACT}}=\chi\left(\hat{J}^2_{\left(\frac{\pi}{2},\frac{\pi}{4}\right)}-\hat{J}^2_{\left(\frac{\pi}{2},-\frac{\pi}{4}\right)}\right), \tag{II.60}$$

$$=\chi\left(\hat{J}_x\hat{J}_y+\hat{J}_y\hat{J}_x\right), \tag{II.61}$$

$$=\frac{\chi}{2i}\left(\hat{J}^2_+-\hat{J}^2_-\right). \tag{II.62}$$

  The unitary operator has the form

$$\hat{U}_{\mathrm{TACT}}(\chi)=\exp\left(i\chi\left(\frac{N}{2}\right)^{-\frac{2}{3}}\left(\hat{J}_x\hat{J}_y+\hat{J}_y\hat{J}_x\right)\right), \tag{II.63}$$

  where χ is effective coupling constant, $\left(\frac{N}{2}\right)^{-\frac{2}{3}}$ is the scaling parameter depending on the number of particles in the system.

  With the help of the TACT operation, achieving a higher level of squeezing of the state is possible compare to OAT itself [44]. This is one of the advantages of this operation, and at the same time, the squeezed state is still in the axes, unlike OAT when the state constantly rotates around the axis of the input state. The disadvantage is that the dynamics are more complicated than in the previous case [45]. The visualization of state squeezed via TACT on the Bloch sphere is in FIG II.2 (d)-(f), when the initial state is a coherent state in the J_x axis up to a squeezed state with an effective interaction time $\chi=0.3$ ($N=60$) of time evolution (II.63) in

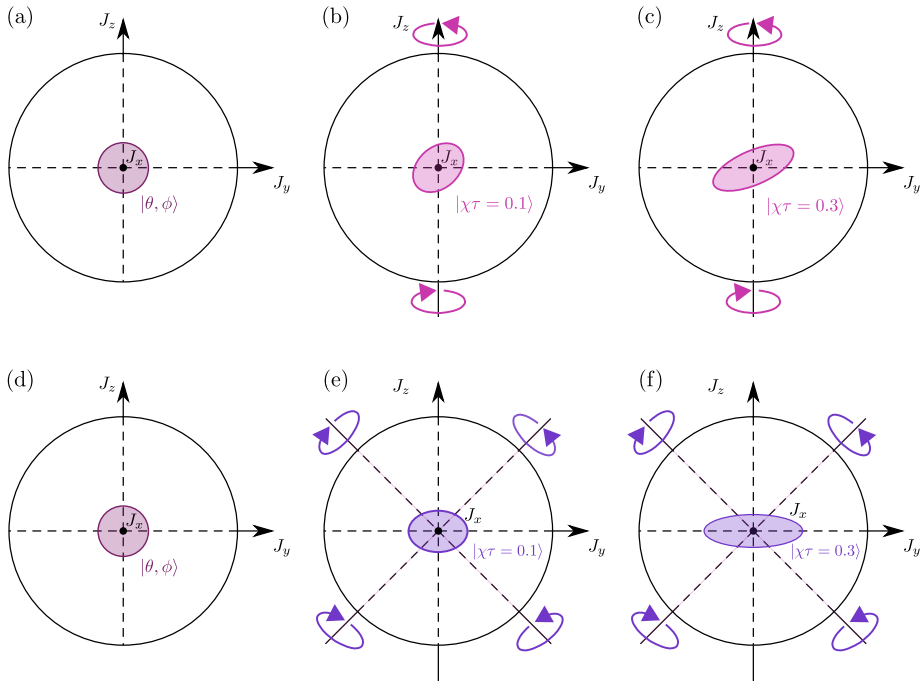

Figure II.2: Visualisation of squeezing on the Bloch sphere. (a) Coherent spin state as an initial state for OAT operation. (b) Squeezed state after effective time $\chi t = 0.1$ (time evolution via (II.54), $N = 60$). (c) Squeezed state after effective time $\chi t = 0.3$ (time evolution via (II.54), $N = 60$) (d) Coherent spin state as an initial state for TACT operation. (e) Squeezed state after effective time $\chi t = 0.1$ (time evolution via (II.63), $N = 60$). (f) Squeezed state after effective time $\chi t = 0.3$ (time evolution via (II.63), $N = 60$)

y, z axes, and the form of the unitary operator is

$$\hat{U}_{\mathrm{TACT}}(\chi) = \exp\left(i\chi\left(\frac{N}{2}\right)^{-\frac{2}{3}}(\hat{J}_z\hat{J}_y + \hat{J}_y\hat{J}_z)\right). \tag{II.64}$$

These are examples where we have rotated perpendicular axes, we can consider the simplest case where our twisting axes are directly J_x and J_y, then the shape of the Hamiltonian

$$\hat{H}_{\mathrm{TACT}} = \chi\left(\hat{J}_x^2 + \hat{J}_y^2\right). \tag{II.65}$$

II.4.3 Higher-order operations

A higher order of operation is considered when the Hamiltonian contains a higher power of operators than the quadratic one, i.e., cubic, quartic, and higher. Compared to quadratic and linear operations, higher-order operations are much harder to achieve experimentally.

Although we do not have these operations at our disposal, the effort is to reach states squeezed in these higher orders, i.e., states that we would get through evolution, for example, by cubic operation or higher. The motivation is quantum metrology [42, 46, 47] and the possibility of more precise measurements with states that are squeezed in the sense of higher orders of operations. There are various procedures to achieve these operations or at least emulate these operations. We will focus on an example with a cubic operation defined by a unitary operator

$$\hat{U}_c(\chi t) = \exp\left(i\frac{\chi t}{3}\left(\frac{N}{2}\right)^{-\frac{2}{3}}\hat{J}_x^3\right). \tag{II.66}$$

It is possible to emulate the effect of such an operation by a suitable series of lower-order operations. Specifically, OAT operation combined with rotation and time-reversed OAT [42]. In this way, it is possible to create a cubically squeezed state, similar to the state we would get from the original operation (II.66).

Another possible procedure is using commutators of operators [19] of lower orders (quadratic and linear) to implement a cubic operation [48]; in principle, this method should work subsequently for higher orders of operations. The formula for obtaining the cubic operator

$$\begin{aligned}\hat{J}_x^3 &= \frac{i}{4}\left[\left(\hat{J}_z^2 - \hat{J}_y^2\right), \left(\hat{J}_y\hat{J}_z + \hat{J}_z\hat{J}_y\right)\right] \\ &= \frac{i}{4}\left[\left(\hat{J}_x\hat{J}_z + \hat{J}_z\hat{J}_x\right), \left(\hat{J}_x\hat{J}_y + \hat{J}_y\hat{J}_x\right)\right] + \frac{1}{4}\hat{J}_x. \end{aligned} \tag{II.67}$$

II.5 Approximation by a plane

In cases of a large number of atoms in the system, when $N \gg 1$, it is possible to select an area near the pole that appears to be a plane, and thus it is possible to move from a three-dimensional space to a two-dimensional space (also known as Holstein - Primakoff transformation [49]). The operator $\hat{J}_z$ thus changes to its mean value

$$\hat{J}_z \approx \frac{N}{2}. \tag{II.68}$$

Then the commutation relation becomes from (II.15) to the form

$$\left[\hat{J}_x, \hat{J}_y\right] = i\frac{N}{2}. \tag{II.69}$$

We have moved from commutation relations with the operator on the right-hand side to commutation relations with the constant on the right-hand side. The next step is to move from the collective spins to the phase space, that is, to establish a relation between $\hat{J}_x$, $\hat{J}_y$ and observables $\hat{x}$, $\hat{p}$. So once we substitute $\hat{J}_x$ and $\hat{J}_y$ into the commutation relations, they are equal to the commutation relations for the observables $\hat{x}$ and $\hat{p}$:

$$\sqrt{\frac{2}{N}}\hat{J}_x = \hat{x}, \tag{II.70}$$

$$\sqrt{\frac{2}{N}}\hat{J}_p = \hat{p}, \tag{II.71}$$

which leads to the commutation relations of the harmonic oscillator

$$[\hat{x}, \hat{p}] = i. \tag{II.72}$$

They are then motivated by comparing the results obtained in the harmonic oscillator system and the system of collective spins, comparing the properties of the states. For example, Gaussian states (more details in section III.3.2),

which are defined in linear harmonic oscillator systems, on the Bloch sphere are not directly defined, but we can say that Guass-like states are precisely those states that change to the Gaussian states in the H-P transformation, the same for non-Gaussian states.

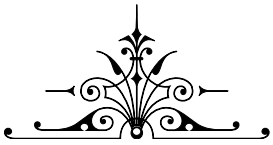

Chapter III

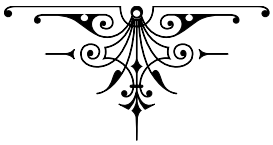

Theoretical basis of Harmonic oscillators

In this chapter, we describe one mode of light as a harmonic oscillator. We mention different classes of states, their definitions, and the ways in which we can create such states, i.e. the operations by which they can be achieved. An important aspect is Gaussianity and non-Gaussianity as a property of states and how it can be defined.

III.1 Definition

Quantum light is described within the framework of quantum field theory as a quantized electromagnetic field. We describe one mode of the electromagnetic field using the linear harmonic oscillator model, which is defined by the Hamiltonian

$$\hat{H} = \hbar\omega\hat{a}^\dagger\hat{a}. \tag{III.1}$$

In the next, we consider constant $\hbar = 1$ and frequency $\omega = 1$. The creation $\hat{a}^\dagger$ and annihilation $\hat{a}$ operators satisfying

$$\left[\hat{a}, \hat{a}^\dagger\right] = \mathbb{1}, \tag{III.2}$$

where $\mathbb{1}$ is the identity operator. This commutation relation reflects the quantized nature of the electromagnetic field.

The momentum and position operators for quantum light can be expressed in terms of these creation and annihilation operators. The momentum operator $\hat{p}$ and the position operator $\hat{x}$ are defined as follows

$$\hat{x} = \frac{(\hat{a}^\dagger + \hat{a})}{\sqrt{2}}, \tag{III.3}$$

$$\hat{p} = i\frac{(\hat{a}^\dagger - \hat{a})}{\sqrt{2}}. \tag{III.4}$$

The commutation relations for the $\hat{x}$ and $\hat{p}$ can be derived from the commutation relations of the creation and annihilation operators. They are given by

$$[\hat{x}, \hat{p}] = i. \tag{III.5}$$

The uncertainty relations for quantum light, based on these momentum and position operators, can be expressed as

$$\Delta x^2 \Delta p^2 \geq \frac{1}{4}, \tag{III.6}$$

where Δx^2 and Δp^2 are the variances of the operators in the form

$$\Delta x^2 = \langle\hat{x}^2\rangle - \langle\hat{x}\rangle^2, \tag{III.7}$$

$$\Delta p^2 = \langle\hat{p}^2\rangle - \langle\hat{p}\rangle^2. \tag{III.8}$$

III.2 States and representation of states

III.2.1 Representation of the states

Fock state representation

Fock states $|n\rangle$ are eigenstates of the number operator, which counts the photons in a given mode of the field. This representation is particularly useful for analyzing the behavior of quantum light in terms of discrete quanta. The number operator denoted as

$$\hat{N} = \hat{a}^\dagger \hat{a}, \tag{III.9}$$

acts on Fock states as follows

$$\hat{N} |n\rangle = n |n\rangle \tag{III.10}$$

This equation expresses the eigenvalue property of Fock states with respect to the number operator.

The creation and annihilation operators, $\hat{a}^\dagger$ and $\hat{a}$, operate on Fock states as

$$\hat{a} |n\rangle = \sqrt{n} |n-1\rangle , \tag{III.11}$$

$$\hat{a}^\dagger |n\rangle = \sqrt{n+1} |n+1\rangle . \tag{III.12}$$

The Fock states form an orthogonal basis of an infinite dimensional Hilbert space,

$$\langle n|m\rangle = \delta_{n,m}, \tag{III.13}$$

$$\sum_{n=0}^{\infty} |n\rangle \langle n| = \mathbb{1}. \tag{III.14}$$

A general pure quantum state in the Fock basis is represented as a superposition of Fock states as

$$|\psi\rangle = \sum_{n=0}^{\infty} c_n |n\rangle , \tag{III.15}$$

where c_n are complex coefficients satisfying $\sum_{n=0}^{\infty} |c_n|^2 = 1$. A mixed state with a density operator $\hat{\rho}$ is given by

$$\hat{\rho} = \sum_{n=0}^{\infty} p_n |n\rangle \langle n| , \tag{III.16}$$

where p_n are probabilities satisfying $\sum_{n=0}^{\infty} p_n = 1$.

Fock states are a class of states that have inherently uncertain phases but well-defined numbers of particles. This relationship is part of the quantum mechanical principle that states conjugate variables (like particle number and phase) cannot be simultaneously well-defined. On the opposite side, coherent states

$$|\alpha\rangle = \exp\left(-\frac{1}{2}|\alpha|^2\right) \sum_{n=0}^{\infty} \frac{\alpha^n}{\sqrt{n!}} |n\rangle \,, \tag{III.17}$$

have a well-defined phase and amplitude, resembling classical waves (more details about coherent states in subsection III.2.2).

Quadrature state representation

The position and momentum operators, $\hat{x}$ and $\hat{p}$, have eigenvectors $|x\rangle$ and $|p\rangle$ satisfying

$$\hat{x}\,|x\rangle = x\,|x\rangle \,, \tag{III.18}$$

$$\hat{p}\,|p\rangle = p\,|p\rangle \,. \tag{III.19}$$

These eigenvectors collectively form a complementary pair, constituting a complete orthogonal basis.

$$\langle x|x'\rangle = \delta(x-x)', \tag{III.20}$$

$$\langle p|p'\rangle = \delta(p-p)', \tag{III.21}$$

$$\langle x|p\rangle = \frac{\mathrm{e}^{ixp}}{\sqrt{2\pi}}, \tag{III.22}$$

$$\int_{-\infty}^{+\infty} |x\rangle\langle x|\,dx = \int_{-\infty}^{+\infty} |p\rangle\langle p|\,dp = \mathbb{1}. \tag{III.23}$$

In the quadrature representation a pure state $|\psi\rangle$ has the form

$$|\psi\rangle = \int_{-\infty}^{+\infty} \psi(x)\,|x\rangle\,dx, \tag{III.24}$$

where $\psi(x) = \langle x|\psi\rangle$ is a wave function of the state.

The quadrature representation has a continuous basis in contrast to the discrete basis of Fock states. In comparing these formalisms, the quadrature representation is useful for describing continuous degrees of freedom, whereas the Fock representation is more appropriate for systems characterized by discrete energy levels.

Wigner function

The Wigner function $\mathcal{W}(x,p)$ associated with a quantum state $\hat{\rho}$ is defined as follows

$$\mathcal{W}(x,p) = \frac{1}{2\pi}\int_{-\infty}^{+\infty} \exp(ipx)\left\langle x-\frac{y}{2}\right|\hat{\rho}\left|x+\frac{y}{2}\right\rangle dy. \tag{III.25}$$

Sometimes it is more efficient to overwrite real variables x and p with a complex variable α

$$\alpha = \frac{x+ip}{\sqrt{2}}, \tag{III.26}$$

as in the case of the definition of the Wigner function through the displaced parity operator

$$W(\alpha) = \frac{1}{2\pi}\langle \hat{D}^{\dagger}(\alpha^*)(-\hat{\Pi})^{\hat{a}^{\dagger}\hat{a}}\hat{D}(\alpha)\rangle, \tag{III.27}$$

where $\hat{\Pi}$ is the parity operator and $\hat{D}(\alpha)$ is unitary operator of displacement (III.39). $\hat{\Pi}$ operator is defined as

$$\hat{\Pi} = \sum_n (-1)^n |n\rangle\langle n|, \tag{III.28}$$

The Wigner function is normalized as

$$\int_{-\infty}^{+\infty}\int_{-\infty}^{+\infty} \mathcal{W}(x,p)\,dxdp = 1. \tag{III.29}$$

The marginal distributions of the Wigner function provide the probability distributions in the position and momentum spaces. The position probability distribution is obtained by integrating the Wigner function overall momentum values

$$p(x) = \int_{-\infty}^{+\infty} \mathcal{W}(x,p)\,dp. \tag{III.30}$$

Similarly, the momentum probability distribution is obtained by integrating overall position values

$$p(p) = \int_{-\infty}^{+\infty} \mathcal{W}(x,p)\,dx. \tag{III.31}$$

Unlike classical probability distributions, the Wigner function can take negative values. Negative regions in the Wigner function indicate the presence of non-classical correlations and inherently quantum features.

Wigner function can be used for finding expectation values of symmetrically ordered operators

$$\mathrm{Tr}[\hat{\rho}(\hat{x}^m\hat{p}^n)_{sym}] = \int_{-\infty}^{+\infty} x^m p^n \mathcal{W}(x,p)\, dxdp, \tag{III.32}$$

where symmetrical ordering $(\cdot)_{sym}$, means that the operator is actually an average of all possible combinations of ordering. For example for $m = 1$ and $n = 1$ – $(\hat{x}\hat{p})_{sym} = \frac{1}{2}(\hat{x}\hat{p} + \hat{p}\hat{x})$.

Understanding these properties facilitates interpreting the Wigner function as a versatile tool for characterizing quantum states in quantum optics. Its unique features provide insights into the non-classical nature of quantum states and the intricacies of quantum uncertainties.

P - function

The P-function is also known as a Glauber-Sudarshan quasidistribution. P-function is defined as a Fourier transform of the characteristic function $\bar{P}$,

$$P(x,p) = \frac{1}{(2\pi)^2}\int_{-\infty}^{+\infty}\int_{-\infty}^{+\infty} \bar{P}(x',p')\exp\left(-i(xp' - px')\right)dx'dp', \tag{III.33}$$

where

$$\bar{P}(x',p') = \mathrm{Tr}\left[\hat{\rho}\exp\left(\frac{x'+ip'}{\sqrt{2}}\hat{a}^\dagger\right)\exp\left(\frac{x'-ip'}{\sqrt{2}}\hat{a}\right)\right]. \tag{III.34}$$

The P-function can be used to express any state by projections on coherent states

$$\hat{\rho} = \int_{-\infty}^{+\infty}\int_{-\infty}^{+\infty} P(\alpha)\,|\alpha\rangle\langle\alpha|\, d^2\alpha. \tag{III.35}$$

Similarly, as the Wigner function, the P-function is normalized

$$\int_{-\infty}^{+\infty}\int_{-\infty}^{+\infty} P(x,p)\, dxdp = 1. \tag{III.36}$$

In contrast to a regular probability distribution, for some states, this function can have negative values or display irregularities as the Dirac δ-function and its derivatives.

Husimi's - function

Husimi's $\mathcal{Q}$-function is a quasiprobability distribution defined as a projection of the state on coherent state $|\alpha\rangle$, i.e.,

$$\mathcal{Q}(x,p) = \mathcal{Q}(\alpha) = \frac{1}{2\pi}\mathrm{Tr}\left[\hat{\rho}\,|\alpha\rangle\,\langle\alpha|\right] = \frac{1}{2\pi}\,\langle\alpha|\,\hat{\rho}\,|\alpha\rangle\,, \tag{III.37}$$

where coherent amplitude $\alpha = \frac{x+ip}{\sqrt{2}}$. The $\mathcal{Q}$-function is real, regular, non-negative, and normalized to unity. It can be utilized to derive statistics for anti-normally ordered operators

$$\mathrm{Tr}\left[\hat{\rho}\hat{a}^m\hat{a}^{\dagger n}\right] = \int_{-\infty}^{+\infty} \alpha^m, \alpha^{*n}\,\mathcal{Q}(\alpha)d^2\alpha. \tag{III.38}$$

III.2.2 Quantum states of light

In this subsection, we present the definition of coherent, thermal, and squeezed vacuum states. Then, we classify the states according to their properties, as classical and non-classical states, and further, we classify non-classical states into Gaussian and non-Gaussian states.

Coherent state

The coherent state $|\alpha\rangle$ can be defined as displaced vacuum state $|0\rangle$,

$$|\alpha\rangle = \exp\left(\alpha\hat{a}^\dagger - \alpha^*\hat{a}\right)|0\rangle\,, \tag{III.39}$$

where α is a complex number representing the displacement amplitude. In Fock notation, a quantum coherent state can be expressed as

$$|\alpha\rangle = \exp\left(-\frac{1}{2}|\alpha|^2\right)\sum_{n=0}^{\infty}\frac{\alpha^n}{\sqrt{n!}}\,|n\rangle\,. \tag{III.40}$$

If follows from (III.40) that a coherent state has Poissonian photon statistics (an example is shown in the figure III.1(a)),

$$p_n = |\,\langle n|\alpha\rangle\,|^2 = \frac{|\alpha|^{2n}}{n!}\exp\left(-|\alpha|^2\right). \tag{III.41}$$

Quantum coherent states are eigenstates of the annihilation operator $\hat{a}$

$$\hat{a}\,|\alpha\rangle = \alpha\,|\alpha\rangle\,. \tag{III.42}$$

This results in the minimum uncertainty in position and momentum, so they saturate the Heisenberg uncertainty principle [50]. The variance in the position and momentum quadratures of a coherent state is minimized and equal to $\frac{1}{2}$.

The best approximation of coherent state in quantum optics can be generated using laser light [51].

The Wigner function of the coherent state is

$$W_\alpha(x,p) = \frac{1}{\pi}\exp\left(-(x-x_0)^2-(p-p_0)^2\right), \tag{III.43}$$

which corresponds to a Gaussian distribution, with mean values x_0 and p_0.

The P-function of the coherent state is

$$\begin{aligned} P_\alpha(\alpha) &= \frac{1}{\pi^2}e^{|\alpha|^2-|\alpha_0|^2}\int_{-\infty}^{+\infty}\int_{-\infty}^{+\infty}\exp\left[-\beta(\alpha^*-\alpha_0^*)+\beta^*(\alpha-\alpha_0)\right]d^2\beta, \\ &= \delta^{(2)}(\alpha-\alpha_0), \end{aligned} \tag{III.44}$$

i.e., a two-dimensional delta function.

The $\mathcal{Q}$-function of the coherent state is

$$\mathcal{Q}_\alpha(\alpha) = \frac{1}{\pi}e^{-|\alpha-\beta|^2}, \tag{III.45}$$

which is a Gaussian distribution in α centered on β, of unit variance.

Thermal state

A general quantum thermal state is a type of quantum state that represents a system in thermal equilibrium with a heat bath. Since they are mixed states, thermal states are described by a density operator. The density operator for a quantum thermal state is given by the Gibbs canonical ensemble

$$\hat{\rho}_{Th} = \frac{\exp\left(-\beta\hat{H}\right)}{\mathrm{Tr}\left(\exp\left(-\beta\hat{H}\right)\right)}. \tag{III.46}$$

Here $\hat{H}$ is the Hamiltonian of the system, $\beta = \frac{1}{k_B T}$, where k_B is the Boltzmann constant, and T is the temperature of the system. In the Fock representation, the state can be expressed as

$$\hat{\rho}_{Th} = \sum_{n=0}^{\infty} p_n(n)\left|n\right\rangle\left\langle n\right|, \tag{III.47}$$

where $p_n(n)$ is the probability of finding n photons in a certain mode of the thermal state and can be expressed for a single mode as

$$p_n(n) = \frac{\langle \hat{n} \rangle^n}{(1 + \langle \hat{n} \rangle)^{n+1}}. \tag{III.48}$$

$p_n(n)$ has the form of a Bose-Einstein distribution (see the figure III.1(b)) and $\langle \hat{n} \rangle = \frac{1}{e^{\beta}-1}$. The state with the highest probability is always the vacuum state.

As the temperature increases, more energy levels are populated with higher probability, leading to a broader distribution. Consequently, the variance in observables, reflecting the spread of possible outcomes, tends to increase with temperature

$$\Delta x^2 = \Delta p^2 = \langle \hat{n} \rangle + \frac{1}{2}, \tag{III.49}$$

and variance of photon number operator $\hat{n}$

$$\Delta n^2 = \langle \hat{n} \rangle (1 + \langle \hat{n} \rangle). \tag{III.50}$$

The Wigner function of the thermal state is

$$W_T(x, p) = \frac{1}{\pi(2\bar{n} + 1)} \exp\left(-\frac{x^2 + p^2}{2\bar{n} + 1} \right), \tag{III.51}$$

where $\bar{n}$ is average photon number.

The P-function of the thermal state is

$$P_T(x, p) = \frac{1}{2\pi\bar{n}} \exp\left(-\frac{x^2 + p^2}{2\bar{n}} \right). \tag{III.52}$$

The $\mathcal{Q}$-function of the thermal state is

$$\mathcal{Q}_T(x, p) = \frac{1}{\pi(2\bar{n} + 2)} \exp\left(-\frac{x^2 + p^2}{2\bar{n} + 2} \right). \tag{III.53}$$

Quantum thermal states are associated with maximum entropy for a given average energy. This is a manifestation of the principle of maximum entropy in statistical mechanics. They find applications in various fields, including condensed matter physics, quantum information theory, and quantum optics. Experimental realization and manipulation of quantum thermal states are essential for studying the thermal properties of quantum systems in different physical platforms.

Squeezed state

Quantum squeezed states are nonclassical states of light that exhibit reduced uncertainty in one of the complementary observables, such as position and momentum. If the variance in at least one of the quadratures ($\hat{\tilde{x}}(\phi)$, $\hat{\tilde{p}}(\phi)$) is smaller than the vacuum variance, it is a squeezed state. $\hat{\tilde{x}}(\phi)$ and $\hat{\tilde{p}}(\phi)$ are generally rotated quadratures

$$\hat{\tilde{x}}(\phi) = \cos(\phi)\hat{x} + \sin(\phi)\hat{p}, \tag{III.54}$$

$$\hat{\tilde{p}}(\phi) = -\sin(\phi)\hat{x} + \cos(\phi)\hat{p}. \tag{III.55}$$

The squeezed states play a crucial role in quantum optics and quantum information processing due to their unique properties, which can be quantified using the concept of squeezing.

A typical squeezed state $|\psi\rangle$ is created by applying a squeezing operator $\hat{S}(\zeta)$ to the vacuum state $|0\rangle$

$$\begin{aligned} |\psi(\zeta)\rangle &= \hat{S}(\zeta)\,|0\rangle\,, \\ &= \exp\left(\frac{\zeta}{2}(\hat{a}^2 - \hat{a}^{\dagger 2})\right)|0\rangle\,, \end{aligned} \tag{III.56}$$

where ζ is the squeezing parameter. From this definition of the squeezing parameter, we can see this operation preserves state parity. Thus, the photon statistics after squeezing look as follows: for even states, the photon statistics have only even contributions, and for odd states, again, odd contributions. For example, the squeezed vacuum in the Fock representation reads

$$|\psi(\zeta)\rangle_{|0\rangle} = \frac{1}{\sqrt{\cosh(\zeta)}} \sum_{n=0}^{\infty} \frac{\sqrt{(2n)!}}{n!2^n} \left(\tanh(\zeta)\right)^n |2n\rangle\,, \tag{III.57}$$

where $\frac{1}{\sqrt{\cosh(\zeta)}} \sum_{n=0}^{\infty} \frac{\sqrt{(2n)!}}{n!2^n} \left(\tanh(\zeta)\right)^n$ is photon distribution (see the figure III.1(c)).

The variance of the squeezed quadrature is given by

$$\Delta x^2 = \frac{1}{2}\exp(-2\zeta), \tag{III.58}$$

$$\Delta p^2 = \frac{1}{2}\exp(2\zeta). \tag{III.59}$$

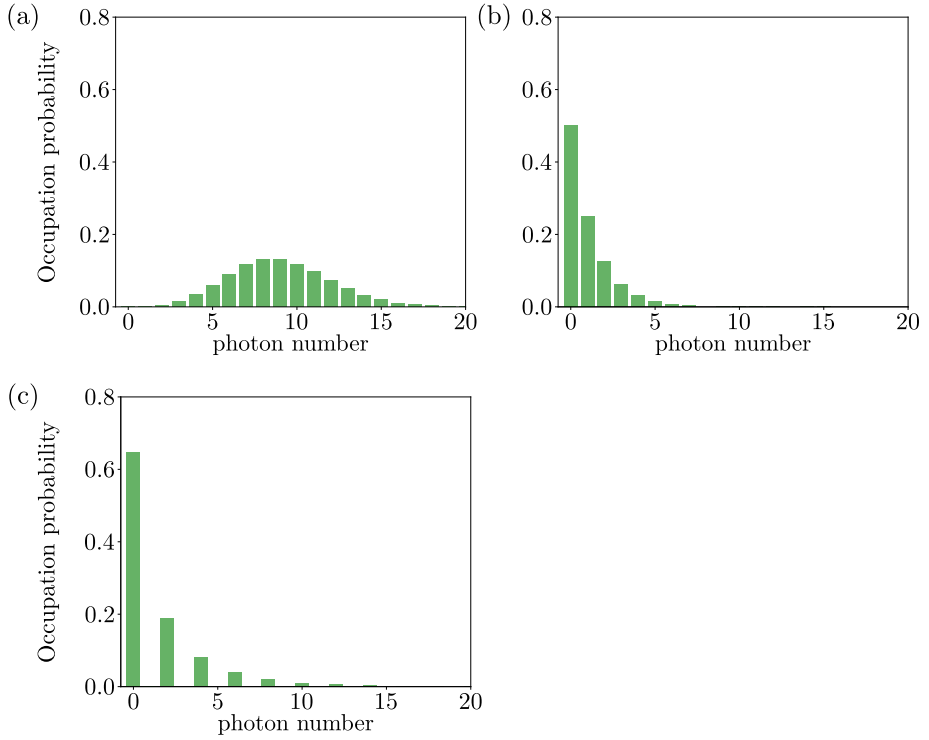

Figure III.1: Photon statistics of (a) the coherent state ($\alpha = 3$), (b) the thermal state ($\langle \hat{n} \rangle = 1$) and (c) squeezed vacuum state (III.56) ($\zeta = 1$).

The Wigner function of the squeezed vacuum state is

$$W_S(x,p) = \frac{1}{\pi} \exp\left(-e^{2\zeta}x^2 - e^{-2\zeta}p^2\right), \tag{III.60}$$

where ζ is the squeezing parameter.

The P-function of the squeezed vacuum state is

$$P_S(\alpha) = \exp\left[-\frac{(V_x - V_p)}{8}\right]\left\{\frac{\partial^2}{\partial\alpha^2} + \frac{\partial^2}{\partial\alpha^{*2}} - 2\left[\frac{V_x + V_p - 2}{V_x - V_p}\right]\frac{\partial}{\partial\alpha}\frac{\partial}{\partial\alpha^*}\right\}, \tag{III.61}$$

where V_x and V_p are variances of quadratures.

The $\mathcal{Q}$-function of the squeezed vacuum state is

$$\mathcal{Q}_S(\alpha) = \frac{\text{sech}(\zeta)}{\pi} \exp[-|\alpha|^2 + (\alpha^* + \alpha)\text{sech}(\zeta) - \frac{\tanh(\zeta)}{2}\left(e^{i\theta}\alpha^{*2} + e^{-i\theta}\alpha^2\right)]. \tag{III.62}$$

Experimental generation of quantum squeezed states often involves nonlinear optical processes [52]. One common method is the parametric down-conversion in a nonlinear crystal [53–55], where a pump photon is split into two photons, creating a squeezed state. Another technique involves using an optical cavity with a nonlinear medium, where the Kerr nonlinearity induces squeezing [23].

These experimental setups are designed to manipulate the quantum state of light and achieve the desired squeezing. Measurement of the resulting state typically involves homodyne or double-homodyne detection to characterize the squeezing in the relevant quadratures [12, 53].

Quantum squeezed states find applications in quantum communication [1–4], quantum metrology [7], and quantum information processing [8, 56], where the reduction of uncertainty in specific observables can enhance precision and sensitivity in measurements beyond classical limits.

III.3 Distinguishing "classical" and "non-classical" quantum states

In this section, we deal with the division of quantum light states into two large classes, namely classical and non-classical quantum states, in relation to the values of the P-function.

III.3.1 Classical states

As classical states, we denote states with non-negative P-functions, i.e., states that are either coherent or can be expressed as mixtures of coherent states.

A typical example of a mixed classical state is the thermal state, which can be constructed as a mixture of coherent states with Gaussian distribution centered at the origin.

III.3.2 Non-classical states

The second class of states is the class of non-classical states [57–60]. If we start from the properties associated with the P-function, they are states with a negative P-function in some region in the phase space, or their P-function is more singular than the delta function. We will further divide this class into subclasses according to the shape of the quasi-probability distribution into quantum Gaussian [12, 61] and non-Gaussian states [60, 62].

Gaussian states

Gaussian states are described by the Wigner function in the form of a Gaussian function (this property is based on the characteristic function). At the same time, it is possible to fully describe these states with only the first two moments

$$\mu = \begin{pmatrix} \langle \hat{x} \rangle \\ \langle \hat{p} \rangle \end{pmatrix}, \tag{III.63}$$

$$\Sigma = \begin{pmatrix} \langle \hat{\hat{x}}^2 \rangle & \frac{1}{2}\langle \hat{\hat{x}}\hat{\hat{p}} + \hat{\hat{p}}\hat{\hat{x}} \rangle \\ \frac{1}{2}\langle \hat{\hat{x}}\hat{\hat{p}} + \hat{\hat{p}}\hat{\hat{x}} \rangle & \langle \hat{\hat{p}}^2 \rangle \end{pmatrix}; \hat{\hat{x}} = \hat{x} - \bar{x}, \hat{\hat{p}} = \hat{p} - \bar{p}. \tag{III.64}$$

Higher moments are composed of a combination of only the first two moments. We start with a vacuum state, that is a classical Gaussian state, and then we can create any Gaussian state, even a non-classical one, just by using Gaussian operations. Gaussian operations are operations preserving the Gaussianity of the state:

- Displacement ... $\hat{D}(\alpha) = \exp\left(\alpha \hat{a}^\dagger - \alpha^* \hat{a}\right)$
- Linear squeezing ... $\hat{S}(\zeta) = \exp\left(\frac{\zeta}{2}(\hat{a}^2 - \hat{a}^{\dagger 2})\right)$
- Phase shift ... $\hat{R}(\phi) = \exp\left(i\phi\hat{n}\right)$

In general, the Wigner function of any Gaussian state can be written in this form (for one mode)

$$W_{\boldsymbol{X},\Sigma}(\boldsymbol{Y}) = \frac{1}{(2\pi)} \exp\left(\frac{1}{2}\left(\boldsymbol{Y} - \boldsymbol{X}\right)^T \Sigma^{-1} \left(\boldsymbol{Y} - \boldsymbol{X}\right)\right), \tag{III.65}$$

where Σ is the covariance matrix and $\mathbf{X} = \left(\langle \hat{x} \rangle, \langle \hat{p} \rangle\right)^T$ (vector of mean values).

By squeezing operation, it is possible to generate non-classical states from classical ones; other Gaussian operations do not have this property. A squeezed state cannot be written as a mixture of coherent states.

Non-Gaussian states

While Gaussian distributions dominate classical statistics, quantum non-Gaussian states are much more diverse. Wigner functions of these states deviate from the Gaussian form and can read negative values. Non-Gaussianity, as such, is a witness of higher-order nonlinearities. There are many ways to achieve non-Gaussian states from Gaussian states, such as conditional measurement and nonlinear optical processes. In the following chapters, we use a non-linear optical process called Kerr nonlinearity to generate Non-gaussian states.

The Kerr nonlinearity is an operation that can be used in several different ways to generate different states, such as cat states, cubically squeezed states, and or quartic squeezed states. It is a non-linear process where the phase of the state evolves proportionally to the intensity. We further divide this nonlinear phenomenon into two specific cases, namely the case where the mode itself affects the phase change in the nonlinear system - self-Kerr

$$\hat{H}_{Kerr_s} = \chi \hat{n}^2, \tag{III.66}$$

or the case where two modes influence each other, and this case is called cross-Kerr

$$\hat{H}_{Kerr_c} = \chi \hat{n}_1 \hat{n}_2. \tag{III.67}$$

In both cases, the χ parameter symbolizes the strength of the nonlinear interaction.

Kerr nonlinearity is, of course, one of the non-Gaussian operations that can be realized experimentally across many platforms, such as in electromagnetically induced transparency [63–65], Bose-Einstein condensates of interacting atoms [66], cold atoms [67], Josephson junctions [68, 69], and even light in resonators [70, 71],

Chapter IV

Heat machine based on Kerr nonlinearities

This chapter is based on results published in the article [72]. All images found in this chapter are taken from the article [72]. A more detailed description and derivation of formulas are in Appendix A.

IV.1 Motivation

A heat engine may be viewed as a device that concentrates energy from several degrees of freedom (modes) into a single one in a selected degree of freedom called the working mode. For example, a combustion engine concentrates the energy of $\sim 10^{30}$ motional modes of individual molecules into the single mode of moving piston. This happens within the limits given by the laws of thermodynamics:

- The first law — whereby the working-mode energy cannot exceed the total energy of all the input modes.

- The second law — whereby the input energy cannot be entirely concentrated in the working mode: part of it must spill over to initially colder modes that contain, on average, less energy than the thermal mean.

The enormous ($\sim 10^{30}$) number of hot and cold modes involved in heat machines (HM) justifies the adoption of their thermodynamic (TD) description: HM are open systems wherein hot and cold baths couple to a working medium (WM) or heat-controlling device [73–75]. Accordingly, HM must be dissipative (a thermodynamically open system operating out of, and often far from, thermodynamic equilibrium in an environment with which it exchanges energy and matter). This paradigm underlies HM also in the quantum domain [76–78], notwithstanding the effects of quantum coherence or entanglement on their operation [79–86]. The "smallest" (or minimal) heat engines in the quantum domain have thus far been defined as those having the fewest degrees of freedom in the working medium (WM): a single qubit [86–88] or two coupled qubits [89], a single atom or molecule [82, 90, 91], but their hot and cold baths have been invariably comprised of mode continua that give rise to destruction of coherences in the WM (unless external control prevents this destruction [80, 92]).

In our work, we introduce the concept of a purely coherent, autonomous, closed-system HE, using nonlinear coupling of thermal, continuous-variable, bosonic field modes. This makes these devices fundamentally different from existing HE that is energized by macroscopic baths composed of linearly coupled oscillator modes [75, 76, 87, 93–95]. The Kerr nonlinearities are non-Gaussian operations (NGOs) that have been conceived in quantum optical and quantum information schemes [96, 97] but are mostly least used in the context of HE, with few exceptions [98, 99].

The envisaged NGO can achieve both HE functionalities:

1. Concentrate the energy of a heat bath in a selected degree of freedom called the working mode, within limits dictated by the first and second laws of thermodynamics.

2. The concentrated heat must be partly converted into work output, which requires the state of the working mode to store energy in a nonpassive form[1].

Thanks to their nonlinearity, they can cause output field modes to constructively or destructively interfere despite the randomness of the input phase. These NGOs cause information flow among the modes, resulting in autonomous feed-forward of the information instead of externally controlled HE [76, 93, 94, 101, 102]. In contrast, linear Gaussian operations (LIGOs) cannot perform this feat. In quantum optics, LIGOs encompass all energy-conserving linear interference operations caused by beam splitters (BSs) and phase shifters. In contrast, squeezing is neither linear nor energy conserving, but it is a Gaussian operation whose effect on HEs has been studied in [85, 103, 104].

The proposed machines are dubbed here as nonlinear interferometric heat machines (NIHM). NIHMs lie beyond the present scope of the resource theory of quantum thermodynamics [105–108] based on LIGO, which relies on energy-preserving joint unitaries performed on quantum systems and their thermal bath ancillae.

IV.2 NIHM principle

Consider a multiport linear interferometer with m input modes and m output modes that contain only (energy-conserving and therefore passive) linear mode couplers or beam splitters (figure IV.1(a)). If the input is a multimode factorized coherent state $|\beta_1\rangle |\beta_2\rangle \dots |\beta_m\rangle$ one can find parameters of the interferometer such that there is a coherent state $|\alpha\rangle$ in one output mode, all the remaining output modes are empty. Such an idealized scenario would achieve full energy concentration.

If, however, the input is thermal noise, which can be treated as a mixture of coherent states $|\beta_1\rangle |\beta_2\rangle \dots |\beta_m\rangle$ with random amplitudes of β_1, β_2, …,β_m that have Gaussian distributions with zero mean, then neither of the heat engine

[1] A quantum state is nonpassive [100] if there exists at least one unitary operation that can extract work from it. Nonpassive states are essential in quantum thermodynamics because they represent resources from which work can be extracted, similar to how a charged battery can do work in classical thermodynamics.

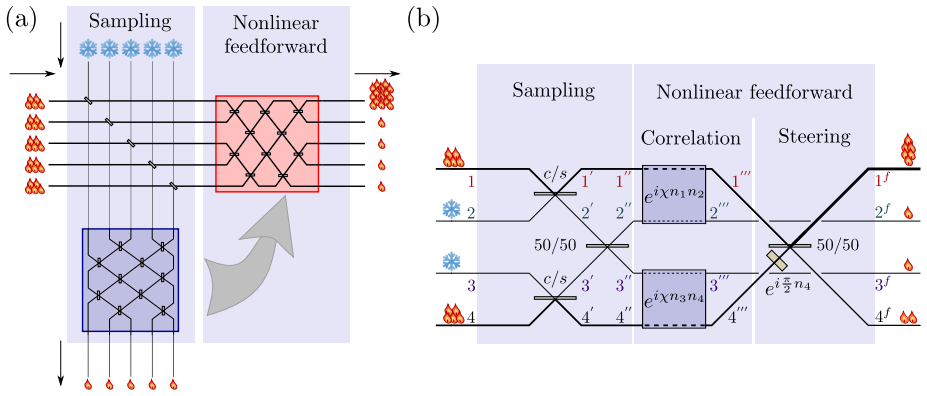

Figure IV.1: (a) (i)A fraction of the energy of the hot modes is split off by BSs (in the bottom blue box) to carry information about the remaining hot modes(in the right red box). (ii) Nonlinear interactions correlate these two boxes and autonomously feedforward the information such that (iii) the output fields can be steered to interfere constructively in one preselected mode. (b) A four-mode NIHM in which the input modes (1 and 4, hot; 2 and 3, cold) undergo the aforesaid stages. For optimal parameter choice, the interference is predominantly constructive in mode 1^f and destructive in mode 4^f.

functionalities is then achievable via linear interferometric network [109, 110], as the thermal randomness prevents selected-mode amplification or heat-to-work conversion [111, 112].

However, if we could estimate the magnitudes and phases of $|\beta_1\rangle\,|\beta_2\rangle\ldots|\beta_m\rangle$ and feedforward the results for each realization of the random input, we would be able to choose the interferometer parameters such that the energy is mostly concentrated in nonpassive form in one mode (a quantum state is nonpassive if there exists at least one unitary operation that can extract work from it, nonpassive states have populations that are not ordered in a way that maximizes entropy, meaning they are not in thermal equilibrium). Instead of conventional measurements that can provide this information nearly perfectly [95], we show that it is possible to partially estimate and forward them autonomously by nonlinear intermode coupling, which is inevitably NGO. Note that, according to the Second law of thermodynamics, this feat cannot be achieved at all if all the input modes are in the same thermal state. Some of the inputs have to be colder than others, forming distinct cold and hot few-mode baths.

The general m-mode NIHM protocol consists of two major stages (figure IV.1(a)):

1. Sampling: A fraction of each hot input field mode is split off and mixed with a corresponding cold field mode by imbalanced BS. The cold-mode states then become weak copies of the respective hot-mode states. These $m/2$ weak copies are pairwise mixed by a 50/50 merger. These LIGOs "sample" the random distribution of the input modes: The "sampled" phase differences are encoded by the intensity mixing ratio of the weak-copy outputs.

2. Nonlinear feedforward: Subsequently, these weak-copy outputs are nonlinearly cross-correlated by NGO (here, nonlinear cross-Kerr coupling) with the dominant hot-mode fractions. Since the cross-Kerr Hamiltonian commutes with the bare Hamiltonian of the hot and cold modes, it does not require energy investment, nor does it require external control, so that NIHM is a self-contained (autonomous) heat-to-work converter. An additional m-mode basis rotation and phase shifting exploit this autonomous nonlinear feedforward of the sampling to steer the energy mainly to the desired mode. The output distributions become nonthermal (non-Gaussian).

The minimal version of NIHM (figure IV.1(b)) contains two hot and two cold input modes, for simplicity, at the same frequency (nondegenerate mode analysis is laborious and does not reveal essentially new insights). The coherence length of this interferometer should be much longer than its spatial size so that temporal evolution can be replaced by discrete steps, each described by a unitary evolution operator. We analyze the autonomous feedforward of the a priori unknown amplitudes of the hot modes 1 and 4 and their steering that maximize the energy and work capacity (ergotropy or nonpassivity) [83, 85, 100, 113] of mode 1 at the output:

1. At the sampling stage, the first BS, with low transmissivity $s = \sin(\theta) \ll 1$ (high reflectivity $c = \cos(\theta) \lesssim 1$), causes small fractions of the hot input modes 1 and 4 to split off and merge, respectively, with the empty modes 2 and 3, so that we have weak copies $2'$ and $3'$ of 1 and 4, respectively. For each coherent-state realization, these weak copies have the same phase difference ϕ as the input modes 1 and 4 and mean intensity difference proportional to the mean quanta number difference n_-. The weak copies then merge on a 50/50 BS whose output modes are $2''$ and $3''$. The correlations generated between n_- and ψ are quantified by the mutual

information [114]. At the output of the 50/50 merger, modes $2''$ and $3''$ become correlated. Their correlation encodes (samples) n_- of modes 1 and 4. Consequently, in the weak copies, the n_- distribution broadens (increases its entropy), while the ϕ distribution is still uniform.

2. At the nonlinear feedforward stage, two cross-Kerr couplers cause, in the classical approximation [115], the phase difference of the hot modes $1''$ and $4''$ to be shifted proportionally to the intensity difference of modes $2''$ and $3''$, respectively, so that $\phi \to \phi + \chi n''_-$, where χ is the nonlinear phase shift. For each set of coherent-state amplitudes in the thermal input distribution, $|\alpha_1\rangle$, $|0_2\rangle$, $|0_3\rangle$, $|\alpha_4 e^{i\phi}\rangle$, the coherent states in the strong-fraction hot modes $1'''$ and $4'''$ then become, after the cross-Kerr couplers (for more details of the calculation see Appendix A, section A.2)

$$|\alpha_1'''\rangle = \left| c\alpha_1 \exp\left(i\chi \frac{s^2}{2} |\alpha_1 + \alpha_4 e^{i\phi}|^2 \right) \right\rangle \tag{IV.1}$$

$$|\alpha_4'''\rangle = \left| c\alpha_4 \exp\left(i\chi \frac{s^2}{2} |\alpha_1 - \alpha_4 e^{i\phi}|^2 + \phi \right) \right\rangle \tag{IV.2}$$

3. At the steering stage, the final 50/50 BS, preceded by a $\frac{\pi}{2}$ shift of mode $4'''$, yields at the two outputs the coherent-state amplitudes

$$\alpha_{1,4}^f = \frac{1}{\sqrt{2}} \left(\alpha_1''' \pm \alpha_4''' \right), \tag{IV.3}$$

which determines the output intensities

$$|\alpha_{1,4}^f|^2 = \frac{c^2}{2} \left[\alpha_1^2 + \alpha_4^2 \pm 2\alpha_1\alpha_4 \sin\left(2s^2\alpha_1\alpha_4\chi\cos(\phi) - \phi \right) \right]. \tag{IV.4}$$

This nonsinusoidal dependence of the interference term on the phase difference ϕ of the input fields stems from the nonlinear coupling.

The mean intensities at the output of the final 50/50 BS in the strong-fraction hot modes are found to be, after averaging over the coherent inputs we get,

$$\bar{n}_{1,4}^f = c^2\bar{n} \left[1 \pm \frac{s^2\chi\bar{n}}{(1 + s^4\chi^2\bar{n}^2)^2} \right], \tag{IV.5}$$

where $\bar{n}$ (for thermal states) is equals temperature in the hot modes 1 and 4.

IV.3 Full density matrix description

It should be noted that the analytical approach includes the computation of the entire scheme with coherent states, and the final step is averaging over a Gaussian distribution of coherent states with a random phase (at the input) to obtain a result for the thermal states. It is more difficult to calculate the higher moments, and the calculation of the first two moments, i.e., the mean value of the number of photons and the variance, was carried out (see Appendix A for more details).

A full quantum description is obtained by applying unitary operators to the input quantum state. Full photon statistics can be obtained in this way. Of course, this procedure also has its pitfalls; it is a numerical procedure, and thus, we run into computational complexity since it is a four-mode scheme.

We start with a density matrix

$$\hat{\rho}_0 = \hat{\rho}^{(T)} \otimes \hat{\rho}^{(0)} \otimes \hat{\rho}^{(0)} \otimes \hat{\rho}^{(T)}, \tag{IV.6}$$

where $\hat{\rho}^{(T)}$ is a single-mode thermal state of temperature T, and $\hat{\rho}^{(0)}$ is single-mode vacuum state (empty mode). The output state is $\hat{\rho}_f = \hat{U}\hat{\rho}_0\hat{U}^\dagger$, where

$$\hat{U} = \hat{U}_5\left(\frac{\pi}{2}\right)\hat{U}_4(\chi)\hat{U}_3\left(\frac{\pi}{2}\right)\hat{U}_2\left(\frac{\pi}{2}\right)\hat{U}_1(\theta). \tag{IV.7}$$

The unitary operator

$$\hat{U}_1(\theta) = \exp\left(i\hat{J}_x^{(1,2)}\theta\right) \otimes \exp\left(i\hat{J}_x^{(3,4)}\theta\right) \tag{IV.8}$$

is the first BS operation coupling mode 1 with 2 and 3 with 4, where

$$\hat{J}_x^{(k,l)} = \left(\frac{1}{2}\left[\hat{a}_k^\dagger\hat{a}_l + \hat{a}_k\hat{a}_l^\dagger\right]\right). \tag{IV.9}$$

$\hat{U}_2(\frac{\pi}{2}) = \exp\left(i\hat{J}_x^{(2,3)}\frac{\pi}{2}\right)$ describes the first 50-50 BS operator coupling modes 2 and 4. $\hat{U}_3(\frac{\pi}{2}) = \exp\left(i\frac{\pi}{2}\hat{n}_4\right)$ is the $\pi/2$ phase shifter in mode 4,

$$\hat{U}_4(\chi) = \exp(i\chi\hat{n}_1\hat{n}_2) \otimes \exp(i\chi\hat{n}_3\hat{n}_4) \tag{IV.10}$$

describes the cross-Kerr couplers between modes 1 and 2 and modes 3 and 4, and $\hat{U}_5(\frac{\pi}{2}) = \exp\left(i\frac{\pi}{2}\hat{J}_x^{(1,4)}\right)$ is the last 50-50 BS operator coupling modes 1 and 4.

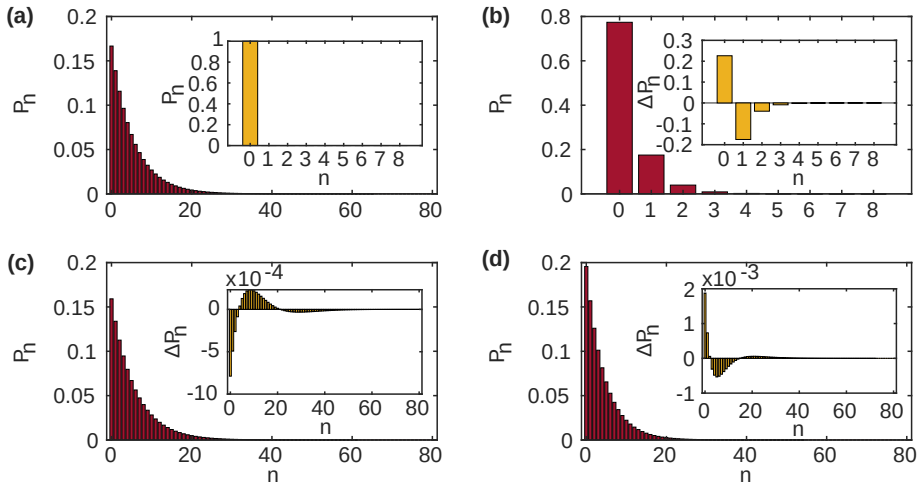

Figure IV.2: Results of numerical calculations with the full entangled density matrix, input thermal state with $\bar{n} = 5$. The Hilbert space is truncated at $n = 80$ for the hot modes and $n = 8$ for the cold modes. The total dimensionality is thus $81 \times 81 \times 9 \times 9 = 531,441$. The figures show photon number distributions in individual modes. (a) Red - input hot mode (1 and 4 in the figure IV.1(b)); yellow - input vacuum mode (2 and 3 in the figure IV.1(b)); (b) red - "waste" output modes 2^f and 3^f (originally input vacuum mode); yellow - the difference between photon number distribution of the "waste" output mode 2^f and a thermal state with the same mean photon number; (c) Red - "working" output mode 1^f; yellow - the difference between photon number distribution of the "working" output 1^f mode and a thermal state with the same mean photon number; (d) red - "waste" output mode 4^f (originally input thermal mode); yellow - difference between photon number distribution of the "waste" output mode 4^f and a thermal state with the same mean photon number.

Independently of the analytical calculations, the optimization task of the entire scheme was performed so that the energy was concentrated in the first output mode. The free parameters in the optimization were θ in equation (IV.8) and the strength of nonlinear interaction χ in equation (IV.10). Sequential quadratic programming was used as the optimization method. First, however, the parameter θ in equation (IV.8) was divided into θ_1 and θ_2 – $\hat{U}_1(\theta_1, \theta_2) =$

$\exp\left(i\hat{J}_x^{(1,2)}\theta_1\right)\otimes\exp\left(i\hat{J}_x^{(3,4)}\theta_2\right)$, but due to the use of a symmetrical input, i.e., all warm modes have the same mean energy, and similarly for the cold modes, so there is no reason to have a different dividing ratio at of these BSs; therefore the parameters were subsequently unified into one.

Due to the numerical complexity, it was necessary to write a library of functions that stored as little data as possible and only the really necessary information, due to the occupancy of the RAM memory and also by reducing the amount of data with which the optimizations had to be performed. For this reason, it was not possible to use the *qutip* library in Python fully, but only with a limited number of functions. A library of functions written for a 4-mode heat engine (*power*) is included on GitHub [116].

Since the Hilbert space of a four-mode state is rather large, the numerical calculation of NIHM unitary operation was truncated at $n = 80$ for the hot modes and $n = 8$ for the cold modes, the total Hilbert space dimension being $81 \times 81 \times 9 \times 9 = 531,441$ (the probability distributions of the output modes are shown in figure IV.2, where it can be seen that the 1^f output mode no longer has the photon statistics of a thermal state), consequently, individual density matrices or unitary operators have dimension $531,441 \times 531,441$. therefore, it was necessary to use sparse matrices. However, we can only use this for weak thermal states; if we wanted to perform numerical simulations for thermal states where $\bar{n}$ corresponds to 10 or more, the dimensions would have to be beyond the capacity of the computational resources available to us.

IV.4 Cascading

One can concentrate the energy to higher values by cascading the scheme as in shown figure IV.3. In a sense, it can be viewed as an analogy to the cycles of a heat engine. In each stage, the mean energy is higher, and the relative fluctuation is smaller than in the preceding one. We explored whether this can lead to a non-monotonous photodistribution indicating a (single-mode) non-passive state [113, 117]. Since we have analytical formulas only for the first two moments of the photodistribution and the full density matrix calculation would be impossible due to the large Hilbert space, the following approximation has been used. Knowing the first two moments, one takes the most conservative approach and, according to the Jaynes principle [118], chooses the photodistribution of the highest entropy that corresponds to these moments. This leads to a quadratically exponential distribution $p_n \approx \exp(\lambda_1 n + \lambda_2 n^2)$ with $\lambda_{1,2}$ Lagrange multiplicators that follow from the two known moments. One then finds

numerically the Glauber-Sudarshan distribution corresponding to this photodistribution and uses it to calculate the first two moments in the next stage. In this way, the photodistribution of eight cascades has been calculated in figure IV.3. As can be seen, starting from about the fourth cascade, the photodistribution is nonmonotonous. Notice, however, that the interferometer parameters χ and s are optimized to maximize $\bar{n}-\Delta n$ (i.e., the nonmonotonicity) and not just $\bar{n}$.

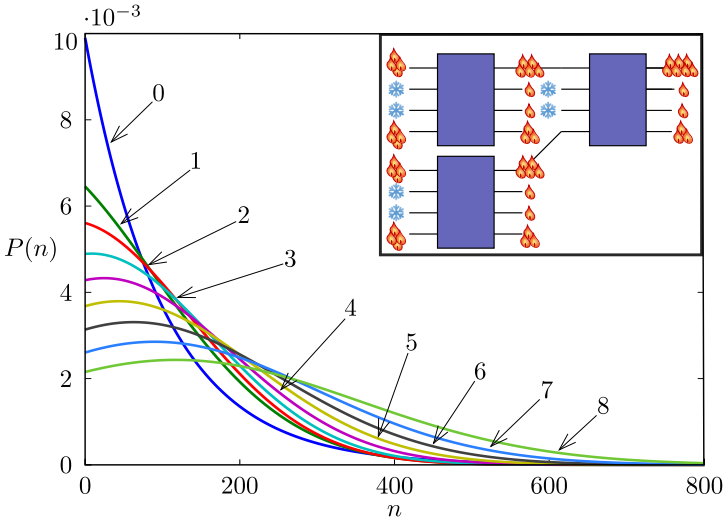

Figure IV.3: Photodistribution in the highest energy outputs in eight subsequent cascades. Cascading the scheme: the highest temperature outputs of each stage are used as the hot inputs of the next stage, thus gradually increasing the mean energy of a preselected mode to arbitrarily high values.

IV.5 Conclusion

Nonlinear interferometric networks have been proposed in our work as heat engines via nonlinear interferometry−NIHM. Conceptually, they allow us to treat baths as dynamical systems, in contrast to existing classical and quantum heat engines, for which the working-medium-bath exchange has not yet been described as a coherent process. Such a description is indeed unfeasible for

infinite/macroscopic baths, but we consider only a few-mode "baths". Notwithstanding its coherent-nonlinear nature, NIHM adheres to the second law and acts as a genuine heat machine cycle, albeit only a few modes are involved in the operation.

The minimal version of the NIHM−4-mode cross-Kerr coupled network has been analyzed to illustrate the operation principles. These nonlinearly coupled modes replace both the working medium and the piston (working mode), so NIHM is conceptually much simpler than a traditional heat engine.

On the applied side, (a) NIHM practical value is their ability to interfere and thereby concentrate energy from independent heat channels. This feat is impossible in conventional heat devices whose heat channels do not interfere. (b) The cascading process depicted here (figure IV.3) may pave the way to manipulating and enhancing the information hidden in noisy input via controllable nonlinear operations. This perspective is based on the fact that NIHM bears an analogy to a quantum computer with continuous variables [19], if inter-mode quantum correlations are accounted for, or to a semiclassical optical computer if they are neglected. (c) The feasibility of NIHM for few-photon or few-phonon input may add impetus to the creation of quantum nonlinear interference devices [19, 119–123].

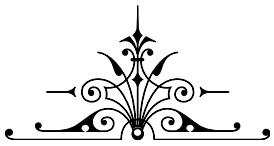

Chapter V

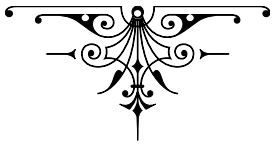

Generation of Non-Gaussian states

In this chapter, we show how the Kerr nonlinearity can be straightforwardly used for generating quantum states with the cubic and quartic nonlinear squeezing [23]. Such states are the required resource for the deterministic implementation of the quadrature phase gates and the quantum nonlinear measurements. All images found in this chapter are taken from the article [23].

V.1 Motivation

The unitary operation with the lowest order of nonlinearity sufficient for the universal quantum information processing is the cubic phase gate [11, 124]. In some systems, the gate can be implemented by direct dynamical control of the system's parameters [15, 18, 125], but it can be universally realized through a measurement-induced scheme [126–129] with the help of suitably prepared ancillary states.

The key property of the required ancillary states is the reduction of noise in the nonlinear quadrature corresponding to the cubic operation. The quantum states exhibiting such nonlinear squeezing are nonclassical and must be prepared by specifically tailored techniques. This can be accomplished for the continuous-variables (CV) traveling light by preparing specific superpositions of photon number states using suitable projections by single photon detectors [130, 131]. Other physical systems, such as the optomechanical systems [132], the microwave resonators [15], or the trapped ion systems [125, 133], can take advantage of the ability to dynamically control the coupling between the CV system and the ancillary mode. It is also possible to take advantage of the high-order nonlinearity that already exists in the physical system, such as suitably transforming quantum states produced by the three-photon downconversion [134]. Another prominent kind of nonlinearity intensively pursued on a broad range of physical platforms is the Kerr nonlinearity, which shifts the phase of the state proportionally to the energy. It is a non-Gaussian operation with broad applications in quantum logic [135–138], quantum teleportation [139–141], or quantum non-demolition measurements [142, 143]. The Kerr operation was already considered for a preparation of highly nonclassical superposed coherent states [144] and, together with the Gaussian operations, they can be employed for an incremental realization of the nonlinear operations of the third order [19]. It is, therefore, no surprise that it is being intensively studied across many scenarios, such as in electromagnetically induced transparency [63–65, 145], Bose-Einstein condensates [146], cold atoms [67], Josephson junctions [68, 69, 147], even light in resonators [70, 71].

V.2 Nonlinear squeezing parameter

The main questions are how to identify state squeezing and how to measure its quality. In many cases, fidelity is used as an indicator of the quality of state preparation. For metrology, quantum computing, or quantum cryptography,

fidelity does not make that much sense since this indicator of the quality of preparation will only tell us how well our state overlaps with the target state, but it will not tell us anything about the squeezing of the state. The point is that even if we have a lower fidelity, our state may be squeezed as much as the target state and the fidelity may be low, for example, due to the misalignment. Or, on the contrary, in the opposite case, when we can get high fidelity (e.g. around 90%), while the state is not sufficiently squeezed.

For these reasons, we introduce a nonlinear squeezing parameter

$$\xi_n = \frac{\mathrm{Tr}\left[\hat{\rho}\hat{O}_n^2\right] - \mathrm{Tr}\left[\hat{\rho}\hat{O}_n\right]^2}{\min_{\hat{\rho}_G}\left(\mathrm{Tr}\left[\hat{\rho}_G\hat{O}_n^2\right] - \mathrm{Tr}\left[\hat{\rho}_G\hat{O}_n\right]^2\right)}, \tag{V.1}$$

where $\hat{O}_n$ is the operator in which the states[1] (represented by $\hat{\rho}$) are squeezed. The minimization is taken over the set of all Gaussian states (represented by $\hat{\rho}_G$). Operator $\hat{O}_n$ is normally defined through the unitary operators and the quadrature operator, but in the case of cubic and quartic squeezing in the harmonic oscillator system, it is possible to analytically express the operator $\hat{O}_n$ in the form (for x-axis)

$$\hat{O}_n = \hat{x} - \hat{p}^{n-1}, \tag{V.2}$$

and (for p-axis)

$$\hat{O}_n = \hat{p} - \hat{x}^{n-1}. \tag{V.3}$$

When $\xi < 1$ (from (V.1)) we can say the quantum state $\hat{\rho}$ has genuine nonlinear squeezing of the n-th order (for $n \geq 3$, because $n = 1$ and $n = 2$ is Gaussian squeezing (III.56), $n = 3$ for cubic squeezing and $n = 4$ for quartic squeezing).

V.3 Nonlinear squeezing by Kerr operation

We use the Kerr operation as the only source of nonlinear squeezing in our procedures; the other operations are Gaussian. We will specifically focus on the cases $\hat{H} = \hat{p}^3$ and $\hat{H} = \hat{p}^4$.

First, we begin by presenting the procedure for the deterministic generation of cubic squeezed states. Such states can be, in the idealized scenario, generated by applying a unitary cubic nonlinear operation given by Hamiltonian $\hat{H} = \hat{p}^3$

[1] with cubic and quartic nonlinear squeezing

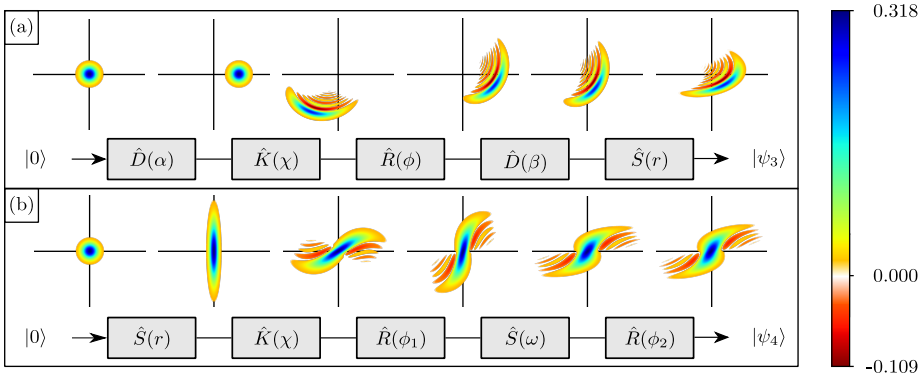

Figure V.1: A schematic depiction of using the Kerr operation together with Gaussian gates for preparation of quantum states with (a) nonlinear cubic squeezing, (b) nonlinear quartic squeezing. For better illustration, the gates are supplemented by schematic depictions of the Wigner functions of the states along different steps of the procedures, starting as the Wigner functions of vacuum states on the left and ending as the Wigner functions of the respective squeezed states on the right. The boxes represent the unitary operations displacement ($\hat{D}(\alpha)$, $\hat{D}(\beta)$), phase shift ($\hat{R}(\phi)$,$\hat{R}(\phi_1)$,$\hat{R}(\phi_2)$), Kerr nonlinearity ($\hat{K}(\chi)$), and squeezing ($\hat{S}(r)$, $\hat{S}(\omega)$).

onto a Gaussian squeezed state. We can generate them by applying Kerr nonlinearity to an initial coherent state, unitary operation of the Kerr nonlinearity has the shape

$$\hat{K}(\chi) = \exp\left[i\chi(\hat{x}^2 + \hat{p}^2)^2\right]. \tag{V.4}$$

In the generation itself, we also use other Gaussian operations, namely squeezing, displacement, and phase shift, which can be used to adjust the state after the Kerr operation. The resulting shape of the state on which the nonlinear squeezing calculation is performed has the form

$$|\psi_3(\alpha,\chi,\phi,\beta,r)\rangle = \hat{S}(r)\hat{D}(\beta)\hat{R}(\phi)\hat{K}(\chi)\hat{D}(\alpha)\,|0\rangle\,, \tag{V.5}$$

where $\hat{S}(r)$ represents squeezing (defined in (III.56)), $\hat{D}(\alpha) = \exp\left(-i\alpha\hat{p}\right)$ represents displacement in $\hat{x}$ quadrature, $\hat{K}(\chi)$ represents Kerr operation (defined in (V.4)) and $\hat{R}(\phi) = \exp\left[-\frac{i}{2}\phi\left(\hat{x}^2 + \hat{p}^2\right)\right]$ represent phase shift (the whole process is illustrated in figure V.1(a)). The nonlinear squeezing parameter (V.1)

takes the form $\xi_3(\alpha, \chi, \phi, \beta, r)$, is then a five-parameter function that can be numerically optimized to achieve the largest possible nonlinear squeezing.

In the case of quartic nonlinear squeezing, we start with a different input state than in the cubic case, namely with a linearly squeezed state. The reason is the different symmetry of the operation. Ideal cubic squeezed states are symmetric with respect to the change $\hat{p} \to -\hat{p}$, which geometrically represents symmetry with respect to one axis in phase space. Meanwhile, ideal states with quartic nonlinear squeezing have symmetry with respect to simultaneous exchange $\hat{x} \to -\hat{x}$ and $\hat{p} \to -\hat{p}$, which geometrically represent symmetry with respect to the point of origin. For this reason, a coherent state displaced in $\hat{x}$ quadrature cannot be used, but this type of symmetry is satisfied precisely by a Gaussian squeezed vacuum state. Subsequently, the form of notation of the approximate quartic squeezed state

$$|\psi_4(r, \chi, \phi_1, \omega, \phi_2)\rangle = \hat{R}(\phi_2)\hat{S}(\omega)\hat{R}(\phi_1)\hat{K}(\chi)\hat{S}(r)\,|0\rangle\,. \tag{V.6}$$

The main nonlinear properties of the state are represented by the squeezing parameter r and the Kerr parameter χ. The other three parameters, phase ϕ_1 and ϕ_2, and the second squeezing parameter ω represent the Gaussuan processing with the purpose of adjusting the geometry of the quantum state (as can be seen in the figure V.1(b)).

V.4 Numerical results and error analysis

In our numerical simulations, we optimized all relevant parameters and thus found the maximum squeezing achievable with our procedures. We then analyzed the robustness of our method against imprecise parameter settings.

In preparing the cubically squeezed state (V.5), the Kerr nonlinearity is an operation applied after the displacement. This means that the whole process is dependent on the choice of the input coherent state. For this reason, we scanned a relatively wide interval of the real parameter α of the input coherent state and plotted the strength of the Kerr nonlinearity (to achieve maximum cubic squeezing) in this dependence. As we can see from the figure V.2(a), with a larger value of α, a weaker Kerr nonlinearity is needed. This follows from the fact that the higher the intensity of the state, the stronger the effect of the Kerr nonlinearity. The result is then the possibility of experimental realization since a really weak Kerr nonlinearity is needed only at the price of a strong coherent state (which is experimentally feasible). Details of numerical simulations and optimization for cubic squeezing can be found in Appendix B in the section

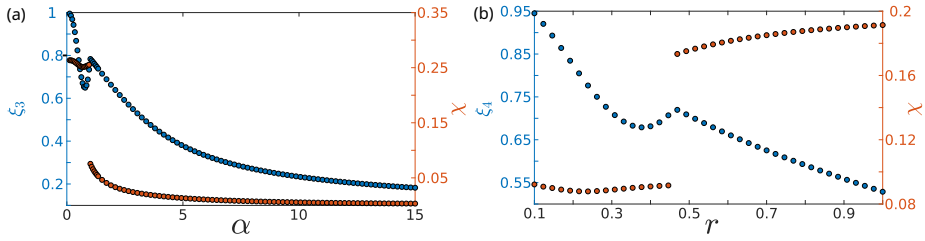

Figure V.2: (a) The minimized cubic squeezing parameter ξ_3 (left y-axis, blue) and χ coefficient of the Kerr nonlinearity required (right y-axis, red) relative to the displacement α of the initial state. (b) The minimized quartic squeezing parameter ξ_4 (left y-axis, blue) and the χ coefficient of the Kerr nonlinearity required (right y-axis, red) relative to the squeezing parameter r of the initial state.

B.2. Also, the minimum variance of the Gaussian state for cubic squeezing was calculated analytically and is attached in the Appendix B, in the section B.1.

In the case of the quartic squeezed state approximation (V.6), the initial state before applying the Kerr operation is the Gaussian squeezed state. Therefore, as in the case of cubic squeezing, we performed a simulation for a range of Gaussian squeezed states (expressed by the squeezing parameter r - the strength of the unitary operator). It is clear from the figure V.2(b) that it is much more difficult to carry out experimentally because, with increasing squeezing of the input state, the maximum achievable nonlinear squeezing also increases, but the necessary strength of the Kerr nonlinearity also increases. However, this does not change the fact that it is achievable only with Kerr nonlinearity and Gaussian operations. As in the case for cubic squeezing as well as for quartic, details about the simulations and variance calculation for Gaussian states are in Appendix B in the section B.2.

To analyze the robustness of the methods, we have studied the error deviations of the resulting state from the target for different input states. With both cases of squeezing (cubic and quartic), we performed two scenarios of inaccurate settings:

1. inaccurate settings of all parameters, i.e., the parameter describes the input state;

2. ideal input state but errors in the other parameters.

In both scenarios, we let the parameters fluctuate with Gaussian distributions with mean values $\mu_1, \ldots, \mu_5$ and standard deviations $\sigma_1, \ldots, \sigma_5$.

Figures V.3(a) and V.3(b) refer to cubic squeezing; we can see the blue-dotted ideal case showing the optimal choice of parameters, while the blue area indicates an error rate of 1% and therefore $\sigma_j = 0.01\mu_j$, and a brown area where the error rate is 5%. 10,000 iterations of parameter randomization were performed for each α of these areas. In the case of a one percent error rate (blue area), the output nonlinear squeezing differs very little from the ideal case. However, with an increase to 5% error, the rate becomes a significant difference. In the case of the precisely prepared input state V.3(b), most of the brown area is under the red curve. We still achieve nonlinear squeezing, but not the maximum one. For case V.3(a), i.e., even with an inaccurate input state, we get above the red limit, but even so, in 77.4% of cases, we achieve nonlinear squeezing.

Next, we analyzed the method's robustness for quartic squeezing. In the case of the perfectly prepared input state V.3(d), we see that even if the other parameters have an error rate of 1% (blue region) or 5% (green region), we will always be below the red limit. That means that we always achieve a nonlinear squeezing not very different from the optimally chosen parameters (blue dotted curve). In case of a random selection of all parameters, in figure V.3(c), we can see that the quartic squeezing is significantly more vulnerable to the imperfections as even for the errors with $\sigma_j = 0.01\mu_j$, the quartic squeezing does not surpass $\xi_4 \approx 0.7$, that can be achieved only by considering superposition of the Fock states $|0\rangle$ and $|2\rangle$. While 61% of all the data points lie under the mean value for $\sigma_j = 0.05\mu_j$, and 67% of all data points lie under the mean value for $\sigma_j = 0.01\mu_j$, the outliers show the values large enough to practically prevent the generation of the quartic nonlinear squeezing in this fashion.

V.5 Conclusion

In principle, quantum states exhibiting nonlinear squeezing can be generated with the help of an arbitrary high-order nonlinearity through the geometry of the phase space. However, such an approach is incremental and requires a large number of individual nonlinear operations to achieve the desired result. We have shown that states exhibiting the nonlinear squeezing of the third and the fourth order can be generated with the help of only a single Kerr gate with a constant interaction strength and a set of suitably chosen Gaussian operations. In both cases, the key step is applying the Kerr gate onto a Gaussian quantum

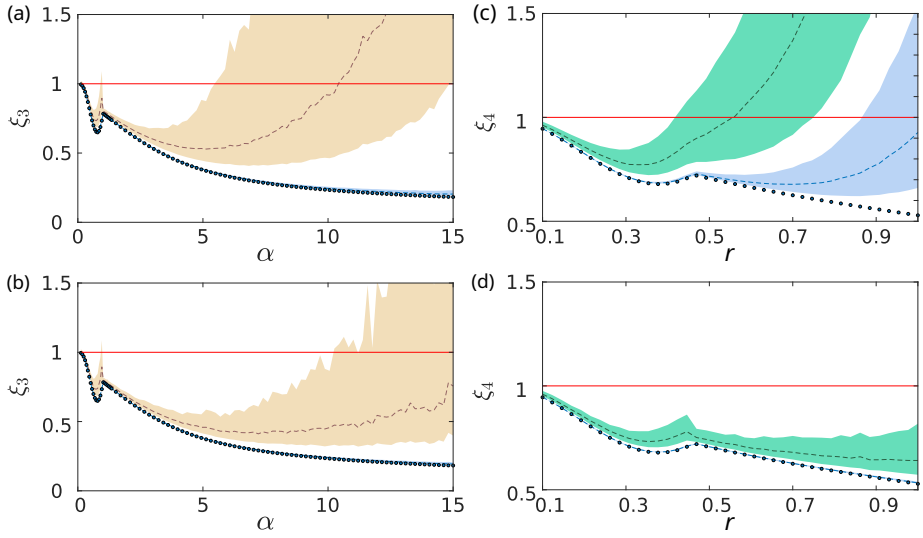

Figure V.3: (a) Cubic nonlinear squeezing ξ_3 (V.1) for quantum state (V.5) with parameters α, χ, ϕ, β, and r fluctuating with Gaussian distribution with the respective mean values $\mu_1, \cdots, \mu_5$ and with the standard deviations $\sigma_1, \cdots, \sigma_5$. (b) Same as (a), but the initial displacements α are set to the optimal theoretical values. The red lines mark $\xi_3 = 1$, and the areas below correspond to quantum states with cubic nonlinear squeezing. The blue dots represent the ideal scenario without the fluctuations. The dashed lines show the mean value of ξ_3 in the simulated sample, while the color-filled areas mark the interval between the upper and the lower standard deviation (see Appendix B, section B.3 for more details). The red and the blue areas then mark the simulations with $\sigma_j = 0.05\mu_j$ and $\sigma_j = 0.01\mu_j$ for all j, respectively. (c) Quartic nonlinear squeezing ξ_4 (V.1) for a quantum state (V.6) with parameters r, χ, ϕ_1, w, and ϕ_2 fluctuating with Gaussian distribution with the respective mean values $\mu_1, \cdots, \mu_5$ and with the standard deviations $\sigma_1, \cdots, \sigma_5$. (d) Same as (c), but the Kerr interaction strengths χ are set to the optimal theoretical values. The red lines mark $\xi_4 = 1$ and the areas below correspond to states with the quartic nonlinear squeezing. The blue dots represent the ideal scenario without the fluctuations. The dashed lines show the mean value ξ_4 in the simulated sample, while the color-filled areas mark span between the upper and the lower standard deviation (see Appendix B, section B.3 for more details). The green and the blue areas then mark the simulations with $\sigma_j = 0.05\mu_j$ and $\sigma_j = 0.01\mu_j$ for all j, respectively.

state - a coherent state for the cubic operation and a squeezed state for the quartic operation, the particular choice being determined by the symmetry of the required nonlinear squeezing. In both cases, some nonlinear effect can be already obtained by considering the first three nonzero terms in the Fock state representation of the quantum states. However, this can explain only part of the nonlinear effect, and taking advantage of the full Hilbert space is always beneficial.

Successfully preparing the desired quantum states requires a precise alignment of all parameters of both the Gaussian and the non-Gaussian constituent operations. To test the experimental viability of the proposed operations, we have to analyze their performance under the fluctuations of these parameters numerically. Gaussian fluctuations in all parameters with the standard deviations on the order of 5% of the means for the cubic states and 1% of the means for the quartic states can be roughly tolerated (the selected percentage corresponds to the error rate of parameter selection in the experiment). We, therefore, expect that this technique could be experimentally tested on the platforms on which is the Kerr gate currently available [64–71, 147].

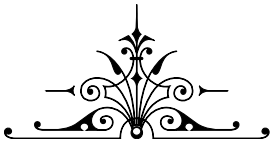

Chapter VI

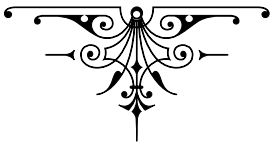

General squeezing parameter as a witness

This chapter discusses a general squeezing parameter that can be used as a witness. The reason why we don't write witness of what in the title is that the choice of what is witnessed is up to the user, as it depends on the choice of the operator that is selected in the squeezing parameter (an example is witnesses of nonlinear squeezing, non-Gaussianity, entanglement, and others).

VI.1 Motivation

Many applications of quantum physics are built upon specific quantum states and their properties. The main examples of this are quantum computing employing quantum states that have both the computational capacity and potential for fault tolerance [124, 148], and quantum metrology with probes sensitive to some particular form of disturbance. Such protocols are often designed for specific quantum states [124], but it is often practical to consider a specific feature of quantum states instead [23, 60, 149]. For example, in the metrology application of squeezed light [7, 150], it is the squeezing that is important and not the exact form of the specific squeezed vacuum state. Along the same line, it can be argued that moments of specific operators are also determining factors for the quality of the quintessential quantum protocol — deterministic unity gain teleportation, but also deterministic implementation of cubic phase gate [124] and preparation of fault-tolerant bosonic qubits [124, 149, 151].

This approach is not completely separated from the concept of ideal quantum states proposed by the theory — the optimal states are often defined as eigenstates of the chosen operators [23, 124, 149, 152]. The variance of the operators, the generalized squeezing, then serves as a way to quantify the performance of certain protocols by exploiting the difference between the optimal and the realistic state [23, 128, 129, 149, 152]. The squeezing can also be used to benchmark the performance of a certain class of quantum states, such as separable or Gaussian, and thus can serve as a witness of important quantum properties, such as entanglement [153] or quantum non-Gaussianity [62].

This is nicely demonstrated in the case of cubic nonlinearity. This deterministic non-Gaussian nonlinear operation is sufficient for quantum computation [124] and can be deterministically implemented with the help of Gaussian operations and a single non-Gaussian ancillary state [124–126, 154]. The ideal state is the eigenstate of the cubic operator but is unphysical. Still, it can be approximately prepared looking either for fidelity with some specific states [155] or for states minimizing the variance of the cubic operator and thus maximizing the nonlinear squeezing [23, 152].

The cubic operation can also be relevant in systems of collective spins. A useful application is to create highly non-Gaussian states of collective spins that can serve as a resource for quantum metrological protocols [156–158]. It was also proposed to use this kind of operation for counter-diabatic driving for fast preparation of Dicke states [159]. Moreover, one can use collective spins as the basis for quasi-continuous variable quantum computation for which higher

nonlinearities in the dynamics are essential.

In this chapter, we present the general concept of nonlinear squeezing and discuss its ramifications in the areas of preparing quantum states and verifying their quantum properties. We then demonstrate the concept of cubic squeezing for systems of collective spins.

VI.2 Squeezing parameter

The concept of squeezing originally comes from continuous variable quantum optics, where it describes a state of harmonic oscillator for which fluctuations in a single quadrature are reduced below the ground state level at the cost of increasing fluctuations in the complementary quadrature [160]. Such squeezed states are an approximation of the quadrature eigenstates, and the strength of squeezing, represented by the number of fluctuations, is a way to characterize the distance between the approximation and the ideal state. As a metric, squeezing in quantum harmonic oscillators is much more practical than, for example, fidelity or distance [161, 162], which cannot be effectively evaluated because the target state is not normalized.

In more detail, for the harmonic oscillator with quadrature operators commuting to $[\hat{x}, \hat{p}] = i$, squeezing in quadrature operator $\hat{x}$ is defined as

$$\tilde{\xi}_x = \frac{\mathrm{var}_{\hat{\rho}} \hat{x}}{\mathrm{var}_{|0\rangle\langle 0|} \hat{x}}, \tag{VI.1}$$

where $\mathrm{var}_{\hat{\rho}}[\hat{\mathcal{O}}] = \mathrm{Tr}[\hat{\rho}\hat{\mathcal{O}}^2] - (\mathrm{Tr}[\hat{\rho}\hat{\mathcal{O}}])^2$ and $|0\rangle$ denotes the ground state of the harmonic oscillator. The denominator represents the baseline - the classical limit to the approximation that needs to be surpassed. This parameter directly quantifies the squeezing in $\hat{x}$ and can be used to assess the quality of specific quantum states with respect to their performance in quantum protocols. It is also possible to extend this definition to take into account a set of Gaussian operations that cannot increase the squeezing of the state:

$$\xi_x = \frac{\min_{\hat{U}_F} \mathrm{var}_{\hat{\rho}} \hat{U}_F^\dagger \hat{x} \hat{U}_F}{\mathrm{var}_{|0\rangle\langle 0|} \hat{x}}. \tag{VI.2}$$

These operations, represented by unitary operator $\hat{U}_F$ and also called the *free operations* in quantum resource theories [163–166], transform the state and cannot create squeezing. However, they can increase the value of ξ_x by hiding the

squeezing to an unobserved operator, specifically, in the case of quadrature squeezing, to a quadrature operator that has been rotated ($\hat{R}(\phi) = \exp(i\phi\hat{n})$) and displaced (III.39). So, while (VI.1) represents squeezing of a specific operator, (VI.2) quantifies the amount of any quadrature squeezing present in the state that can be extracted by non-squeezing operations. The quantity (VI.2) also cannot increase under such operations and is, therefore, better suited for the description of squeezing as a quantum resource.

We can extend the concept of squeezing to evaluate approximations of eigenstates of other operators. In analogy with quadrature squeezing, we will, for any quantum state $\hat{\rho}$, define squeezing with respect to a specific operator $\hat{O}$,

$$\tilde{\xi}_{\mathcal{O}}(\hat{\rho}) = \frac{\left[\mathrm{var}_{\hat{\rho}}\left(\hat{\mathcal{O}}\right)\right]}{\min_{\hat{\rho}_F}\left[\mathrm{var}_{\hat{\rho}_F}\left(\hat{U}_F\hat{\mathcal{O}}\hat{U}_F^\dagger\right)\right]}, \tag{VI.3}$$

and also squeezing as a resource

$$\xi_{\mathcal{O}}(\hat{\rho}) = \frac{\min_{\hat{U}_F}\left[\mathrm{var}_{\hat{\rho}}\left(\hat{U}_F\hat{\mathcal{O}}\hat{U}_F^\dagger\right)\right]}{\min_{\hat{U}_F}\min_{\hat{\rho}_F}\left[\mathrm{var}_{\hat{\rho}_F}\left(\hat{U}_F\hat{\mathcal{O}}\hat{U}_F^\dagger\right)\right]}. \tag{VI.4}$$

In both definitions, $\hat{\rho}_F$ describes a class of *free states* and $\hat{U}_F$ a class of *free operations*. The free states provide us with a normalization baseline for the squeezing. These are states that either do not possess the properties required by applications or states that are experimentally feasible and can be considered readily available. Similarly, free operations are those that cannot create the desired property - applying them to a free state only results in another free state. Such states and operations could be chosen arbitrarily, but the squeezing parameters (VI.3) and (VI.4) have the highest practical impact when the choice of free states and operations is driven by some experimental reality. In the case of regular squeezing (VI.1) and (VI.2), the free states are coherent states, and the free operations are phase-shift and displacement. For squeezing in a nonlinear combination of quadrature operators of quantum harmonic oscillator [163–166], the desired non-Gaussianity, the free states are Gaussian states, and the free operations are Gaussian operations.

Each of the two definitions has its application. The direct squeezing (VI.3) is best used in state preparation tasks, in which the goal is to obtain quantum states best approximating the desired eigenstate of $\hat{\mathcal{O}}$ to be used as a resource [149, 166]. In this case, the preparation procedure is optimized to minimize

over the set of preparable states to obtain $\tilde{\xi}_{\min} = \min_{\hat{\rho}} \tilde{\xi}_{\mathcal{O}}(\hat{\rho})$. On the other hand, squeezing as a resource (VI.4) can be used as a general quantifier for the chosen property. For example, it can be applied to an experimentally generated state with the goal of determining whether it possesses the required property, either directly or in an extractable form. In all cases, value $\xi = 0$ confirms the investigated state as the perfect eigenstate of the target operator, best suited for any application. On the other hand, $\xi \geq 1$ implies the state is no better than a free state and is therefore unsuitable for further applications. For any quantum state, the intermediate value $0 < \xi < 1$ can then serve as a quantifier for the given resource, which can be expressed either directly or in the dB scale, $\xi[dB] = 10 \log_{10} \xi$.

VI.3 Example of cubic squeezing in collective spin systems

We already demonstrated an example of cubic squeezing in chapter V. There, we focused on generating a cubically squeezed state realized by Gaussian operations and Kerr nonlinearity, so we completed an example of cubic squeezing in a linear harmonic oscillator. In this chapter, we apply the concept to a different system, namely the system of collective spins, and compare how it works across the two systems.

Under the term cubic operation, we consider the unitary operator, defined

$$\hat{U}_c(\chi) = \exp\left(i \frac{\chi}{3} \left(\frac{N}{2} \right)^{-\frac{3}{2}} \hat{J}_z^3 \right). \tag{VI.5}$$

The term $\left(\frac{N}{2}\right)^{-\frac{3}{2}}$ represents the scaling parameter of the cubic nonlinearity. Interaction strength depends on the size of the system, where N is the number of particles in the system.

Still, since this is a system where the commutator of collective spin operators is not equal to a constant, as in the case of linear harmonic oscillators, we cannot use the same procedure. We have to introduce the definition through the unitary evolution of the operator $\hat{J}_k$. For cubic squeezing, the $\hat{\mathcal{O}}$ operator takes this form

$$\hat{\mathcal{O}}_c(\chi) = \hat{U}_c(\chi) \hat{J}_k \hat{U}_c^\dagger(\chi), \tag{VI.6}$$

for $k \in (x, y, z)$.

Suppose we substitute the operator $\hat{\mathcal{O}}_c(\chi)$ from equation (VI.6) into equation (VI.3), we get the nonlinear squeezing parameter for cubic squeezing. When choosing the operator $\hat{\mathcal{O}}$, it is necessary to choose a benchmark class of states against which we want to define ourselves. In this case, these are the ground states of the Hamiltonian defined as

$$\hat{H}(\beta) = \left(\frac{g^2}{1+g^2}\right)\hat{J}_z^2 + \left(\frac{1}{1+g^2}\right)\hat{J}_y^2 + \left(\frac{g}{1+g^2}\right)\hat{J}_x. \tag{VI.7}$$

This Hamiltonian, based on the general twist and turn Hamiltonian [167], represents two types of operations depending on the choice of the g parameter

- if g belongs to the interval $(0,\infty) \setminus \{1\}$, then it is a two-axis counter-twisting (TACT) operation,
- in the second case, when $g \in \{0,1\}$, it is a one-axis twisting (OAT) operation.

The ground states (together with rotations) of the Hamiltonian defined in this way cover the entire class of squeezed Gaussian-like states, including the coherent state.[1] Gaussian-like states are states in the Holstein-Primakoff approximation (subsection II.5) that belong to the class of Gaussian states in harmonic oscillator phase space. From now on, we will use the term Gaussian and non-Gaussian states to mean Gaussian-like and non-Gaussian-like states.

In the case of cubic squeezing, we can demonstrate the squeezing parameter in two ways: (i) we get a specific state as the output state of the experiment, and we need to evaluate the state and find out if it is nonlinearly squeezed. (ii) we prepare the state (optimization of the state preparation) corresponding to a specific nonlinear squeezing.

(i) **Evaluation of the state**. For the case of state quantification, a modification of the equation for the nonlinear squeezing parameter (VI.4) is needed. By searching for which squeezing force the variance of the tested state is minimal, we minimize the entire fraction over the possible nonlinear interaction strength χ. The resulting relation has the form

$$\xi = \min_{\chi} \frac{\min_{\hat{U}_F}\left[\mathrm{var}_{\hat{\rho}}\left(\hat{U}_F\hat{\mathcal{O}}_c(\chi)\hat{U}_F^\dagger\right)\right]}{\min_{\hat{U}_F}\min_{\hat{\rho}_F}\left[\mathrm{var}_{\hat{\rho}_F}\left(\hat{U}_F\hat{\mathcal{O}}_c(\chi)\hat{U}_F^\dagger\right)\right]}, \tag{VI.8}$$

[1] It is with the parameter g that we determine the orientation of squeezing of the ground state, i.e. if it is in a horizontal or vertical direction, and squeezing ratio of the ground state of the Hamiltonian. The linear term in the Hamiltonian (VI.7) takes the degeneracy, so the eigenstates are only on one hemisphere of the Bloch sphere.

(ii) **State preparation**. It is necessary to change the form of the expression for nonlinear squeezing from equation (VI.4)

$$\xi_{\hat{\mathcal{O}}_\chi} = \frac{\min_{\hat{\rho}} \min_{\hat{U}_F} \left[\mathrm{var}_{\hat{\rho}} \left(\hat{U}_F \hat{\mathcal{O}}_\chi \hat{U}_F^\dagger \right) \right]}{\min_{\hat{U}_F} \min_{\hat{\rho}_F} \left[\mathrm{var}_{\hat{\rho}_F} \left(\hat{U}_F \hat{\mathcal{O}}_\chi \hat{U}_F^\dagger \right) \right]}, \tag{VI.9}$$

when we want to achieve the maximal squeezing using a series of operations ($\hat{\mathcal{O}}_\chi$ corresponds to the $\hat{\mathcal{O}}_c(\chi)$ with specific parameter χ). Minimization over the density matrix $\hat{\rho}$ symbolizes only the free parameters of the experiment, which can be optimized (so as to get as close as possible to a given nonlinear squeezing with a given value of χ).

In case (i) and (ii), the formula contains unitary operations $\hat{U}_F$ through which we minimize. We always solve this step by centering the tested state in one preselected axis (in the given axis we rotate the state so that its variance matrix is diagonal), in which we calculate the given variance. Details of this ´´calibration" are contained in Appendix C, section C.2.

VI.3.1 Elementary scenario with numerical simulation

As an illustrative example, we chose to test a state that is defined as a superposition of two Dicke states with a free parameter γ

$$|\psi\rangle = \sqrt{\gamma}\,|0\rangle + \sqrt{(1-\gamma)}\,|1\rangle\,. \tag{VI.10}$$

We could have chosen other states, but we chose this state, which is used as an approximation of a cubically squeezed state [128, 130, 152]. There are two reasons for the choice — the first is that this state is defined the same way in the systems with a small number of atoms as in the systems with a large number of atoms (it is not truncated by the available dimension of Dicke states). The second reason is that this state is defined in exactly the same way in the linear harmonic oscillator system, which we will later demonstrate (as the functionality of the nonlinear squeezing parameter across different types of systems).

- **Evaluation of the squeezing of the state.**
  For this case, we performed a numerical simulation where we chose the balanced case of (VI.10)($\gamma = 1/2$) in the system corresponding to $N = 80$. We minimize the squeezing parameter (VI.8) over the possible nonlinear

interaction strength χ. We found that the tested state is non-Gaussian, cubically squeezed, and its maximum squeezing corresponds to $\frac{\chi}{3}\left(\frac{N}{2}\right)^{-\frac{3}{2}} = 7.959 \times 10^{-4}$. For this χ, the squeezing parameter is minimal (this can be seen in figure VI.1(a)), and its value is equal to $\xi_c = 0.748$. When we convert the squeezing parameter value to the squeezing in decibels, we get -1.262dB. The value of the selected χ corresponds to the maximal cubical squeezing of the tested state; for all other χ values, where the value of the squeezing parameter $\xi_c < 1$, the state is also cubically squeezed and non-Gaussian, just not maximally.

- **State preparation.**
  It is necessary to slightly change the form of the expression for nonlinear squeezing from equation (VI.9) when we want to achieve the maximal squeezing using a series of operations. We chose the already used superposition (VI.10) for consistency. We are looking for the optimal ratio in the superposition (the parameter γ) to achieve maximal squeezing, corresponding to minimization via state preparation, i.e., minimization via $\hat{\rho}$. As can already be seen from figure VI.1(b), it is not difficult to find the value of γ for which the maximal cubic squeezing is achieved, and as we can see, even in the previous case, the used $\gamma = \frac{1}{2}$ is not optimal. The optimum is $\gamma = 0.551$, and we achieve squeezing $\xi_c = 0.715$, which corresponds to -1.459dB. χ parameter was set $\frac{\chi}{3}\left(\frac{N}{2}\right)^{-\frac{3}{2}} = 7.959 \times 10^{-4}$ to match the previously used optimal value.

If we compare the two different simulations that we performed, in figure VI.1(a) and in figure VI.1(b), we can see that with the selected input state, we found the maximal squeezing. Still, when we have a possible choice of state preparation (we can choose the parameter γ), we can achieve even greater squeezing in the case of $\gamma = 0.551$. The system of collective spins depends on the number of atoms in the system, and the dimensions in which we solve problems also change accordingly. For this reason, it is necessary to analyze the behavior of the squeezing parameter across cases of systems of different sizes. Numerical simulations, already presented in figures VI.1(a) and (b), were performed with the number of atoms $N = 80$. However, we now show smaller and larger numbers of atoms to clarify the behavior of the squeezing parameter. We divided the simulation into two segments; the first was purely in the interval $N = [4, 100]$, and then we expanded the system by simulating the interval $N = [100, \infty)$. The first interval starts with $N = 4$ because the system size for the m-th order operation is at least $N = m + 1$, so for the cubic operation, we start with a

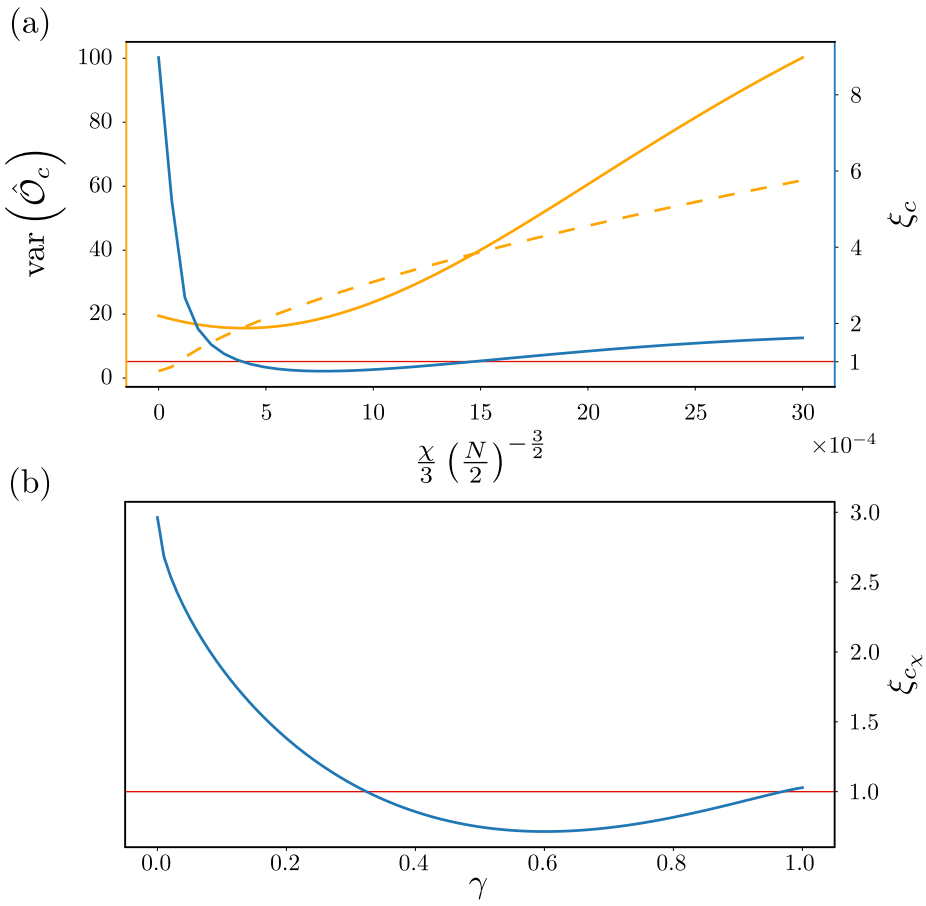

Figure VI.1: (a) Results of numerical simulation - finding the minimum value of the squeezing parameter with the help of (VI.8). The yellow dashed curve corresponds to the variance of the benchmark state; the yellow full line corresponds to the variance of our analyzed state (the yellow curves are connected to the left y-axis, which is also yellow). The blue curve describes the resulting parameter of equation (VI.8) (the values of the blue curve correspond to the right y-axis, which is also blue, and the red curve also belongs to this axis), the red curve is the limit corresponding to $\xi_c = 1$, i.e. when we are below this limit, the state is non-linearly cubically squeezed, when above the limit, we achieve better values with the benchmark states (thus the test case is not nonlinearly squeezed in $\hat{\mathcal{O}}$). (b) Results of numerical simulation - finding of state for corresponding cubic squeezing operation (VI.8). Finding γ for the state described by equation (VI.10). The red curve is the limit corresponding to $\xi_c = 1$, i.e. when we are below this limit, the state is non-linearly cubically squeezed, when above the limit, we achieve better values with the benchmark states (thus, the test case is not nonlinearly squeezed in $\hat{\mathcal{O}}$). The size of the system for simulations is $N = 80$ atoms, for both figures.

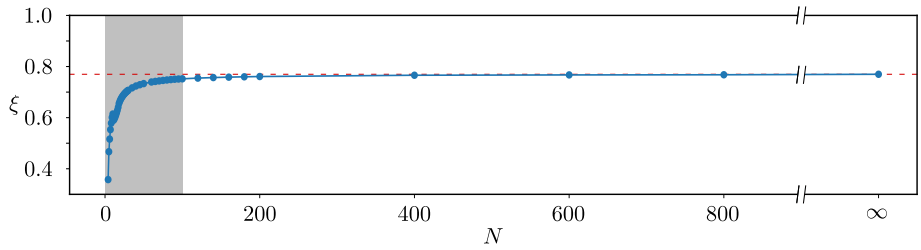

Figure VI.2: Results of numerical simulation of minimizing nonlinear squeezing parameter with testing state (VI.10)(with $\gamma = 1/2$) in the interval of N, where the grey area corresponds to the $N \in [4, 100]$, ∞ point in the x-axis corresponds to the transition to the phase space approximation - Holstein-Primakoff transformation.

system of size $N = 4$. Cubic squeezing cannot be observed in systems with fewer atoms than $N = 4$. The second interval ($N = [100, \infty)$) does not have such a fine sampling due to computational complexity. The case $N = \infty$ is the case when we use the Holstein - Primakoff approximation (for more details, see section II.5) and calculate the values in the phase space with LHO quadrature operators.

In figure VI.2, we can see different regions, namely the gray zone in the interval $N \in [4, 100]$, then $N \in [100, 800]$, and then the point for $N = \infty$.

The gray area indicates the largest changes in the values of the nonlinear parameter for cubic squeezing. These changes are based on the very properties of the system in which we observe it. By changing the number of atoms in the system, we also change the number of Dicke states in the system. Let's focus on the lowest parameter value for $N = 4$. For our tested state, we observe the smallest value of the nonlinear squeezing parameter (from the entire range of tested systems with different numbers of N atoms) in this system.This is because in the $N = 4$ system there are only the following Dicke states: $|0\rangle, |1\rangle, |2\rangle, |3\rangle, |4\rangle$. Thus, the eigenstate of the operator $\hat{\mathcal{O}}$ (VI.6) can be described by the superposition of these five Dicke states, and our tested state describes 40% of this space of Dicke states. For this reason, the value of the nonlinear squeezing parameter subsequently increases as N increases (and the squeezing diminishes). This is because the space of Dicke states gets larger, and the number of Dicke states that describe the ground state of the operator $\hat{\mathcal{O}}$ increases. However, our test state is described by the superposition of only two Dicke states. It thus

describes a gradually smaller part of the total space of Dicke states depending on the increasing number of atoms in the system. An example of comparing

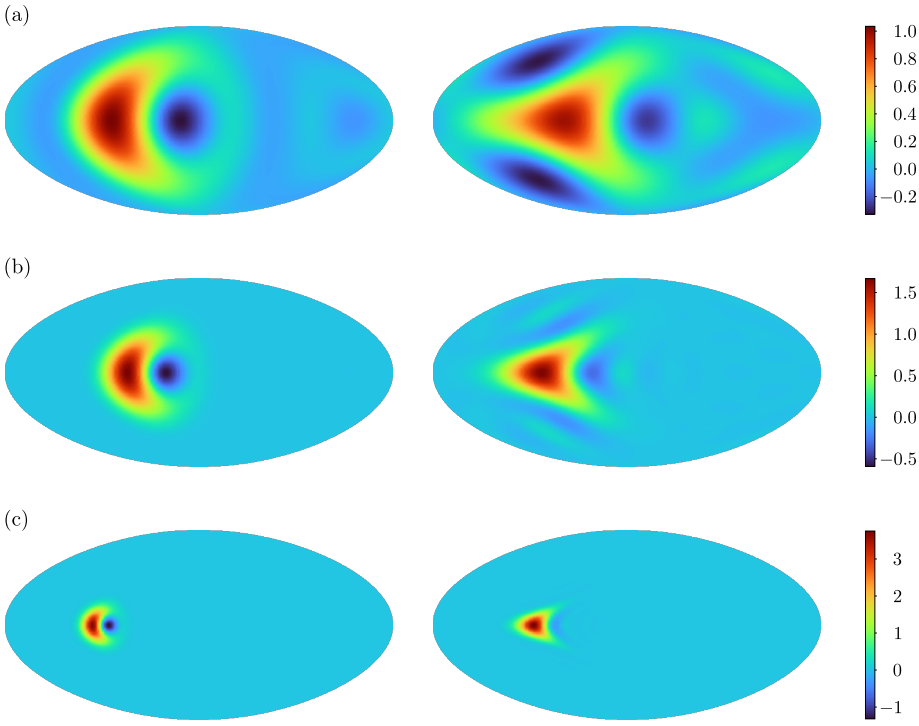

Figure VI.3: Bloch spheres in Hammers projection. The left column corresponds to the tested state (VI.10), i.e. the superposition of $|0\rangle$ and $|1\rangle$ for different numbers of atoms in the systems (where $\gamma = 1/2$). The right column shows the ground states of the operator $\hat{\mathcal{O}}$ (VI.6) for systems with different numbers of atoms. (a) $N = 4$ (b) $N = 10$ (c) $N = 50$.

the tested state with the ground state of the operator $\hat{\mathcal{O}}$ is shown in figure VI.3. There, we can see how the similarity of the tested state with the ground state changes with the increasing number of atoms in the system.

From $N = 100$ we see that we asymptotically approach the nonlinear squeezing value for LHO ($N = \infty$). The value is no longer very different and differs by only 0.015 from the LHO case (which corresponds to 1.95% of the value of

non-linear squeezing in LHO).

The last part of the graph corresponds to a point in ∞. This is the case when using the Holstein-Primakoff approximation, we move into the dynamics of a linear harmonic oscillator system. In this case, too, we use the superposition of $|0\rangle$ and $|1\rangle$ as a test state, only in this case they are Fock states.

As can be seen, the nonlinear squeezing parameter (VI.8) defined for higher numbers of atoms converges to the same squeezing value as in LHO. Then, we have a region of the number of atoms in the system where we achieve a higher squeezing for the same test state, but only because of the limited number of Dicke states in the system.

All points of this simulation were calculated with the normalized cubic squeezing parameter in the unitary operator with respect to the system size (VI.5). The evaluated state was the same for all cases; it was a superposition of the vacuum $|0\rangle$ and the Dicke state $|1\rangle$ in the equation (VI.10) with the setting $\gamma = \frac{1}{2}$.

VI.4 Conclusion

We have shown that it is possible to take the general concept of squeezing and relate it to a specific operator $\hat{\mathcal{O}}$. With this operator, we define the type of squeezing or the property we want to assess. We introduced the squeezing parameter as the ratio of the variance of the tested state with respect to the specific operator $\hat{\mathcal{O}}$ and the variance of the boundary state due to the same specific operator $\hat{\mathcal{O}}$.

The squeezing parameter, as defined in this way, can act as a witness and tell whether the tested state is outside the class of boundary states or not, just in case the value of the squeezing parameter is less than 1, in other cases, we know nothing. Cubically squeezed states of collective spin states ($\xi < 1$) are non-Gaussian and also entangled between the individual spins [153]. When $\xi > 1$ we have no information about either property.

Subsequently, we demonstrated this method for cubic squeezing in systems of collective spins, using the example of the superposition of vacuum state $|0\rangle$ and Dicke state $|1\rangle$. The example was the state evaluation and how to use the squeezing parameter in the preparation of the state.

In conclusion, we can say that the superposition of vacuum state $|0\rangle$ and Dicke state $|1\rangle$ can be cubically squeezed, both in collective spin systems and in the case of a linear harmonic oscillator, and even for spin systems $N \geq 100$ we achieve not too different squeezing as in phase space. In the case of

the $N = 800$ atoms system, the value is then identical to the value in LHO. This points to the possibility of using the same defined parameter of nonlinear squeezing in two different systems, namely in the system of collective spins and the linear harmonic oscillator. At the same time, with a large number of atoms in the system, it is possible to compare the squeezing obtained in both systems directly.

Chapter VII

Summary

This thesis includes the results obtained during my studies. Chapters IV, V, and VI contains work that has been published in articles or is ready for publication. In these chapters, we present the motivation of individual topics, their methodology, results, and conclusions. The title of this work also shows its path — Utilization and quantification of quantum nonlinearity.

Chapter IV is based on the results obtained in our article ´´Nonlinear coherent heat machines". My main task was complete numerics and design of the cascading scheme. We dealt with using the Kerr operation as a source of nonlinearity in the interferometer to obtain the smallest possible heat machine.

We have shown that it is possible to realize a four-mode thermal machine in which two input modes are hot (thermal or coherent states of the same temperature/energy), and the remaining 2 input modes are cold (empty modes — vacuum states). It is, therefore, possible to concentrate energy into one output mode without violating the first or second law of thermodynamics. This nonlinear interferometer scheme can be made more efficient by cascading. In this way, a nonmonotonous photodistribution can be gradually obtained.

The following chapter V of the thesis uses nonlinearity to realize cubic and quartic squeezed states and then quantify the state squeezing. We deal with this issue in the article ´´Generation of quantum states with nonlinear squeezing by Kerr nonlinearity". I am the main author of this article, and I therefore took part in the majority of the writing itself, as well as in all numerical and analytical work. We have shown that it is possible to create a deterministically cubically and quartically squeezed state using Kerr nonlinearity and Gaussian operations. The cubically squeezed state can be realized experimentally due to the attainable Kerr nonlinearity interaction strength values.

The last thematic chapter from the work done during my doctoral studies is chapter VI. We introduced the concept of nonlinear squeezing and generalized it. This article is being finalized for submission. Here, I will also be the main author and, therefore, have a majority share in all the work. We have shown how, depending on the choice of the state property, it is possible to modify the nonlinear squeezing parameter so that we can describe it ourselves. We have demonstrated an example of cubic squeezing on two different systems, namely the collective spin systems and the LHO. We also presented how this parameter can be used (and what needs to be minimized) — use in state evaluation and use in state preparation.

Appendix A - Heat machine based on Kerr nonlinearities

A.1 Mean output photon numbers

Assume that the input field can be constructed as a mixture of coherent states, and let us first study the evolution of each coherent state (figure IV.1(b)). Assume first that the four input modes have amplitudes $a_1, 0, 0, a_4 e^{i\phi}$, where a_1 and a_4 are real (note that only the phase difference between them matters so that one can set the phase of the first mode equal to zero). We assume that the first beam splitters have reflectivity c and transmissivity s given as

$$c = \cos\alpha, \tag{A.1}$$
$$s = \sin\alpha, \tag{A.2}$$

so that the coherent amplitudes transform to

$$a_1' = ca_1, \tag{A.3}$$
$$a_2' = sa_1, \tag{A.4}$$
$$a_3' = sa_4 e^{i\phi}, \tag{A.5}$$
$$a_4' = ca_4 e^{i\phi}. \tag{A.6}$$

After the 50/50 beam splitter between modes 2 and 3 the field amplitudes are

$$a_1'' = ca_1, \tag{A.7}$$
$$a_2'' = \frac{s}{\sqrt{2}}\left(a_1 + a_4 e^{i\phi}\right), \tag{A.8}$$
$$a_3'' = \frac{s}{\sqrt{2}}\left(a_1 - a_4 e^{i\phi}\right), \tag{A.9}$$
$$a_4'' = ca_4 e^{i\phi}. \tag{A.10}$$

The cross-Kerr effect entangles modes 1 with 2 and 3 with 4. However, to find photon number statistics at the output, we can use the reduced density matrices of modes 1 and 4 as described in A.4. Assume that the annihilation operators of modes 1 and 2 after the cross-Kerr coupling are $\hat{a}_1'''$ and $\hat{a}_4'''$. Their mean values are, according to (A.81)

$$\langle \hat{a}_1''' \rangle = ca_1 \exp\left\{\frac{s^2}{2}\left[\left|a_1 + a_4 e^{i\phi}\right|^2\left(e^{i\chi} - 1\right)\right]\right\}, \tag{A.11}$$
$$\langle \hat{a}_4''' \rangle = ca_4 \exp\left\{\frac{s^2}{2}\left[\left|a_1 - a_4 e^{i\phi}\right|^2\left(e^{i\chi} - 1\right)\right] + i\phi\right\}, \tag{A.12}$$

and for the mean photon numbers (using (A.82))

$$\langle \hat{a}_1'''^{\dagger} \hat{a}_1''' \rangle = c^2 a_1^2, \tag{A.13}$$
$$\langle \hat{a}_4'''^{\dagger} \hat{a}_4''' \rangle = c^2 a_4^2. \tag{A.14}$$

Before the last beam splitter, the phase of mode 4 is shifted by $\pi/2$ (this can also be contained in the parameters of the beam splitter). The output fields coming from the last beam splitter have annihilation operators given by

$$\hat{a}_{1,f} = \frac{1}{\sqrt{2}}\left(\hat{a}_1''' + \hat{a}_4''' e^{i\frac{\pi}{2}}\right), \tag{A.15}$$
$$\hat{a}_{4,f} = \frac{1}{\sqrt{2}}\left(\hat{a}_1''' - \hat{a}_4''' e^{i\frac{\pi}{2}}\right). \tag{A.16}$$

Thus, one finds the mean output photon numbers

$$\begin{aligned}\langle\hat{n}_{1,f}\rangle &= \frac{c^2}{2}\{a_1^2+a_4^2+a_1a_4e^{i\left(\phi+\frac{\pi}{2}\right)} \\ &\quad\times e^{\frac{s^2}{2}\left[\left|a_1+a_4e^{i\phi}\right|^2\left(e^{-i\chi}-1\right)+\left|a_1-a_4e^{i\phi}\right|^2\left(e^{i\chi}-1\right)\right]}+c.c.\} \quad \text{(A.17)} \\ \langle\hat{n}_{4,f}\rangle &= \frac{c^2}{2}\{a_1^2+a_4^2-a_1a_4e^{i\left(\phi+\frac{\pi}{2}\right)} \\ &\quad\times e^{\frac{s^2}{2}\left[\left|a_1+a_4e^{i\phi}\right|^2\left(e^{-i\chi}-1\right)+\left|a_1-a_4e^{i\phi}\right|^2\left(e^{i\chi}-1\right)\right]}+c.c.\}. \quad \text{(A.18)}\end{aligned}$$

On expanding the exponentials, one finds

$$\begin{aligned}\langle\hat{n}_{1,f}\rangle &= \frac{c^2}{2}\left\{a_1^2+a_4^2+2a_1a_4\exp\left[-2s^2(a_1^2+a_4^2)\sin^2\frac{\chi}{2}\right]\right. \\ &\quad\left.\times\sin\left(2s^2a_1a_4\sin\chi\cos\phi-\phi\right)\right\}, \quad \text{(A.19)} \\ \langle\hat{n}_{4,f}\rangle &= \frac{c^2}{2}\left\{a_1^2+a_4^2-2a_1a_4\exp\left[-2s^2(a_1^2+a_4^2)\sin^2\frac{\chi}{2}\right]\right. \\ &\quad\left.\times\sin\left(2s^2a_1a_4\sin\chi\cos\phi-\phi\right)\right\}. \quad \text{(A.20)}\end{aligned}$$

So far, these results are valid for coherent input states. If the input states are mixtures of coherent states described by regular Glauber Sudarshan distribution P, one gets the resulting mean photon numbers by averaging over this distribution. Note that a single-mode state can be expressed as

$$\hat{\rho}=\int\int P(\alpha,\phi)|\alpha e^{i\phi}\rangle\langle\alpha e^{i\phi}|\;d\alpha\;d\phi \quad \text{(A.21)}$$

with $\alpha\geq 0$ real and $\phi\in(0,2\pi)$. If the input state is described by the Glauber Sudarshan distribution $P(a_1,\psi,a_4,\psi+\phi)$ describing a mixture of two-mode coherent states $|a_1e^{i\psi}\rangle|a_4e^{i(\psi+\phi)}\rangle$, the mean photon numbers are

$$\begin{aligned}\langle\langle\hat{n}_{1,f}\rangle\rangle &= \int_0^\infty\int_0^\infty\int_0^{2\pi}\int_0^{2\pi}\langle\hat{n}_{1,f}\rangle P(a_1,\psi,a_4,\psi+\phi)\;d\phi\;d\psi\;da_1\;da_4, \quad \text{(A.22)} \\ \langle\langle\hat{n}_{4,f}\rangle\rangle &= \int_0^\infty\int_0^\infty\int_0^{2\pi}\int_0^{2\pi}\langle\hat{n}_{4,f}\rangle P(a_1,\psi,a_4,\psi+\phi)\;d\phi\;d\psi\;da_1\;da_4. \quad \text{(A.23)}\end{aligned}$$

A.1.1 Coherent states with random phases

As a special case, consider two coherent states with equal amplitudes but random phases, i.e.,

$$P(a_1, \psi, a_4, \psi + \phi) = \frac{1}{(2\pi)^2}\delta(a_1 - \sqrt{\bar{n}})\delta(a_4 - \sqrt{\bar{n}}). \tag{A.24}$$

Using the property of Bessel functions

$$\int_0^{2\pi} \sin(a\cos\phi - \phi)d\phi = 2\pi J_1(a), \tag{A.25}$$

the integrals in (A.22) and (A.23) can be evaluated as

$$\langle\langle \hat{n}_{1,f} \rangle\rangle = c^2\bar{n} + G, \tag{A.26}$$

$$\langle\langle \hat{n}_{4,f} \rangle\rangle = c^2\bar{n} - G \tag{A.27}$$

with

$$G = c^2\bar{n}\exp\left(-4s^2\bar{n}\sin^2\frac{\chi}{2}\right) J_1\left(2s^2\bar{n}\sin\chi\right). \tag{A.28}$$

A.1.2 Thermal inputs of equal temperature

For a thermal state with mean photon number $\bar{n}$, the single mode probability distribution is

$$P(\alpha, \phi) = \frac{1}{\pi\bar{n}}\alpha e^{-\frac{\alpha^2}{\bar{n}}}. \tag{A.29}$$

Assuming that both the hot modes are at the same temperature with mean photon number $\bar{n}$, the integrals (A.22) and (A.23) lead to

$$\langle\langle \hat{n}_{1,f} \rangle\rangle = c^2\bar{n} + G, \tag{A.30}$$

$$\langle\langle \hat{n}_{4,f} \rangle\rangle = c^2\bar{n} - G, \tag{A.31}$$

where

$$\begin{aligned} G &= c^2 \int_0^\infty\int_0^\infty\int_0^{2\pi}\int_0^{2\pi} a_1 a_4 e^{-2s^2(a_1^2+a_4^2)\sin^2\frac{\chi}{2}} \\ &\times \sin\left(2s^2 a_1 a_4 \sin\chi\cos\phi - \phi\right) \frac{1}{(\pi\bar{n})^2} a_1 a_4 e^{-\frac{a_1^2+a_4^2}{\bar{n}}} d\phi d\psi da_1 da_4 \\ &= \frac{4c^2}{\bar{n}^2}\int_0^\infty\int_0^\infty x^2y^2\exp\left[-\left(\frac{1}{\bar{n}} + 2s^2\sin^2\frac{\chi}{2}\right)(x^2+y^2)\right] \\ &\times J_1\left(2s^2\sin\chi xy\right) dxdy. \end{aligned} \tag{A.32}$$

The integrals can be evaluated as follows. Substituting

$$
\begin{aligned}
a &\equiv \frac{1}{\bar{n}} + 2s^2 \sin^2 \frac{\chi}{2}, && \text{(A.33)}\\
b &\equiv 2s^2 \sin\chi, && \text{(A.34)}\\
x &= r\cos\xi, && \text{(A.35)}\\
y &= r\sin\xi, && \text{(A.36)}\\
dx\ dy &= r dr\ d\xi, && \text{(A.37)}
\end{aligned}
$$

we get

$$
\begin{aligned}
G &= \frac{4c^2}{\bar{n}^2} \int_0^{\pi/2} \cos^2\xi \sin^2\xi \\
&\times \int_0^{\infty} r^5 \exp\left(-ar^2\right) J_1\left(b\sin\xi\cos\xi\ r^2\right) dr\ d\xi && \text{(A.38)}\\
&= \frac{2c^2}{\bar{n}^2} \int_0^{\pi/2} \cos^2\xi \sin^2\xi \\
&\times \int_0^{\infty} u^2 \exp\left(-au\right) J_1\left(b\sin\xi\cos\xi\ u\right) du\ d\xi. && \text{(A.39)}
\end{aligned}
$$

Integral over u can be evaluated using (A.84) getting

$$
G = \frac{6c^2 ab}{\bar{n}^2} \int_0^{\pi/2} \frac{\sin^3\xi\cos^3\xi}{\left(a^2 + b^2\sin^2\xi\cos^2\xi\right)^{5/2}} d\xi, \qquad \text{(A.40)}
$$

and using (A.88) we arrive at

$$
G = \frac{8c^2 b}{\bar{n}^2(4a^2+b^2)^2} = \frac{c^2 s^2 \sin\chi}{\bar{n}^2\left[\left(\frac{1}{\bar{n}} + 2s^2\sin^2\frac{\chi}{2}\right)^2 + s^4\sin^2\chi\right]^2}. \qquad \text{(A.41)}
$$

Using this result in (A.30), one finds

$$
\bar{n}_{f+} \equiv \langle\langle \hat{n}_{1,f}\rangle\rangle = c^2\bar{n} + \frac{c^2 s^2 \sin\chi}{\bar{n}^2\left[\left(\frac{1}{\bar{n}} + 2s^2\sin^2\frac{\chi}{2}\right)^2 + s^4\sin^2\chi\right]^2}, \qquad \text{(A.42)}
$$

in which one can optimize the values χ and α to get maximum energy in the selected mode.

A.2 Classical approximation

Approximate results can be obtained by assuming that the cross-Kerr coupler mutually changes the phases of coherent states as

$$|\alpha\rangle|\beta\rangle \rightarrow |\alpha e^{i\chi|\beta|^2}\rangle|\beta e^{i\chi|\alpha|^2}\rangle \tag{A.43}$$

that would neglect the correlation of quantum fluctuations. This would modify Eqs. (A.11) and (A.12) for the coherent state amplitudes after the Kerr-couplers to

$$a_1''' = ca_1 \exp\left\{i\chi\frac{s^2}{2}\left|a_1 + a_4 e^{i\phi}\right|^2\right\}, \tag{A.44}$$

$$a_4''' = ca_1 \exp\left\{i\left[\chi\frac{s^2}{2}\left|a_1 + a_4 e^{i\phi}\right|^2 + \phi\right]\right\}, \tag{A.45}$$

and the output intensities of the coherent states after the terminal beam splitter would be

$$\langle n_{1,f}\rangle = \frac{c^2}{2}\left[a_1^2 + a_4^2 + 2a_1a_4\sin\left(2s^2a_1a_4\chi\cos\phi - \phi\right)\right], \tag{A.46}$$

$$\langle n_{4,f}\rangle = \frac{c^2}{2}\left[a_1^2 + a_4^2 - 2a_1a_4\sin\left(2s^2a_1a_4\chi\cos\phi - \phi\right)\right]. \tag{A.47}$$

These results differ from Eqs. (A.19) and (A.20) by the missing factor $\exp\left[-2s^2(a_1^2 + a_4^2)\sin^2\frac{\chi}{2}\right]$ that decreases the interference visibility and by having factor χ rather than $\sin\chi$ in the argument of the interference term. Similarly, as in the fully quantum situation, we can study the special cases of two coherent states of equal intensity and two thermal states of equal temperature.

A.2.1 Coherent states with random phases

The results of (A.26) and (A.27) are modified such that the interference term is

$$G = c^2\bar{n}J_1\left(2s^2\bar{n}\chi\right). \tag{A.48}$$

A.2.2 Thermal inputs of equal temperature

The resulting intensity of (A.30) and (A.31) is modified with G being now

$$G = \frac{c^2s^2\chi}{\bar{n}^2\left(\frac{1}{\bar{n}^2} + s^4\chi^2\right)^2} \tag{A.49}$$

so that the output energy in mode 1 is

$$\langle\langle \hat{n}_{1,f} \rangle\rangle = c^2\bar{n} + \frac{c^2 s^2 \chi}{\bar{n}^2 \left(\frac{1}{\bar{n}^2} + s^4\chi^2\right)^2}. \tag{A.50}$$

This formula allows for analytical optimization. Searching for the optimum value of χ one finds

$$\chi_{\text{opt}} = \frac{1}{\sqrt{3}\bar{n}s^2} \tag{A.51}$$

which inserted to (A.50) yields

$$\langle\langle \hat{n}_{1,f} \rangle\rangle = c^2\bar{n}\left(1 + \frac{9}{16\sqrt{3}}\right) \approx 1.325c^2\bar{n}. \tag{A.52}$$

This result shows that classically, it would be the best strategy to split off as small part of the incoming energy as possible (s^2 small, $c^2 \to 1$) and allow for a correspondingly large Kerr nonlinearity. Fully quantized results show that the strong Kerr nonlinearity would lead to smearing the interference, so one has to find the nontrivial optimum.

A.3 Photon number dispersion

The photon number dispersion is calculated as $\Delta n^2 = \langle n^2 \rangle - \langle n \rangle^2 = \langle \hat{a}^\dagger \hat{a}^\dagger \hat{a}\hat{a} \rangle + \langle \hat{a}^\dagger \hat{a} \rangle - \langle \hat{a}^\dagger \hat{a} \rangle^2$, where the operators are in the final output. The quartic term is thus

$$\langle \hat{a}^\dagger \hat{a}^\dagger \hat{a}\hat{a} \rangle = \frac{1}{4}\left\langle \left(\hat{a}_1^{\dagger\prime\prime\prime} + \hat{a}_4^{\dagger\prime\prime\prime}\right)\left(\hat{a}_1^{\dagger\prime\prime\prime} + \hat{a}_4^{\dagger\prime\prime\prime}\right)\left(\hat{a}_1^{\prime\prime\prime} + \hat{a}_4^{\prime\prime\prime}\right)\left(\hat{a}_1^{\prime\prime\prime} + \hat{a}_4^{\prime\prime\prime}\right)\right\rangle. \tag{A.53}$$

Expressing this for a coherent state with real amplitudes a_1 and a_4 and phase difference ϕ one gets

$$\begin{aligned} \langle \hat{a}^\dagger \hat{a}^\dagger \hat{a}\hat{a} \rangle \quad = \quad & \frac{c^4}{4}\{a_1^4 + a_4^4 + 4a_1^2a_4^2 + 4a_1a_4(a_1^2 + a_4^2)\exp\left[-2s^2(a_1^2 + a_4^2)\sin^2\frac{\chi}{2}\right] \\ & \times \sin\left(2s^2a_1a_4\sin\chi\cos\phi - \phi\right) - 2a_1^2a_4^2\exp\left[-2s^2(a_1^2 + a_4^2)\sin^2\chi\right] \\ & \times \cos\left(2s^2a_1a_4\sin 2\chi\cos\phi - 2\phi\right)\}. \end{aligned} \tag{A.54}$$

A.3.1 Coherent inputs

Using the coherent state Glauber Sudarshan distribution (A.24) we find

$$\begin{aligned}\langle\langle \hat{a}^\dagger \hat{a}^\dagger \hat{a}\hat{a}\rangle\rangle &= c^2\bar{n}^2 \left\{ \frac{3}{2} + 2\exp\left(-4s^2\bar{n}\sin^2\frac{\chi}{2}\right)\frac{1}{2\pi} \right. \\ &\quad \times \int_0^{2\pi} \sin\left(2s^2\bar{n}\sin\chi\cos\phi - \phi\right) d\phi \\ &\quad -\frac{1}{2}\exp\left(-4s^2\bar{n}\sin^2\chi\right)\frac{1}{2\pi} \\ &\quad \left. \times \int_0^{2\pi} \cos\left[2s^2\bar{n}\sin(2\chi)\cos\phi - 2\phi\right] d\phi. \right\} \end{aligned} \tag{A.55}$$

Using (A.25) and

$$\int_0^{2\pi} \cos(a\cos\phi - 2\phi) d\phi = -2\pi J_2(a), \tag{A.56}$$

we get

$$\begin{aligned}\langle\langle \hat{a}^\dagger \hat{a}^\dagger \hat{a}\hat{a}\rangle\rangle &= c^4\bar{n}^2 \left\{ \frac{3}{2} + 2\exp\left(-4s^2\bar{n}\sin^2\frac{\chi}{2}\right) J_1\left(2s^2\bar{n}\sin\chi\right) \right. \\ &\quad \left. + \frac{1}{2}\exp\left(-4s^2\bar{n}\sin^2\chi\right) J_2\left[2s^2\bar{n}\sin(2\chi)\right] \right\}. \end{aligned} \tag{A.57}$$

Thus we find

$$\begin{aligned}\Delta n^2 &= c^4\bar{n}^2 \left\{ \frac{1}{2} + 2\exp\left(-4s^2\bar{n}\sin^2\frac{\chi}{2}\right) J_1\left(2s^2\bar{n}\sin\chi\right) \right. \\ &\quad \left. + \frac{1}{2}\exp\left(-4s^2\bar{n}\sin^2\chi\right) J_2\left[2s^2\bar{n}\sin(2\chi)\right] \right\} \\ &\quad + c^2\bar{n}(1-2G) + G(1-G) \end{aligned} \tag{A.58}$$

with G from (A.28).

A.3.2 Thermal inputs

To find the mean value over a thermal state, one averages these values as

$$\langle\langle f(a_1,a_4,\phi,\psi)\rangle\rangle = \frac{1}{(\pi\bar{n})^2}\int_0^\infty\int_0^\infty\int_0^{2\pi}\int_0^{2\pi} f(a_1,a_4,\phi,\psi) \times \exp\left(-\frac{a_1^2+a_4^2}{\bar{n}}\right) a_1 a_4 d\phi\ d\psi\ da_1\ da_4. \quad \text{(A.59)}$$

One thus finds

$$\langle\langle a_1^4\rangle\rangle = \langle\langle a_4^4\rangle\rangle = 2\bar{n}^2, \quad \text{(A.60)}$$

$$\langle\langle a_1^2 a_4^2\rangle\rangle = \bar{n}^2. \quad \text{(A.61)}$$

The other terms can be evaluated as follows.

$$\begin{aligned}\mathcal{A} &\equiv \langle\langle a_1 a_4 (a_1^2+a_4^2)\exp\left[-2s^2(a_1^2+a_4^2)\sin^2\frac{\chi}{2}\right]\sin\left(2s^2 a_1 a_4\sin\chi\cos\phi-\phi\right)\rangle\rangle \\ &= \frac{1}{(\pi\bar{n})^2}\int_0^\infty\int_0^\infty\int_0^{2\pi}\int_0^{2\pi} x^2y^2(x^2+y^2)\exp\left[-\left(\frac{1}{\bar{n}}+2s^2\sin^2\frac{\chi}{2}\right)\right. \\ &\quad \left.\times(x^2+y^2)\right]\sin\left(2s^2xy\sin\chi\cos\phi-\phi\right)d\phi\ d\psi\ dx\ dy \\ &= \frac{4}{\bar{n}^2}\int_0^\infty\int_0^\infty x^2y^2(x^2+y^2) \\ &\quad \times\exp\left[-\left(\frac{1}{\bar{n}}+2s^2\sin^2\frac{\chi}{2}\right)(x^2+y^2)\right]J_1\left(2s^2\sin\chi xy\right)\ dx\ dy. \quad \text{(A.62)}\end{aligned}$$

Using the substitution as in (A.33)–(A.37) we have

$$\mathcal{A} = \frac{4}{\bar{n}^2}\int_0^{\pi/2}\cos^2\xi\sin^2\xi\int_0^\infty r^7 e^{-ar^2}J_1\left(b\cos\xi\sin\xi r^2\right)dr\ d\xi \quad \text{(A.63)}$$

$$= \frac{2}{\bar{n}^2}\int_0^{\pi/2}\cos^2\xi\sin^2\xi\int_0^\infty u^3 e^{-au}J_1\left(b\cos\xi\sin\xi u\right)du\ d\xi. \quad \text{(A.64)}$$

Using (A.85) we get

$$\begin{aligned}
\mathcal{A} &= \frac{2}{\bar{n}^2}\int_0^{\pi/2}\cos^2\xi\sin^2\xi\frac{3b\sin\xi\cos\xi\left(4a^2-b^2\sin^2\xi\cos^2\xi\right)}{\left(a^2+b^2\sin^2\xi\cos^2\xi\right)^{7/2}}\,d\xi \\
&= \frac{24a^2b}{\bar{n}^2}\int_0^{\pi/2}\frac{\sin^3\xi\cos^3\xi}{\left(a^2+b^2\sin^2\xi\cos^2\xi\right)^{7/2}}\,d\xi \\
&\quad -\frac{6b^3}{\bar{n}^2}\int_0^{\pi/2}\frac{\sin^5\xi\cos^5\xi}{\left(a^2+b^2\sin^2\xi\cos^2\xi\right)^{7/2}}\,d\xi. \qquad \text{(A.65)}
\end{aligned}$$

These integrals are evaluated as (A.89) and (A.90) finding

$$\begin{aligned}
\mathcal{A} &= \frac{32b(20a^2+b^2)}{5a\bar{n}^2\left(4a^2+b^2\right)^3}-\frac{32b^3}{5a\bar{n}^2\left(4a^2+b^2\right)^3} \\
&= \frac{128ab}{\bar{n}^2\left(4a^2+b^2\right)^3}=\frac{4s^2\sin\chi\left(\frac{1}{\bar{n}}+2s^2\sin^2\frac{\chi}{2}\right)}{\bar{n}^2\left[\left(\frac{1}{\bar{n}}+2s^2\sin^2\frac{\chi}{2}\right)^2+s^4\sin^2\chi\right]^3}. \qquad \text{(A.66)}
\end{aligned}$$

The average of the last term in (A.54) can be evaluated as follows.

$$\begin{aligned}
\mathcal{B} &\equiv \langle\langle a_1^2a_4^2\exp\left[-2s^2(a_1^2+a_4^2)\sin^2\chi\right]\cos\left(2s^2a_1a_4\sin2\chi\cos\phi-2\phi\right)\rangle\rangle \\
&= \frac{1}{(\pi\bar{n})^2}\int_0^\infty\int_0^\infty\int_0^{2\pi}\int_0^{2\pi}x^3y^3\exp\left[-\left(\frac{1}{\bar{n}}+2s^2\sin^2\chi\right)(x^2+y^2)\right] \\
&\quad \times\cos\left(2s^2xy\sin2\chi\cos\phi-2\phi\right)d\phi\;d\psi\;dx\;dy \\
&= \frac{1}{(\pi\bar{n})^2}\int_0^\infty\int_0^\infty\int_0^{2\pi}\int_0^{2\pi}x^3y^3\exp\left[-a(x^2+y^2)\right] \\
&\quad \times\cos\left(bxy\cos\phi-2\phi\right)d\phi\;d\psi\;dx\;dy \qquad \text{(A.67)}
\end{aligned}$$

with the substitution (note that this is a different substitution than in the preceding cases)

$$a \equiv \frac{1}{\bar{n}}+2s^2\sin^2\chi, \qquad \text{(A.68)}$$

$$b \equiv 2s^2\sin2\chi \qquad \text{(A.69)}$$

we can write

$$\begin{aligned}\mathcal{B} &= -\frac{4}{\bar{n}^2}\int_0^\infty\int_0^\infty x^3y^3\exp\left[-a(x^2+y^2)\right]J_2(bxy)\;dx\;dy\\ &= -\frac{4}{\bar{n}^2}\int_0^{\pi/2}\sin^3\xi\cos^3\xi\int_0^\infty r^7e^{-ar^2}J_2\left(b\sin\xi\cos\xi r^2\right)dr\;d\xi\\ &= -\frac{2}{\bar{n}^2}\int_0^{\pi/2}\sin^3\xi\cos^3\xi\int_0^\infty u^3e^{-au}J_2\left(b\sin\xi\cos\xi u\right)du\;d\xi. \quad \text{(A.70)}\end{aligned}$$

Using (A.87) we have

$$\begin{aligned}\mathcal{B} &= -\frac{30ab^2}{\bar{n}^2}\int_0^{\pi/2}\frac{\sin^5\xi\cos^5\xi}{\left(a^2+b^2\sin^2\xi\cos^2\xi\right)^{7/2}}d\xi \quad \text{(A.71)}\\ &= -\frac{32b^2}{\bar{n}^2\left(4a^2+b^2\right)^3}\\ &= -\frac{2s^4\sin^2(2\chi)}{\bar{n}^2\left[\left(\frac{1}{\bar{n}}+2s^2\sin^2\chi\right)^2+s^4\sin^2(2\chi)\right]^3}, \quad \text{(A.72)}\end{aligned}$$

where (A.90) was used.

Thus we find

$$\begin{aligned}\langle\langle\hat{a}^\dagger\hat{a}^\dagger\hat{a}\hat{a}\rangle\rangle &= c^4\left(2\bar{n}^2+\mathcal{A}-\frac{1}{2}\mathcal{B}\right)\\ &= c^4\left\{2\bar{n}^2+\frac{4s^2\sin\chi\left(\frac{1}{\bar{n}}+2s^2\sin^2\frac{\chi}{2}\right)}{\bar{n}^2\left[\left(\frac{1}{\bar{n}}+2s^2\sin^2\frac{\chi}{2}\right)^2+s^4\sin^2\chi\right]^3}\right.\\ &\qquad\left.+\frac{s^4\sin^2(2\chi)}{\bar{n}^2\left[\left(\frac{1}{\bar{n}}+2s^2\sin^2\chi\right)^2+s^4\sin^2(2\chi)\right]^3}\right\} \quad \text{(A.73)}\\ &= c^4\bar{n}^2\left\{2+\frac{4\left(1+2\bar{n}_1\sin^2\frac{\chi}{2}\right)\bar{n}_1\sin\chi}{\left[\left(1+2\bar{n}_1\sin^2\frac{\chi}{2}\right)^2+\bar{n}_1^2\sin^2\chi\right]^3}\right.\\ &\qquad\left.+\frac{\bar{n}_1^2\sin^2(2\chi)}{\left[\left(1+2\bar{n}_1\sin^2\chi\right)^2+\bar{n}_1^2\sin^2(2\chi)\right]^3}\right\}, \quad \text{(A.74)}\end{aligned}$$

where

$$\bar{n}_1 \equiv s^2\bar{n} \tag{A.75}$$

is the mean photon number split off from the hot beam.

Therefore, the photon number dispersion is

$$\begin{aligned}\Delta n^2 \;=\; & c^4\bar{n}^2 + c^2\bar{n} + \frac{c^2s^2\left(1-2c^2\bar{n}\right)\sin\chi}{\bar{n}^2\left[\left(\frac{1}{\bar{n}}+2s^2\sin^2\frac{\chi}{2}\right)^2+s^4\sin^2\chi\right]^2} \\ & -\frac{c^4s^4\sin^2\chi}{\bar{n}^4\left[\left(\frac{1}{\bar{n}}+2s^2\sin^2\frac{\chi}{2}\right)^2+s^4\sin^2\chi\right]^4} \\ & +\frac{4c^4s^2\sin\chi\left(\frac{1}{\bar{n}}+2s^2\sin^2\frac{\chi}{2}\right)}{\bar{n}^2\left[\left(\frac{1}{\bar{n}}+2s^2\sin^2\chi\right)^2+s^4\sin^2\chi\right]^3} \\ & +\frac{c^4s^4\sin^2(2\chi)}{\bar{n}^2\left[\left(\frac{1}{\bar{n}}+2s^2\sin^2\chi\right)^2+s^4\sin^2(2\chi)\right]^3}.\end{aligned} \tag{A.76}$$

The magnitude of the fluctuations in the output mode is similar to that of thermal light but somewhat smaller.

A.4 Reduced density matrix of a coherent state coupled by a cross-Kerr coupler

The Fock representation of a two-mode coherent state is

$$|\alpha\rangle|\beta\rangle = e^{-\frac{|\alpha|^2}{2}}e^{-\frac{|\beta|^2}{2}}\sum_{m,n}\frac{\alpha^n}{\sqrt{n!}}\frac{\beta^m}{\sqrt{m!}}|n\rangle|m\rangle. \tag{A.77}$$

The cross-Kerr interaction changes Focks states as $|n\rangle|m\rangle \rightarrow e^{i\chi nm}|n\rangle|m\rangle$, so that the input coherent state changes to

$$U_{\mathrm{Kerr}}|\alpha\rangle|\beta\rangle = e^{-\frac{|\alpha|^2}{2}}e^{-\frac{|\beta|^2}{2}}\sum_{m,n}\frac{\alpha^n}{\sqrt{n!}}\frac{\beta^m}{\sqrt{m!}}e^{i\chi nm}|n\rangle|m\rangle. \tag{A.78}$$

The density matrix corresponding to this state is

$$\rho = e^{-|\alpha|^2}e^{-|\beta|^2}\sum_{n,m,n',m'}\frac{\alpha^n\alpha^{*n'}\beta^m\beta^{*m'}}{\sqrt{n!n'!m!m'!}}e^{i\chi(nm-n'm')}|n,m\rangle\langle n',m'|. \tag{A.79}$$

The reduced density matrix related to mode α is then

$$\begin{aligned}\mathrm{Tr}\left[\rho\right]_\beta &= e^{-|\alpha|^2}e^{-|\beta|^2}\sum_{n,m,n'}\frac{\alpha^n\alpha^{*n'}|\beta|^{2m}}{\sqrt{n!n'!}\;m!}e^{i\chi(n-n')m}|n\rangle\langle n'| \\ &= e^{-|\alpha|^2}\sum_{n,n'}\frac{\alpha^n\alpha^{*n'}}{\sqrt{n!n'!}}\exp\left\{|\beta|^2\left[e^{i\chi(n-n')}-1\right]\right\}|n\rangle\langle n'|. \quad \text{(A.80)}\end{aligned}$$

This result enables us to find moments of the creation and annihilation operators acting on mode α:

$$\begin{aligned}\langle\hat{a}\rangle &= \mathrm{Tr}[\hat{a}\rho_\alpha] = e^{-|\alpha|^2}\mathrm{Tr}\sum_{n,n'}\frac{\alpha^n\alpha^{*n'}}{\sqrt{n!n'!}}\exp\left\{|\beta|^2\left[e^{i\chi(n-n')}-1\right]\right\}\sqrt{n}|n-1\rangle\langle n'| \\ &= e^{-|\alpha|^2}\mathrm{Tr}\sum_{k,n'}\frac{\alpha^{k+1}\alpha^{*n'}}{\sqrt{(k+1)!n'!}}\exp\left\{|\beta|^2\left[e^{i\chi(k+1-n')}-1\right]\right\}\sqrt{k+1}|k\rangle\langle n'| \\ &= e^{-|\alpha|^2}\sum_{k}\frac{\alpha^{k+1}\alpha^{*k}}{k!}\exp\left[|\beta|^2\left(e^{i\chi}-1\right)\right] \\ &= \alpha\exp\left[|\beta|^2\left(e^{i\chi}-1\right)\right]. \quad \text{(A.81)}\end{aligned}$$

In the same way one can find mean values of normally ordered operators as

$$\langle\hat{a}^{\dagger q}\hat{a}^r\rangle = \alpha^{*q}\alpha^r\exp\left[|\beta|^2\left(e^{i\chi(r-q)}-1\right)\right]. \quad \text{(A.82)}$$

A.5 Bessel function formulas

From the general expression [168] (p. 97)

$$\int_0^\infty e^{au}u^{\mu-1}J_\nu(bu)du = (a^2+b^2)^{-\mu/2}\Gamma(\nu+\mu)\mathrm{P}_{\mu-1}^{-\nu}\left(\frac{a}{\sqrt{a^2+b^2}}\right) \quad \text{(A.83)}$$

we get the special cases used in the text

$$\int_0^\infty e^{-au}u^2 J_1(bu)du = \frac{3ab}{(a^2+b^2)^{5/2}}, \tag{A.84}$$

$$\int_0^\infty e^{-au}u^3 J_1(bu)du = \frac{3b(4a^2-b^2)}{(a^2+b^2)^{7/2}}, \tag{A.85}$$

$$\int_0^\infty e^{-au}u^2 J_2(bu)du = \frac{3b^2}{(a^2+b^2)^{5/2}}, \tag{A.86}$$

$$\int_0^\infty e^{-au}u^3 J_2(bu)du = \frac{15ab^2}{(a^2+b^2)^{7/2}}, \tag{A.87}$$

Eqs. (A.84) and (A.87) also follow from 66, chapt. 25 in [169], Eq. (A.86) follows from 60 in [169].

A.6 Auxiliary integrals

$$\int_0^{\pi/2} \frac{\sin^3\xi\cos^3\xi}{\left(a^2+b^2\sin^2\xi\cos^2\xi\right)^{5/2}}d\xi = \frac{4}{3a(4a^2+b^2)^2}, \tag{A.88}$$

$$\int_0^{\pi/2} \frac{\sin^3\xi\cos^3\xi}{\left(a^2+b^2\sin^2\xi\cos^2\xi\right)^{7/2}}d\xi = \frac{4(20a^2+b^2)}{15a^3(4a^2+b^2)^3}, \tag{A.89}$$

$$\int_0^{\pi/2} \frac{\sin^5\xi\cos^5\xi}{\left(a^2+b^2\sin^2\xi\cos^2\xi\right)^{7/2}}d\xi = \frac{16}{15a(4a^2+b^2)^3}. \tag{A.90}$$

Appendix B - Generation of Non-Gaussian states

B.1 Optimal Gaussian states for evaluating nonlinear squeezing.

To properly evaluate the nonlinear squeezing of quantum states given by $\xi_{3,4}$, we require the knowledge of the optimal variance of the ideal Gaussian state that is used in the denominator. Due to the symmetry of the operator $\hat{O}_3$, the ideal Gaussian state for the cubic nonlinearity is the vacuum state squeezed along the $\hat{x}$ axis. For this state, the optimal squeezing parameter and the minimal variance can be analytically calculated in Heisenberg's picture, in which the operators $\hat{x}$ and $\hat{p}$ evolve as

$$\hat{x} \rightarrow g\hat{x}, \tag{B.1}$$

$$\hat{p} \rightarrow \frac{1}{g}\hat{p}. \tag{B.2}$$

We can then substitute the new $\hat{x}$ and $\hat{p}$ into the variance

$$\text{var}\left(\hat{O}_3\right) = \langle \hat{O}_3^2 \rangle - \langle \hat{O}_3 \rangle^2;\ \hat{O}_3 = \hat{x} - \hat{p}^2, \tag{B.3}$$

$$\langle \hat{O}_3 \rangle = g \langle 0| \hat{x} |0\rangle - \frac{1}{g^2} \langle 0| \hat{p}^2 |0\rangle, \tag{B.4}$$

$$\langle \hat{O}_3^2 \rangle = g^2 \langle 0| \hat{x}^2 |0\rangle - \frac{1}{g} \langle 0| \hat{x}\hat{p}^2 + \hat{p}^2\hat{x} |0\rangle + \\ + \frac{1}{g^4} \langle 0| \hat{p}^4 |0\rangle, \tag{B.5}$$

$$\text{var}\left(\hat{O}_3\right) = \frac{g^2}{2} + \frac{1}{g^4}\frac{3}{4} - \frac{1}{g^4}\frac{1}{4} = \frac{g^2}{2} + \frac{1}{2g^4}. \tag{B.6}$$

The next step is to perform a derivative and to set it equal to the zero value for finding the value of the minimum:

$$\frac{\partial \text{var}\left(\hat{O}_3\right)}{\partial g} = 0, \tag{B.7}$$

$$g - \frac{2}{g^5} = 0 \rightarrow g = \sqrt[6]{2}, \tag{B.8}$$

$$\text{var}_{min}\left(\hat{O}_3\right) = 3 \times 2^{-\frac{5}{3}}. \tag{B.9}$$

For the case of quartic squeezing, the optimal state is a squeezed vacuum state; this time, however, it is squeezed in an arbitrary direction. By applying the same approach as in the previous case, the quadrature operators of the squeezed and rotated vacuum state can be expressed as:

$$\hat{x} \rightarrow g\cos(\phi)\hat{x} + \frac{\sin(\phi)}{g}\hat{p}, \tag{B.10}$$

$$\hat{p} \rightarrow \frac{\cos(\phi)}{g}\hat{p} - g\sin(\phi)\hat{x}. \tag{B.11}$$

Subsequently, we substitute them into the nonlinear variance and obtain

$$\mathrm{var}\left(\hat{O}_4\right) = \langle \hat{O}_4^2 \rangle - \langle \hat{O}_4 \rangle^2;\ \hat{O}_4 = \hat{x} - \hat{p}^3, \tag{B.12}$$

$$\begin{aligned}\mathrm{var}\left(\hat{O}_4\right) =& \frac{g^2\cos^2(\phi)}{2} + \frac{\sin^2(\phi)}{2g^2} + \\ &+ \frac{3}{2}g^2\sin^3(\phi)\cos(\phi) + \frac{3}{2}\sin(\phi)\cos^3(\phi) - \\ &- \frac{3}{2}\sin^3(\phi)\cos(\phi) - \frac{3}{2}\frac{\cos^3(\phi)\sin(\phi)}{g^4} + \\ &+ \frac{15}{8}\frac{\cos^6(\phi)}{g^6} + \frac{45}{8}\frac{\sin^2(\phi)\cos^4(\phi)}{g^2} + \\ &+ \frac{45}{8}g^2\sin^4(\phi)\cos^2(\phi) + \frac{15}{8}g^6\sin^6(\phi).\end{aligned} \tag{B.13}$$

The optimal parameters for the Gaussian state minimizing this formula can be numerically found to be

$$g = -0.637, \tag{B.14}$$

$$\phi = -1.949, \tag{B.15}$$

and the minimal variance of the Gaussian state is $\mathrm{var}_{min}\left(\hat{O}_4\right) = 0.971$.

B.2 Optimization of the state preparation

In the following, we describe the numerical optimization tools employed to achieve the results. The optimized parameter is always the relative squeezing parameter $\xi_{3,4}$. Still, since the denominator of (V.1) is always fixed, it is sufficient to minimize the variance of the quantum operators $\hat{O}_3$ and $\hat{O}_4$ with $\hat{O}_n = \hat{x} - \hat{p}^{n-1}$. These variances, which we denote $V_3(\alpha;\chi,\phi,\beta,r)$ and $V_4(r;\chi,\phi_1,\omega,\phi_2)$, respectively, are the functions of the input parameters of the preparation circuit.

The variances for each combination of parameters were calculated in two steps. In the first step, we numerically applied the Kerr nonlinearity by expressing the input state in the Fock basis of the dimension N and by multiplying it by the matrix form of the unitary operator for the Kerr operation to produce the approximate representation of the states $|\zeta_3\rangle = \hat{K}(\chi)\hat{D}(\alpha)|0\rangle$ and

$|\zeta_4\rangle = \hat{K}(\chi)\hat{S}(r)|0\rangle$ for the preparation of the cubic and the quartic squeezing, respectively.

The application of the Kerr operator could be done perfectly because the operator is diagonal in the Fock basis. In our simulations, we have used dimension $N = 300$, which was sufficient to represent the selected input states faithfully. We then used these quantum states to evaluate the moments of the quadrature operators.

For generation of the cubic squeezing, the relevant moments can be obtained by the Gaussian transformation of the quadrature operators. That leads to the polynomial formula for the variance

$$V_3 = \langle\zeta_3| (\hat{O}_3')^2 |\zeta_3\rangle - \langle\zeta_3| \hat{O}_3' |\zeta_3\rangle^2 , \tag{B.16}$$

where

$$\hat{x}' = g\left(\cos(\phi)x + \sin(\phi)p\right), \tag{B.17}$$

$$\hat{p}' = \frac{1}{g}\left((-\sin(\phi)x + \cos(\phi)p) + \beta\right), \tag{B.18}$$

$$\hat{O}_3' = \hat{x}' - \hat{p}'^3. \tag{B.19}$$

Similarly, for the quartic squeezing, we obtain

$$V_4 = \langle\zeta_4| (\hat{O}_4')^2 |\zeta_4\rangle - \langle\zeta_4| \hat{O}_4' |\zeta_4\rangle^2 , \tag{B.20}$$

where

$$\hat{x}_1 = \omega \sin(\phi_2)\left(\sin(\phi_1)\hat{x} + \cos(\phi_1)\hat{p}\right), \tag{B.21}$$

$$\hat{x}_2 = \frac{1}{\omega}\cos(\phi_2)\left(-\cos(\phi_1)\hat{x} + \sin(\phi_1)\hat{p}\right), \tag{B.22}$$

$$\hat{p}_1 = \frac{1}{\omega}\sin(\phi_2)\left(-\cos(\phi_1)\hat{x} + \sin(\phi_1)\hat{p}\right), \tag{B.23}$$

$$\hat{p}_2 = \omega\cos(\phi_2)\left(\sin(\phi_1)\hat{x} + \cos(\phi_1)\hat{p}\right), \tag{B.24}$$

$$\hat{x}'' = \hat{x}_1 + \hat{x}_2, \tag{B.25}$$

$$\hat{p}'' = \hat{p}_1 - \hat{p}_2, \tag{B.26}$$

$$\hat{O}_4 = \hat{x}'' - \hat{p}''^3. \tag{B.27}$$

The numerical optimization of the functions was performed in Python, with help of the *scipy.optimize.minimize* library and the L-BFGS-B function. This is a quasi-Newtonian optimization method that allows the setting of the intervals

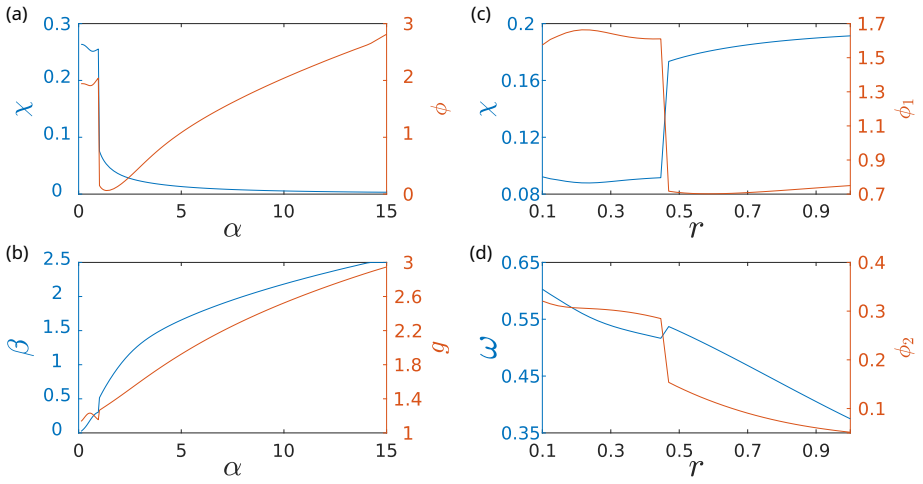

Figure B.1: Left column - the optimal parameters of obtained by the numerical optimization for the given input displacement for the case of the Cubic nonlinear squeezing. (a) The parameters of Kerr nonlinearity χ and phase shift parameter ϕ. (b) The displacement parameter β, and the squeezing parameter g. Right column - the optimal parameters obtained by the numerical optimization for a given input displacement for the case of the Quartic nonlinear squeezing. (c) The parameters of Kerr nonlinearity χ, and rotation ϕ_1. (d) The phase shift parameter ϕ_2, and the squeezing parameter (ω).

of parameters in which the optimization will take place and thus reduces the computational time. This method uses the Broyden-Fletcher-Goldfarb-Shanno algorithm. The optimization searches for the local minima and always starts from the pre-selected entry points. In our analysis, in which we searched for the minimal values for the different fixed values of α (for the cubic squeezing) and r (for the quartic squeezing), we always chose one of the sets of the parameters as those that were optimal for the previously calculated value of α or r, and the other 299 sets were chosen randomly. There were 300 different starting sets of the parameters for each instance of the numerical optimization.

The parameters for which the optimal nonlinear squeezing was found are plotted for the cubic squeezing in Fig. B.1(a),(b) and for the quartic squeezing in Fig. B.1(c),(d).

B.3 Statistical evaluation of errors

In the following, we would like to describe, in detail, the error analysis employed to obtain the results presented. When simulating the errors, we started from the optimal set of the parameters and then simulated the random deviations. This was done by running the Monte Carlo simulation, in which $N_{runs} = 10000$ runs of the quantum state preparation were simulated with parameters that were randomly chosen from Gaussian distributions with mean values μ, that were corresponding to the parameters' optimal value, and standard deviations $\sigma = \gamma\mu$, that was considered to be a certain fraction of the mean value. The obtained nonlinear variances from each run were then statistically evaluated.

In each simulated run of the experiment, the obtained nonlinear variance can be expressed as $\xi_{3,4}(k)$, where $k = 1, \cdots, N_{runs}$ denotes the particular run. The fundamental information is provided by the statistical moments. The most important one is the mean value, $\overline{\xi}_{3,4} = \frac{1}{N_{runs}} \sum_k \xi_{3,4}(k)$, but important insight is also given by the upper and the lower standard deviations

$$\sigma_+^2 = \frac{1}{N_+} \sum_k (\max[\xi_{3,4}(k) - \overline{\xi}_{3,4}, 0])^2, \tag{B.28}$$

$$\sigma_-^2 = \frac{1}{N_-} \sum_k (\min[\xi_{3,4}(k) - \overline{\xi}_{3,4}, 0])^2, \tag{B.29}$$

where N_+ and N_- represent the number of runs in which the measured nonlinear variance $\xi_{3,4}(k)$ is larger or lower, respectively, than the mean-variance $\overline{\xi}_{3,4}$.

B.4 Numerical representation of quantum states and operations

To implement the numerical simulation of the quantum states and operations, we chose the dimension of the Hilbert space to be $N = 300$ to avoid nonphysical results by ensuring the states we work with are faithfully represented. On this dimension, we can represent the truncated annihilation operator by matrix A with elements

$$A_{m,n} = \delta_{m,n+1}\sqrt{m} \quad \forall\, m = 1, 2, \ldots, N-1, .$$

The quadrature operators $\hat{x}$ and $\hat{p}$ can then be represented by matrices

$$X = \frac{\left(A^\dagger + A\right)}{\sqrt{2}},$$
$$P = \frac{i\left(A^\dagger - A\right)}{\sqrt{2}}.$$

Subsequently, we use these matrices to define transformation matrices of displacement $D(\alpha)$, squeezing $S(r)$, phase rotation $R(\phi)$ and Kerr nonlinearity $K(\chi)$,

$$D(\alpha) = \exp\left[-i\alpha X\right],$$
$$S(r) = \exp\left[\frac{ir}{2}\left(XP + PX\right)\right],$$
$$R(\phi) = \exp\left[\frac{i\phi}{2}\left(X^2 + P^2\right)\right],$$
$$K(\chi) = \exp\left[-i\chi\left(X^2 + P^2\right)^2\right],$$

and use them to calculate the vector representation of the quantum state obtained by applying the Kerr operation to a coherent state for the case of preparation of the cubic squeezing,

$$|\zeta_3\rangle = \hat{K}(\chi)\hat{D}(\alpha)\,|0\rangle\,,$$

or to a squeezed state for the case of preparation of the quartic squeezing,

$$|\zeta_4\rangle = \hat{K}(\chi)\hat{S}(r)\,|0\rangle\,.$$

In both cases, the initial vacuum state is represented by a numerical vector

$$|0\rangle = \begin{pmatrix} 1 \\ 0 \\ 0 \\ 0 \\ \vdots \\ 0 \end{pmatrix}.$$

Appendix C - General squeezing parameter as a witness

C.1 Maximal variance value

In this section, we want to present the highest possible value of the variance of the operator $\hat{\mathcal{O}}$ in equation (VI.3). Consider the eigenstates with minimal and maximal energy of the operator $\hat{\mathcal{O}}$ such that

$$\begin{aligned} \hat{O}\,|\lambda_{min}\rangle &= \lambda_{min}\,|\lambda_{min}\rangle\,, \\ \hat{O}\,|\lambda_{max}\rangle &= \lambda_{max}\,|\lambda_{max}\rangle\,. \end{aligned} \tag{C.1}$$

Then consider the state as a superposition of the highest and lowest energy eigenstates

$$|\psi\rangle = \alpha\,|\lambda_{min}\rangle + \beta\,|\lambda_{max}\rangle\,. \tag{C.2}$$

The variance calculation corresponds to

$$\begin{aligned}
\mathrm{var}\left(\hat{O}\right) &= \langle\psi|\,\hat{O}^2\,|\psi\rangle - \langle\psi|\,\hat{O}\,|\psi\rangle^2 \\
&= (\alpha^*\,\langle\lambda_{min}| + \beta^*\,\langle\lambda_{max}|)\hat{O}^2(\alpha\,|\lambda_{min}\rangle + \beta\,|\lambda_{max}\rangle) \\
&- \Big((\alpha^*\,\langle\lambda_{min}| + \beta^*\,\langle\lambda_{max}|)\hat{O}(\alpha\,|\lambda_{min}\rangle + \beta\,|\lambda_{max}\rangle)\Big)^2 \\
&= |\alpha|^2\lambda_{min}^2 + |\beta|^2\lambda_{max}^2 - \left(|\alpha|^2\lambda_{min} + |\beta|^2\lambda_{max}\right)^2 \\
&= |\alpha|^2|\beta|^2\left(\lambda_{min}^2 + \lambda_{max}^2\right) - 2|\alpha|^2|\beta|^2\lambda_{min}\lambda_{max} \\
&= |\alpha|^2|\beta|^2\left(\lambda_{min} - \lambda_{max}\right)^2.
\end{aligned} \tag{C.3}$$

We want the case where the variance value is the highest, then $\alpha = \beta = \frac{1}{\sqrt{2}}$ and $\lambda_{max} = -\lambda_{min}$. In the case of collective spins is $\lambda_{max} = \frac{N}{2}$, where N is the number of atoms in the system. That means the maximum value of variance is dependent on the size of the system and equals to $\left(\frac{N}{2}\right)^2$. If we were to increase the system until N would limitly close to infinity, then the maximum value of the nonlinear variance would be infinity, as it is in the case of a linear harmonic oscillator.

C.2 Rotation calibration, minimization of variance over the general rotation

In the case of cubic squeezing in collective spins, the minimization through the general free operation consists in the fact that we need to rotate the state to the axis perpendicular to the linear operator $\hat{J}_y$ from equation (VI.6). The given axis will be the J_x axis since we are studying the cubic squeezing $\hat{J}_z^3$, and the linear component is $\hat{J}_y$. Subsequently, orient the state so that the covariance matrix is diagonal.

First, we have to calculate the rotation angles so that the state is centered,

and we calculate this using the mean values of the individual operators:

$$\begin{aligned}\gamma &= \arccos\left(\frac{\langle\hat{J}_z\rangle}{\sqrt{\langle\hat{J}_x\rangle^2+\langle\hat{J}_y\rangle^2+\langle\hat{J}_z\rangle^2}}\right)\\ \omega &= \arcsin\left(\frac{\sqrt{\langle\hat{J}_x\rangle^2+\langle\hat{J}_y\rangle^2}}{\sqrt{\langle\hat{J}_x\rangle^2+\langle\hat{J}_y\rangle^2+\langle\hat{J}_z\rangle^2}}\right).\end{aligned} \tag{C.4}$$

Next, let's apply the rotation operators to the given state

$$\hat{\rho}' = \exp\left(i\gamma\hat{J}_y\right)\exp\left(i\omega\hat{J}_z\right)\hat{\rho}\exp\left(-i\omega\hat{J}_z\right)\exp\left(-i\gamma\hat{J}_y\right). \tag{C.5}$$

The next step is to calculate the second moment for the given operators $\hat{J}_y$, $\hat{J}_z$ and their combination. Thus, we get the rotation angle of the state, and then we get the diagonal covariance matrix for the operators $\hat{J}_y$ and $\hat{J}_z$.

$$\beta = \frac{1}{2}\arctan\left(\frac{\langle\hat{J}_z\hat{J}_y+\hat{J}_y\hat{J}_z\rangle}{\langle\hat{J}_z^2\rangle-\langle\hat{J}_y^2\rangle}\right). \tag{C.6}$$

Then, centered and correctly rotated state

$$\hat{\rho}'' = \exp\left(i\beta\hat{J}_x\right)\hat{\rho}'\exp\left(-i\beta\hat{J}_x\right). \tag{C.7}$$

Bibliography

[1] V. Scarani et al. “The Security of Practical Quantum Key Distribution”. In: *Review of Modern Physics* 81 (Sept. 2009), p. 1301. DOI: 10.1103/RevModPhys.81.1301.

[2] H.-K. Lo et al. “Secure quantum key distribution”. In: *Nat. Photonics* 8 (Aug. 2014), pp. 595–604. DOI: 10.1038/nphoton.2014.149.

[3] K. Azuma et al. “All-photonic intercity quantum key distribution”. In: *Nat. Commun.* 6.10171 (Dec. 2015), pp. 1–6. DOI: 10.1038/ncomms10171.

[4] S. Ecker et al. “Strategies for achieving high key rates in satellite-based QKD”. In: *npj Quantum Inf.* 7.5 (Jan. 2021), pp. 1–7. DOI: 10.1038/s41534-020-00335-5.

[5] G. J. Pryde et al. “Creation of maximally entangled photon-number states using optical fiber multiports”. In: *Phys. Rev. A* 68.5 (Nov. 2003), p. 052315. DOI: 10.1103/PhysRevA.68.052315.

[6] M. W. Mitchell et al. “Super-resolving phase measurements with a multiphoton entangled state”. In: *Nature* 429 (May 2004), pp. 161–164. DOI: 10.1038/nature02493.

[7] J. Aasi et al. “Enhanced sensitivity of the LIGO gravitational wave detector by using squeezed states of light”. In: *Nat. Photonics* 7 (Aug. 2013), pp. 613–619. DOI: 10.1038/nphoton.2013.177.

[8] E. Knill et al. “A scheme for efficient quantum computation with linear optics”. In: *Nature* 409 (Jan. 2001), pp. 46–52. DOI: 10.1038/35051009.

[9] J. L. O’Brien. “Optical Quantum Computing”. In: *Science* 318.5856 (Dec. 2007), pp. 1567–1570. DOI: 10.1126/science.1142892.

[10] H.-S. Zhong et al. “Quantum computational advantage using photons”. In: *Science* 370.6523 (Dec. 2020), pp. 1460–1463. DOI: 10.1126/science.abe8770.

[11] S. L. Braunstein et al. “Quantum information with continuous variables”. In: *Rev. Mod. Phys.* 77.2 (June 2005), pp. 513–577. DOI: 10.1103/RevModPhys.77.513.

[12] C. Weedbrook et al. “Gaussian quantum information”. In: *Rev. Mod. Phys.* 84.2 (May 2012), pp. 621–669. DOI: 10.1103/RevModPhys.84.621.

[13] U. Andersen et al. “Hybrid discrete- and continuous-variable quantum information”. In: *Nat. Phys.* 11 (Sept. 2015), pp. 713–719. DOI: 10.1038/nphys3410.

[14] N. Ofek et al. “Extending the lifetime of a quantum bit with error correction in superconducting circuits”. In: *Nature* 536 (Aug. 2016), pp. 441–445. DOI: 10.1038/nature18949.

[15] T. Hillmann et al. “Universal Gate Set for Continuous-Variable Quantum Computation with Microwave Circuits”. In: *Phys. Rev. Lett.* 125.16 (Oct. 2020), p. 160501. DOI: 10.1103/PhysRevLett.125.160501.

[16] M. Aspelmeyer et al. “Cavity optomechanics”. In: *Rev. Mod. Phys.* 86.4 (Dec. 2014), pp. 1391–1452. DOI: 10.1103/RevModPhys.86.1391.

[17] O. Hosten et al. “Measurement noise 100 times lower than the quantum-projection limit using entangled atoms”. In: *Nature* 529 (Jan. 2016), pp. 505–508. DOI: 10.1038/nature16176.

[18] Á. Cuevas et al. “Experimental Detection of Quantum Channel Capacities”. In: *Phys. Rev. Lett.* 119.10 (Sept. 2017), p. 100502. DOI: 10.1103/PhysRevLett.119.100502.

[19] S. Lloyd et al. “Quantum Computation over Continuous Variables”. In: *Phys. Rev. Lett.* 82.8 (Feb. 1999), pp. 1784–1787. DOI: 10.1103/PhysRevLett.82.1784.

[20] A. Mari et al. “Positive Wigner Functions Render Classical Simulation of Quantum Computation Efficient”. In: *Phys. Rev. Lett.* 109.23 (Dec. 2012), p. 230503. DOI: 10.1103/PhysRevLett.109.230503.

[21] A. Ourjoumtsev et al. “Generating Optical Schrödinger Kittens for Quantum Information Processing”. In: *Science* 312.5770 (Apr. 2006), pp. 83–86. DOI: 10.1126/science.1122858.

[22] A. Zavatta et al. “Quantum-to-Classical Transition with Single-Photon-Added Coherent States of Light”. In: *Science* 306.5696 (Oct. 2004), pp. 660–662. DOI: 10.1126/science.1103190.

[23] Š. Bräuer et al. “Generation of quantum states with nonlinear squeezing by Kerr nonlinearity”. In: *Opt. Express* 29.14 (July 2021), pp. 22648–22658. DOI: 10.1364/OE.427637.

[24] R. Landauer. “Irreversibility and Heat Generation in the Computing Process”. In: *IBM J. Res. Dev.* 5.3 (July 1961), pp. 183–191. DOI: 10.1147/rd.53.0183.

[25] C. H. Bennett. “Notes on Landauer’s principle, reversible computation, and Maxwell’s Demon”. In: *Studies in History and Philosophy of Science Part B: Studies in History and Philosophy of Modern Physics* 34.3 (Sept. 2003), pp. 501–510. DOI: 10.1016/S1355-2198(03)00039-X.

[26] J. M. R. Parrondo et al. “Thermodynamics of information”. In: *Nat. Phys.* 11 (Feb. 2015), pp. 131–139. DOI: 10.1038/nphys3230.

[27] M. A. Nielsen et al. *Quantum Computation and Quantum Information*. Cambridge, England, UK: Cambridge University Press, Oct. 2000.

[28] S. Deffner et al. *Quantum Thermodynamics – An introduction to the thermodynamics of quantum information*. Morgan & Claypool Publishers, July 2019. DOI: 10.1088/2053-2571/ab21c6.

[29] K. C. Young et al. “Error Suppression and Error Correction in Adiabatic Quantum Computation: Techniques and Challenges”. In: *Phys. Rev. X* 3.4 (Nov. 2013), p. 041013. DOI: 10.1103/PhysRevX.3.041013.

[30] M. D. Reed et al. “Realization of three-qubit quantum error correction with superconducting circuits”. In: *Nature* 482 (Feb. 2012), pp. 382–385. DOI: 10.1038/nature10786.

[31] A. C. Santos et al. “Superadiabatic Controlled Evolutions and Universal Quantum Computation”. In: *Sci. Rep.* 5.15775 (Oct. 2015), pp. 1–10. DOI: 10.1038/srep15775.

[32] J. Schwinger. “On angular momentum”. In: (Jan. 1952). DOI: 10.2172/4389568.

[33] J. M. Radcliffe. “Some properties of coherent spin states”. In: *J. Phys. A: Gen. Phys.* 4.3 (May 1971), p. 313. DOI: 10.1088/0305-4470/4/3/009.

[34] F. T. Arecchi et al. “Atomic Coherent States in Quantum Optics”. In: *Phys. Rev. A* 6.6 (Dec. 1972), pp. 2211–2237. DOI: 10.1103/PhysRevA.6.2211.

[35] W.-M. Zhang et al. “Coherent states: Theory and some applications”. In: *Rev. Mod. Phys.* 62.4 (Oct. 1990), pp. 867–927. DOI: 10.1103/RevModPhys.62.867.

[36] R. Achilles et al. “The early proofs of the theorem of Campbell, Baker, Hausdorff, and Dynkin”. In: *Arch. Hist. Exact Sci.* 66.3 (May 2012), pp. 295–358. DOI: 10.1007/s00407-012-0095-8.

[37] R. Feynman et al. “Geometrical Representation of the Schrödinger Equation for Solving Maser Problems”. In: *J. Appl. Phys.* (1957).

[38] J. Davis et al. “Wigner negativity in spin-j systems”. In: *Phys. Rev. Res.* 3.3 (Aug. 2021), p. 033134. DOI: 10.1103/PhysRevResearch.3.033134.

[39] J. Ma et al. “Quantum spin squeezing”. In: *Phys. Rep.* 509.2 (Dec. 2011), pp. 89–165. DOI: 10.1016/j.physrep.2011.08.003.

[40] K. Husimi. “Some Formal Properties of the Density Matrix”. In: *Proceedings of the Physico-Mathematical Society of Japan. 3rd Series* 22.4 (1940), pp. 264–314. DOI: 10.11429/ppmsj1919.22.4_264.

[41] M. Kitagawa et al. “Number-phase minimum-uncertainty state with reduced number uncertainty in a Kerr nonlinear interferometer”. In: *Phys. Rev. A* 34.5 (Nov. 1986), pp. 3974–3988. DOI: 10.1103/PhysRevA.34.3974.

[42] S. Colombo et al. “Time-reversal-based quantum metrology with many-body entangled states”. In: *Nat. Phys.* 18 (Aug. 2022), pp. 925–930. DOI: 10.1038/s41567-022-01653-5.

[43] J. Huang et al. “Quantum metrology with spin cat states under dissipation”. In: *Sci. Rep.* 5.17894 (Dec. 2015), pp. 1–10. DOI: 10.1038/srep17894.

[44] D. Kajtoch et al. “Quantum dynamics generated by the two-axis countertwisting Hamiltonian”. In: *Phys. Rev. A* 92.1 (July 2015), p. 013623. DOI: 10.1103/PhysRevA.92.013623.

[45] F. Pan et al. “Exact solution of the two-axis countertwisting Hamiltonian”. In: *Ann. Phys.* 376 (Jan. 2017), pp. 182–193. DOI: 10.1016/j.aop.2016.11.019.

[46] J. Huang et al. “Non-Gaussian precision metrology via driving through quantum phase transitions”. In: *Phys. Rev. A* 97.3 (Mar. 2018), p. 032116. DOI: 10.1103/PhysRevA.97.032116.

[47] K. Xu et al. “Metrological Characterization of Non-Gaussian Entangled States of Superconducting Qubits”. In: *Phys. Rev. Lett.* 128.15 (Apr. 2022), p. 150501. DOI: 10.1103/PhysRevLett.128.150501.

[48] T. Opatrný. “Quasicontinuous-Variable Quantum Computation with Collective Spins in Multipath Interferometers”. In: *Phys. Rev. Lett.* 119.1 (July 2017), p. 010502. DOI: 10.1103/PhysRevLett.119.010502.

[49] T. Holstein et al. “Field Dependence of the Intrinsic Domain Magnetization of a Ferromagnet”. In: *Physical Review* 58.12 (Dec. 1940), pp. 1098–1113. DOI: 10.1103/PhysRev.58.1098.

[50] U. Leonhardt. *Essential Quantum Optics: From Quantum Measurements to Black Holes*. Cambridge, England, UK: Cambridge University Press, Feb. 2010. DOI: 10.1017/CBO9780511806117.

[51] K. Mølmer. “Optical coherence: A convenient fiction”. In: *Phys. Rev. A* 55.4 (Apr. 1997), pp. 3195–3203. DOI: 10.1103/PhysRevA.55.3195.

[52] U. L. Andersen et al. “30 years of squeezed light generation”. In: *Phys. Scr.* 91.5 (Apr. 2016), p. 053001. DOI: 10.1088/0031-8949/91/5/053001.

[53] L. Mandel et al. *Optical Coherence and Quantum Optics*. Cambridge, England, UK: Cambridge University Press, Sept. 1995. DOI: 10.1017/CBO9781139644105.

[54] H. Vahlbruch et al. “Observation of Squeezed Light with 10-dB Quantum-Noise Reduction”. In: *Phys. Rev. Lett.* 100.3 (Jan. 2008), p. 033602. DOI: 10.1103/PhysRevLett.100.033602.

[55] M. Mehmet et al. “Squeezed light at 1550 nm with a quantum noise reduction of 12.3 dB”. In: *Opt. Express* 19.25 (Dec. 2011), pp. 25763–25772. DOI: 10.1364/OE.19.025763.

[56] J. L. O’Brien. “Optical Quantum Computing”. In: *Science* 318.5856 (Dec. 2007), pp. 1567–1570. DOI: 10.1126/science.1142892.

[57] H. J. Kimble et al. “Photon Antibunching in Resonance Fluorescence”. In: *Phys. Rev. Lett.* 39.11 (Sept. 1977), pp. 691–695. DOI: 10.1103/PhysRevLett.39.691.

[58] L. Davidovich. “Sub-Poissonian processes in quantum optics”. In: *Rev. Mod. Phys.* 68.1 (Jan. 1996), pp. 127–173. DOI: 10.1103/RevModPhys.68.127.

[59] A. Sizmann et al. “Observation of amplitude squeezing of the up-converted mode in second harmonic generation”. In: *Opt. Commun.* 80.2 (Dec. 1990), pp. 138–142. DOI: 10.1016/0030-4018(90)90375-4.

[60] L. Lachman et al. “Quantum non-Gaussianity of light and atoms”. In: *Prog. Quantum Electron.* 83 (May 2022), p. 100395. DOI: 10.1016/j.pquantelec.2022.100395.

[61] J. B. Brask. “Gaussian states and operations – a quick reference”. In: *arXiv* (Feb. 2021). DOI: 10.48550/arXiv.2102.05748. eprint: 2102.05748.

[62] M. Walschaers. “Non-Gaussian Quantum States and Where to Find Them”. In: *PRX Quantum* 2.3 (Sept. 2021), p. 030204. DOI: 10.1103/PRXQuantum.2.030204.

[63] H. Schmidt et al. “Giant Kerr nonlinearities obtained by electromagnetically induced transparency”. In: *Opt. Lett.* 21.23 (Dec. 1996), pp. 1936–1938. DOI: 10.1364/OL.21.001936.

[64] M. J. Werner et al. “Photon-photon interactions in cavity electromagnetically induced transparency”. In: *Phys. Rev. A* 61.1 (Dec. 1999), p. 011801. DOI: 10.1103/PhysRevA.61.011801.

[65] T. N. Dey et al. “Observable effects of Kerr nonlinearity on slow light”. In: *Phys. Rev. A* 76.1 (July 2007), p. 015802. DOI: 10.1103/PhysRevA.76.015802.

[66] L. V. Hau et al. “Light speed reduction to 17 metres per second in an ultracold atomic gas”. In: *Nature* 397 (Feb. 1999), pp. 594–598. DOI: 10.1038/17561.

[67] H. Kang et al. “Observation of Large Kerr Nonlinearity at Low Light Intensities”. In: *Phys. Rev. Lett.* 91.9 (Aug. 2003), p. 093601. DOI: 10.1103/PhysRevLett.91.093601.

[68] M. A. Castellanos-Beltran et al. “Widely tunable parametric amplifier based on a superconducting quantum interference device array resonator”. In: *Appl. Phys. Lett.* 91.8 (Aug. 2007). DOI: 10.1063/1.2773988.

[69] F. Mallet et al. “Single-shot qubit readout in circuit quantum electrodynamics”. In: *Nat. Phys.* 5 (Nov. 2009), pp. 791–795. DOI: 10.1038/nphys1400.

[70] Y. Niu et al. “Giant Kerr nonlinearity induced by interacting dark resonances”. In: *Opt. Lett.* 30.24 (Dec. 2005), pp. 3371–3373. DOI: 10.1364/OL.30.003371.

[71] X.-Y. L et al. “Quantum-criticality-induced strong Kerr nonlinearities in optomechanical systems”. In: *Sci. Rep.* 3.2943 (Oct. 2013), pp. 1–9. DOI: 10.1038/srep02943.

[72] T. Opatrný et al. “Nonlinear coherent heat machines”. In: *Sci. Adv.* 9.1 (Jan. 2023). DOI: 10.1126/sciadv.adf1070.

[73] H. B. Callen. *Thermodynamics and an Introduction to Thermostatistics*. Chichester, England, UK: Wiley, 1991.

[74] S. Carnot. *Rflexions sur la puissance motrice du feu et sur les machines propres dvelopper cette puissance*. Chez Bachelier, Libraire, 1824.

[75] D. Kondepudi et al. *Modern Thermodynamics: From Heat Engines to Dissipative Structures*. Chichester, England, UK: Wiley, Dec. 2014.

[76] R. Kosloff. “Quantum Thermodynamics: A Dynamical Viewpoint”. In: *Entropy* 15.6 (May 2013), pp. 2100–2128. DOI: 10.3390/e15062100.

[77] F. Binder et al. *Thermodynamics in the Quantum Regime: Fundamental Aspects and New Directions*. Cham, Switzerland: Springer International Publishing, Apr. 2019.

[78] H. E. D. Scovil et al. “Three-Level Masers as Heat Engines”. In: *Phys. Rev. Lett.* 2.6 (Mar. 1959), pp. 262–263. DOI: 10.1103/PhysRevLett.2.262.

[79] M. O. Scully et al. “Extracting Work from a Single Heat Bath via Vanishing Quantum Coherence”. In: *Science* 299.5608 (Feb. 2003), pp. 862–864. DOI: 10.1126/science.1078955.

[80] R. Uzdin et al. “Equivalence of Quantum Heat Machines, and Quantum-Thermodynamic Signatures”. In: *Phys. Rev. X* 5.3 (Sept. 2015), p. 031044. DOI: 10.1103/PhysRevX.5.031044.

[81] M. Campisi et al. “The power of a critical heat engine”. In: *Nat. Commun.* 7.11895 (June 2016), pp. 1–5. DOI: 10.1038/ncomms11895.

[82] J. Roßnagel et al. “A single-atom heat engine”. In: *Science* 352.6283 (Apr. 2016), pp. 325–329. DOI: 10.1126/science.aad6320.

[83] D. Gelbwaser-Klimovsky et al. “Work and energy gain of heat-pumped quantized amplifiers”. In: *Europhys. Lett.* 103.6 (Oct. 2013), p. 60005. DOI: 10.1209/0295-5075/103/60005.

[84] D. Gelbwaser-Klimovsky et al. “Heat-machine control by quantum-state preparation: From quantum engines to refrigerators”. In: *Phys. Rev. E* 90.2 (Aug. 2014), p. 022102. DOI: 10.1103/PhysRevE.90.022102.

[85] W. Niedenzu et al. “On the operation of machines powered by quantum non-thermal baths”. In: *New J. Phys.* 18.8 (Aug. 2016), p. 083012. DOI: 10.1088/1367-2630/18/8/083012.

[86] A. Ghosh et al. “Two-level masers as heat-to-work converters”. In: *Proc. Natl. Acad. Sci. U.S.A.* 115.40 (Oct. 2018), pp. 9941–9944. DOI: 10.1073/pnas.1805354115.

[87] M. Kol et al. “Quantum Bath Refrigeration towards Absolute Zero: Challenging the Unattainability Principle”. In: *Phys. Rev. Lett.* 109.9 (Aug. 2012), p. 090601. DOI: 10.1103/PhysRevLett.109.090601.

[88] D. Gelbwaser-Klimovsky et al. “Minimal universal quantum heat machine”. In: *Phys. Rev. E* 87.1 (Jan. 2013), p. 012140. DOI: 10.1103/PhysRevE.87.012140.

[89] N. Linden et al. “How Small Can Thermal Machines Be? The Smallest Possible Refrigerator”. In: *Phys. Rev. Lett.* 105.13 (Sept. 2010), p. 130401. DOI: 10.1103/PhysRevLett.105.130401.

[90] M. T. Naseem et al. “Minimal quantum heat manager boosted by bath spectral filtering”. In: *Phys. Rev. Res.* 2.3 (Aug. 2020), p. 033285. DOI: 10.1103/PhysRevResearch.2.033285.

[91] C. Karg et al. “Quantum optical two-atom thermal diode”. In: *Phys. Rev. E* 99.4 (Apr. 2019), p. 042121. DOI: 10.1103/PhysRevE.99.042121.

[92] J. Klatzow et al. “Experimental Demonstration of Quantum Effects in the Operation of Microscopic Heat Engines”. In: *Phys. Rev. Lett.* 122.11 (Mar. 2019), p. 110601. DOI: 10.1103/PhysRevLett.122.110601.

[93] D. Gelbwaser-Klimovsky et al. “Thermodynamics of Quantum Systems Under Dynamical Control”. In: *Advances In Atomic, Molecular, and Optical Physics*. Vol. 64. Cambridge, MA, USA: Academic Press, Jan. 2015, pp. 329–407. DOI: 10.1016/bs.aamop.2015.07.002.

[94] G. Kurizki et al. *Thermodynamics and Control of Open Quantum Systems*. Cambridge, England, UK: Cambridge University Press, Dec. 2021. DOI: 10.1017/9781316798454.

[95] T. Opatrný et al. “Work Generation from Thermal Noise by Quantum Phase-Sensitive Observation”. In: *Phys. Rev. Lett.* 127.4 (July 2021), p. 040602. DOI: 10.1103/PhysRevLett.127.040602.

[96] S. Ding et al. “Cross-Kerr Nonlinearity for Phonon Counting”. In: *Phys. Rev. Lett.* 119.19 (Nov. 2017), p. 193602. DOI: 10.1103/PhysRevLett.119.193602. eprint: 29219528.

[97] N. Imoto et al. “Quantum nondemolition measurement of the photon number via the optical Kerr effect”. In: *Phys. Rev. A* 32.4 (Oct. 1985), pp. 2287–2292. DOI: 10.1103/PhysRevA.32.2287.

[98] A. Ghosh et al. “Catalysis of heat-to-work conversion in quantum machines”. In: *Proc. Natl. Acad. Sci. U.S.A.* 114.46 (Nov. 2017), pp. 12156–12161. DOI: 10.1073/pnas.1711381114. eprint: 29087326.

[99] A. Hovhannisyan et al. “Photon cooling: Linear versus nonlinear interactions”. In: *Phys. Rev. A* 106.3 (Sept. 2022), p. 032214. DOI: 10.1103/PhysRevA.106.032214.

[100] A. E. Allahverdyan et al. “Maximal work extraction from finite quantum systems”. In: *Europhys. Lett.* 67.4 (Aug. 2004), p. 565. DOI: 10.1209/epl/i2004-10101-2.

[101] A. Misra et al. “Quantum Rényi relative entropies affirm universality of thermodynamics”. In: *Phys. Rev. E* 92.4 (Oct. 2015), p. 042161. DOI: 10.1103/PhysRevE.92.042161. eprint: 26565222.

[102] M. T. Mitchison et al. “Coherence-assisted single-shot cooling by quantum absorption refrigerators”. In: *New J. Phys.* 17.11 (Nov. 2015), p. 115013. DOI: 10.1088/1367-2630/17/11/115013.

[103] C. B. Da et al. “Multiatom Quantum Coherences in Micromasers as Fuel for Thermal and Nonthermal Machines”. In: *Entropy* 18.7 (June 2016), p. 244. DOI: 10.3390/e18070244.

[104] W. Niedenzu et al. “Quantum engine efficiency bound beyond the second law of thermodynamics”. In: *Nat. Commun.* 9.165 (Jan. 2018), pp. 1–13. DOI: 10.1038/s41467-017-01991-6.

[105] E. G. Brown et al. “Passivity and practical work extraction using Gaussian operations”. In: *New J. Phys.* 18.11 (Nov. 2016), p. 113028. DOI: 10.1088/1367-2630/18/11/113028.

[106] U. Singh et al. “Quantum thermodynamics in a multipartite setting: A resource theory of local Gaussian work extraction for multimode bosonic systems”. In: *Phys. Rev. A* 100.4 (Oct. 2019), p. 042104. DOI: 10.1103/PhysRevA.100.042104.

[107] A. Serafini et al. “Gaussian Thermal Operations and The Limits of Algorithmic Cooling”. In: *Phys. Rev. Lett.* 124.1 (Jan. 2020), p. 010602. DOI: 10.1103/PhysRevLett.124.010602.

[108] V. Narasimhachar et al. “Thermodynamic resources in continuous-variable quantum systems”. In: *npj Quantum Inf.* 7.9 (Jan. 2021), pp. 1–7. DOI: 10.1038/s41534-020-00342-6.

[109] M. Reck et al. “Experimental realization of any discrete unitary operator”. In: *Phys. Rev. Lett.* 73.1 (July 1994), pp. 58–61. DOI: 10.1103/PhysRevLett.73.58.

[110] W. R. Clements et al. “Optimal design for universal multiport interferometers”. In: *Optica* 3.12 (Dec. 2016), pp. 1460–1465. DOI: 10.1364/OPTICA.3.001460.

[111] E. A. Martinez et al. “Dynamics and Thermodynamics of Linear Quantum Open Systems”. In: *Phys. Rev. Lett.* 110.13 (Mar. 2013), p. 130406. DOI: 10.1103/PhysRevLett.110.130406.

[112] N. Freitas et al. “Analytic solution for heat flow through a general harmonic network”. In: *Phys. Rev. E* 90.4 (Oct. 2014), p. 042128. DOI: 10.1103/PhysRevE.90.042128.

[113] W. Pusz et al. “Passive states and KMS states for general quantum systems”. In: *Commun. Math. Phys.* 58.3 (Jan. 1978), pp. 273–290.

[114] T. M. Cover et al. *Elements of Information Theory*. Chichester, England, UK: Wiley, Nov. 2012.

[115] R. W. Boyd. *Nonlinear Optics*. Elsevier, Academic Press, 2008.

[116] Š. Bräuer. *4-mode heat machine tools*. GitHub repository https://gist.github.com/simon-brauer/debaed2f561186d6d944b34540769a2f.

[117] A. Lenard. “Thermodynamical proof of the Gibbs formula for elementary quantum systems”. In: *J. Stat. Phys.* 19.6 (Dec. 1978), pp. 575–586. DOI: 10.1007/BF01011769.

[118] E. T. Jaynes. “Information Theory and Statistical Mechanics”. In: *Phys. Rev.* 106.4 (May 1957), pp. 620–630. DOI: 10.1103/PhysRev.106.620.

[119] E. Shahmoon et al. “Strongly interacting photons in hollow-core waveguides”. In: *Phys. Rev. A* 83.3 (Mar. 2011), p. 033806. DOI: 10.1103/PhysRevA.83.033806.

[120] I. Friedler et al. “Long-range interactions and entanglement of slow single-photon pulses”. In: *Phys. Rev. A* 72.4 (Oct. 2005), p. 043803. DOI: 10.1103/PhysRevA.72.043803.

[121] O. Firstenberg et al. “Attractive photons in a quantum nonlinear medium”. In: *Nature* 502 (Oct. 2013), pp. 71–75. DOI: 10.1038/nature12512.

[122] J. D. Thompson et al. “Symmetry-protected collisions between strongly interacting photons”. In: *Nature* 542 (Feb. 2017), pp. 206–209. DOI: 10.1038/nature20823.

[123] D. Tiarks et al. “A photon–photon quantum gate based on Rydberg interactions”. In: *Nat. Phys.* 15 (Feb. 2019), pp. 124–126. DOI: 10.1038/s41567-018-0313-7.

[124] D. Gottesman et al. “Encoding a qubit in an oscillator”. In: *Phys. Rev. A* 64.1 (June 2001), p. 012310. DOI: 10.1103/PhysRevA.64.012310.

[125] K. Park et al. “Deterministic nonlinear phase gates induced by a single qubit”. In: *New J. Phys.* 20.5 (May 2018), p. 053022. DOI: 10.1088/1367-2630/aabb86.

[126] P. Marek et al. “Deterministic implementation of weak quantum cubic nonlinearity”. In: *Phys. Rev. A* 84.5 (Nov. 2011), p. 053802. DOI: 10.1103/PhysRevA.84.053802.

[127] L.-S. Guo et al. “Discriminating two nonorthogonal states against a noise channel by feed-forward control”. In: *Phys. Rev. A* 91.2 (Feb. 2015), p. 022321. DOI: 10.1103/PhysRevA.91.022321.

[128] K. Miyata et al. “Implementation of a quantum cubic gate by an adaptive non-Gaussian measurement”. In: *Phys. Rev. A* 93.2 (Feb. 2016), p. 022301. DOI: 10.1103/PhysRevA.93.022301.

[129] P. Marek et al. “General implementation of arbitrary nonlinear quadrature phase gates”. In: *Phys. Rev. A* 97.2 (Feb. 2018), p. 022329. DOI: 10.1103/PhysRevA.97.022329.

[130] S. Konno et al. “Nonlinear Squeezing for Measurement-Based Non-Gaussian Operations in Time Domain”. In: *Phys. Rev. Appl.* 15.2 (Feb. 2021), p. 024024. DOI: 10.1103/PhysRevApplied.15.024024.

[131] M. Yukawa et al. “Emulating quantum cubic nonlinearity”. In: *Phys. Rev. A* 88.5 (Nov. 2013), p. 053816. DOI: 10.1103/PhysRevA.88.053816.

[132] D. W. Moore et al. “Estimation of squeezing in a nonlinear quadrature of a mechanical oscillator”. In: *New J. Phys.* 21.11 (Nov. 2019), p. 113050. DOI: 10.1088/1367-2630/ab5690.

[133] J. S. Pedernales et al. “Quantum Rabi Model with Trapped Ions”. In: *Sci. Rep.* 5.15472 (Oct. 2015), pp. 1–7. DOI: 10.1038/srep15472.

[134] Y. Zheng et al. “Gaussian Conversion Protocols for Cubic Phase State Generation”. In: *PRX Quantum* 2.1 (Feb. 2021), p. 010327. DOI: 10.1103/PRXQuantum.2.010327.

[135] Q. A. Turchette et al. “Measurement of Conditional Phase Shifts for Quantum Logic”. In: *Phys. Rev. Lett.* 75.25 (Dec. 1995), pp. 4710–4713. DOI: 10.1103/PhysRevLett.75.4710.

[136] F. L. Semio et al. “Effective cross-Kerr nonlinearity and robust phase gates with trapped ions”. In: *Phys. Rev. A* 72.6 (Dec. 2005), p. 064305. DOI: 10.1103/PhysRevA.72.064305.

[137] N. Matsuda et al. “Lossless all-optical phase gate using a polarization-division Sagnac interferometer applicable to a waveguide-type Kerr medium”. In: *Appl. Phys. Lett.* 91.17 (Oct. 2007). DOI: 10.1063/1.2801697.

[138] H. Azuma. “Quantum computation with Kerr-nonlinear photonic crystals”. In: *J. Phys. D: Appl. Phys.* 41.2 (Dec. 2007), p. 025102. DOI: 10.1088/0022-3727/41/2/025102.

[139] D. Vitali et al. “Complete Quantum Teleportation with a Kerr Nonlinearity”. In: *Phys. Rev. Lett.* 85.2 (July 2000), pp. 445–448. DOI: 10.1103/PhysRevLett.85.445.

[140] Z. Jian et al. “Nearly Deterministic Teleportation of a Photonic Qubit with Weak Cross-Kerr Nonlinearities”. In: *Chin. Phys. Lett.* 26.10 (Oct. 2009), p. 100301. DOI: 10.1088/0256-307X/26/10/100301.

[141] L. Dong et al. “A nearly deterministic scheme for generating χ-type entangled states with weak cross-Kerr nonlinearities”. In: *Quantum Inf. Process.* 12.4 (Apr. 2013), pp. 1787–1795. DOI: 10.1007/s11128-012-0481-9.

[142] F. Knig et al. “Soliton backaction-evading measurement using spectral filtering”. In: *Phys. Rev. A* 66.4 (Oct. 2002), p. 043810. DOI: 10.1103/PhysRevA.66.043810.

[143] Y.-F. Xiao et al. “Quantum nondemolition measurement of photon number via optical Kerr effect in an ultra-high-Q microtoroid cavity”. In: *Opt. Express* 16.26 (Dec. 2008), pp. 21462–21475. DOI: 10.1364/OE.16.021462.

[144] H. Jeong et al. “Generation of macroscopic superposition states with small nonlinearity”. In: *Phys. Rev. A* 70.6 (Dec. 2004), p. 061801. DOI: 10.1103/PhysRevA.70.061801.

[145] A. xn–Imamolu-4s3c et al. “Strongly Interacting Photons in a Nonlinear Cavity”. In: *Phys. Rev. Lett.* 79.8 (Aug. 1997), pp. 1467–1470. DOI: 10.1103/PhysRevLett.79.1467.

[146] L. V. Hau et al. “Light speed reduction to 17 metres per second in an ultracold atomic gas”. In: *Nature* 397 (Feb. 1999), pp. 594–598. DOI: 10.1038/17561.

[147] N. Bergeal et al. “Phase-preserving amplification near the quantum limit with a Josephson ring modulator”. In: *Nature* 465 (May 2010), pp. 64–68. DOI: 10.1038/nature09035.

[148] S. Konno et al. “Logical states for fault-tolerant quantum computation with propagating light”. In: *Science* 383.6680 (Jan. 2024), pp. 289–293. DOI: 10.1126/science.adk7560.

[149] P. Marek. “Ground State Nature and Nonlinear Squeezing of Gottesman-Kitaev-Preskill States”. In: *Phys. Rev. Lett.* 132.21 (May 2024), p. 210601. DOI: 10.1103/PhysRevLett.132.210601.

[150] Virgo Collaboration et al. “Increasing the Astrophysical Reach of the Advanced Virgo Detector via the Application of Squeezed Vacuum States of Light”. In: *Phys. Rev. Lett.* 123.23 (Dec. 2019), p. 231108. DOI: 10.1103/PhysRevLett.123.231108.

[151] K. Takase et al. “Gottesman-Kitaev-Preskill qubit synthesizer for propagating light”. In: *npj Quantum Inf.* 9.98 (Oct. 2023), pp. 1–11. DOI: 10.1038/s41534-023-00772-y.

[152] V. Kala et al. “Cubic nonlinear squeezing and its decoherence”. In: *Opt. Express* 30.17 (Aug. 2022), pp. 31456–31471. DOI: 10.1364/OE.464759.

[153] A. S. Sørensen et al. “Entanglement and Extreme Spin Squeezing”. In: *Phys. Rev. Lett.* 86.20 (May 2001), pp. 4431–4434. DOI: 10.1103/PhysRevLett.86.4431.

[154] S. Ghose et al. “Non-Gaussian ancilla states for continuous variable quantum computation via Gaussian maps”. In: *J. Mod. Opt.* (Apr. 2007).

[155] R. Yanagimoto et al. “Engineering a Kerr-Based Deterministic Cubic Phase Gate via Gaussian Operations”. In: *Phys. Rev. Lett.* 124.24 (June 2020), p. 240503. DOI: 10.1103/PhysRevLett.124.240503.

[156] H. Strobel et al. “Fisher information and entanglement of non-Gaussian spin states”. In: *Science* 345.6195 (July 2014), pp. 424–427. DOI: 10.1126/science.1250147.

[157] L. Pezz et al. “Quantum metrology with nonclassical states of atomic ensembles”. In: *Rev. Mod. Phys.* 90.3 (Sept. 2018), p. 035005. DOI: 10.1103/RevModPhys.90.035005.

[158] A. Evrard et al. “Enhanced Magnetic Sensitivity with Non-Gaussian Quantum Fluctuations”. In: *Phys. Rev. Lett.* 122.17 (May 2019), p. 173601. DOI: 10.1103/PhysRevLett.122.173601.

[159] T. Opatrný et al. “Counterdiabatic driving in spin squeezing and Dicke-state preparation”. In: *Phys. Rev. A* 93.2 (Feb. 2016), p. 023815. DOI: 10.1103/PhysRevA.93.023815.

[160] D. F. Walls. “Squeezed states of light”. In: *Nature* 306 (Nov. 1983), pp. 141–146. DOI: 10.1038/306141a0.

[161] R. Jozsa. “Fidelity for Mixed Quantum States”. In: *Journal of Modern Optics* 41.12 (Dec. 1994), pp. 2315–2323. DOI: 10.1080/09500349414552171.

[162] S. L. Braunstein et al. “Statistical distance and the geometry of quantum states”. In: *Phys. Rev. Lett.* 72.22 (May 1994), pp. 3439–3443. DOI: 10.1103/PhysRevLett.72.3439.

[163] B. Yadin et al. “Operational Resource Theory of Continuous-Variable Nonclassicality”. In: *Phys. Rev. X* 8.4 (Dec. 2018), p. 041038. DOI: 10.1103/PhysRevX.8.041038.

[164] F. Albarelli et al. “Resource theory of quantum non-Gaussianity and Wigner negativity”. In: *Phys. Rev. A* 98.5 (Nov. 2018), p. 052350. DOI: 10.1103/PhysRevA.98.052350.

[165] E. Chitambar et al. “Quantum resource theories”. In: *Rev. Mod. Phys.* 91.2 (Apr. 2019), p. 025001. DOI: 10.1103/RevModPhys.91.025001.

[166] G. Carrara et al. “Squeezing as a resource to counteract phase diffusion in optical phase estimation”. In: *Phys. Rev. A* 102.6 (Dec. 2020), p. 062610. DOI: 10.1103/PhysRevA.102.062610.

[167] W. Muessel et al. “Twist-and-turn spin squeezing in Bose-Einstein condensates”. In: *Phys. Rev. A* 92.2 (Aug. 2015), p. 023603. DOI: 10.1103/PhysRevA.92.023603.

[168] I. Gradshteyn et al. *Table of Integrals, Series, and Products*. Elsevier Science, 2014.

[169] A. D. Poularikas. *Handbook of Formulas and Tables for Signal Processing*. Berlin, Germany: Springer, Oct. 1998.

Faculty
of Science

Palacký University
Olomouc

Annotation in English

The thesis focuses on two key directions, namely, the use of nonlinearities in quantum thermodynamics and, subsequently, the generation of nonlinear states and their quantification. The thermodynamic part describes the realization of a nonlinear interferometer as the smallest possible quantum heat machine, where the nonlinear process is an integral part of the scheme. With four input modes, it is possible to concentrate energy in one preselected mode at the output of the scheme. The second segment focuses on the realization and quantification of nonlinearly squeezed states — cubic and quartic, where it is a deterministic process with the use of a non-linear operation (Kerr operations). The follow-up is the generalization of the nonlinear squeezing parameter so that it can be used for the classification of different types of states in different systems.

KEYWORDS: quantum optics, quantum thermodynamics, Kerr nonlinearity, nonlinear squeezing

Anotace v češtině

Práce se zaměřuje na dva klavní směry a to využití nelinearit v kvantové termodynamice a následně na generaci nelineárních stavů a jejich kvantifikaci. V termodynamická část popisuje realizace nelineárního interferometru jako nejmenšího možného kvantového tepelného stroje, kdy nelinární proces je nedílnou součástí schématu. Při vstupních čtyřech módech je možné na výstupu schématu koncentrovat energii do jednoho předvybraného módu. Druhý segment se zaměřuje na realizaci a kvantifikaci nelineárně stlačených stavů — kubicky a kvarticky, kdy se jedná o deterministický proces právě s využitím nelineární operace (Kerrovské operace). Na to navazuje zobecnění parametru nelineárního stlačení tak, aby bylo možné ho využít pro klasifikaci různých typů stavů v různých systémech.

KLÍČOVÁ SLOVA: kvantová optika, kvantová termodynamika, Kerrova nelinearita, nelineární stlačení

TITLE:	Utilization and quantification of quantum nonlinearity
AUTHOR:	Šimon Bräuer
ADVISOR:	Tomáš Opatrný
CO-ADVISOR:	Petr Marek
STUDY PROGRAM:	Optics and optoelectronics
STUDY FORM:	Full-time
YEAR:	2024
PAGES:	105

DEPARTMENT OF OPTICS
FACULTY OF SCIENCE
PALACKÝ UNIVERSITY OLOMOUC

NÁZEV:	Využití a kvantifikace kvantové nelinearity
AUTOR:	Šimon Bräuer
ŠKOLITEL:	Tomáš Opatrný
KONZULTANT:	Petr Marek
STUDIJNÍ PROGRAM:	Optika a optoelektronika
VE FORMĚ:	Prezenční
ROK:	2024
STRANY:	105

KATEDRA OPTIKY
PŘÍRODOVĚDECKÁ FAKULTA
UNIVERZITA PALACKÉHO V OLOMOUCI